Three-Dimensional Echocardiographic Guidance of Percutaneous Procedures

Muhamed Saric, Ricardo Benenstein

▌ INTRODUCTION

Catheter-based transcutaneous repair of both congenital and acquired cardiovascular defects has been performed by interventional cardiologists and other interventional specialists for the past half a century. This therapeutic approach was initially spearheaded by pediatric cardiologists. Atrial balloon septostomy, later referred to as the Rashkind procedure, is generally considered to be the first catheter-based transcutaneous repair procedure. The Rashkind procedure was first reported in 1971 as the initial treatment in neonates with transposition of the great arteries to improve mixing of venous and systemic blood through creation of an iatrogenic atrial septal defect (ASD).[1]

In the beginning, catheter-based transcutaneous repairs were developed as less invasive alternatives to established surgical procedure but have since evolved into novel ways of treating structural heart defects. Catheter-based transcutaneous procedures to repair structural heart defects can be divided into the following groups:

- Valvular disease
  - Mitral stenosis (percutaneous balloon valvuloplasty)
  - Mitral regurgitation [mitral valve (MV) clipping]
  - Aortic stenosis (transcatheter aortic valve replacement)
  - Closure of paravalvular prosthetic leaks.
- Device closure of cardiac shunts
  - ASDs [secundum ASDs; patent foramen ovale (PFO)]
  - Ventricular septal defects (VSDs; congenital and acquired)
  - Patent ductus arteriosus (PDA).
- Occlusion of the left atrial appendage (LAA)
  - Intracardiac device closure of LAA
  - Epicardial suturing of LAA.
- Guidance of electrophysiology ablation procedures
  - Pulmonary vein isolation for atrial fibrillation.
- Miscellaneous procedures
  - Left ventricular pseudoaneurysm closure
  - Alcohol septal ablation for hypertrophic obstructive cardiomyopathy
  - Right ventricular endomyocardial biopsy.

In the interventional suites, echocardiography is typically used in conjunction with X-ray-based fluoroscopy in guiding catheter-based transcutaneous repairs in real time. Fluoroscopy and echocardiography images are typically presented side-by-side to interventionalists on adjacent monitors. Recently, commercial products that dynamically combine (coregister) in real time three-dimensional (3D) ultrasound and interventional X-ray images into one are becoming available. Computed tomography (CT) and magnetic resonance imaging (MRI)—although often important in establishing the diagnosis of a structural heart defect—typically do not readily provide real time imaging during percutaneous interventions in standard interventional suites.

Real time 3D transesophageal echocardiography (3D TEE) and intracardiac echocardiography (ICE) are the most useful echocardiographic techniques for real time procedural guidance as their images are typically superior to and/or more relevant to interventionalists compared to images obtained by either two-dimensional transesophageal echocardiography (2D TEE) or transthoracic echocardiography (TTE).[2]

In general, percutaneous coronary interventions (such as angioplasty and stenting) are not typically classified as catheter-based transcutaneous procedures to repair structural heart defects and thus will not be discussed in this chapter. The use of intravascular ultrasound (IVUS) techniques in the diagnosis and treatment of vascular disease is provided elsewhere in this textbook.

FLUOROSCOPY VERSUS ECHOCARDIOGRAPHY IN GUIDING PERCUTANEOUS INTERVENTIONS

Imaging is essential for the diagnosis, guidance, and assessments of results of all catheter-based transcutaneous procedures to repair structural heart defects. Detailed description of basics of fluoroscopy and echocardiography are beyond the scope of this chapter; here we will discuss their advantages and shortcomings from the perspective of catheter-based transcutaneous interventional procedures.

X-ray-based fluoroscopy and contrast angiography have been historically considered as gold standards in guiding percutaneous repairs of structural heart defects. These radiographic techniques, which are very familiar to interventionalists, tend to have poor depth resolution, lack ability to differentiate between various soft tissues, and require the use of ionizing radiation and iodinated contrast agents.

While in principle, TTE can be used to guide catheter-based interventions, its use is limited by both suboptimal imaging of relevant cardiac structures and by difficulties in acquiring TTE images in the sterile environment of an interventional suite.

2D TEE and ICE imaging, although extensively used during percutaneous procedure, suffer from the 2D, cross-sectional nature of their images. As a consequence, movement of wires, catheters, and devices used during interventions cannot be tracked appropriately. In addition, neither 2D TEE nor ICE can typically provide en face views of structures of interest to interventionalists. Furthermore, ICE typically provides only monoplane images. It is also invasive and requires the use of expensive disposable transducers that are advanced under sterile condition into the heart via the venous system. Examples of ICE use are provided in the section on percutaneous ASD closure below.

In our practice, modern 3D TEE imaging is the preferred echocardiography technique for guiding interventional procedures as it provides detailed dynamic images (included en face views) of relevant cardiac structures in real time, something that is not easily achievable by any other imaging technique.[3] Although 3D TEE has been around for decades (primarily as an offline, postprocessed imaging technique), it has been revolutionized by the introduction of a 3D TEE probe with a matrix-array transducer having 3,000 elements in the first decade of the 21st century. This approximately a 25–50-fold increase in the number of imaging elements compared with a standard 2D TEE probe has allowed for real time 3D imaging, making 3D TEE ideally suited for guidance of cardiac interventions. General aspects of 3D echocardiographic imaging have previously been reviewed[4–7] and are also discussed elsewhere in this textbook.

TRANSSEPTAL PUNCTURE: A COMMON ELEMENT OF MANY INTERVENTIONAL PROCEDURES

Many catheter-based transcutaneous procedures (such as those involving the MV, LAA, and pulmonary veins) require a transvenous access to the left atrium. In general, the left atrium is accessed after entering a peripheral vein (typically the femoral vein) followed by threading catheters and other hardware into the right atrium and then performing the transseptal puncture to bring the hardware across the interatrial septum into the left atrium.

The general technique of transseptal puncture was originally described by Ross in 1959; further refinements were published in 1962 by Brockenbrough and colleagues.[8,9] Briefly, a sharp needle that will be used to puncture the interatrial septum (referred to as Brockenbrough needle) is hidden inside a catheter (such as the Mullins™ catheter, Medtronic Inc., Minneapolis, MN). The catheter is advanced through the venous system into the right atrium and then pushed further to cause tenting of the interatrial septum (evagination of the interatrial septum toward the left atrium). Thereafter, the Brockenbrough needle is advanced through the catheter until it punctures the interatrial septum.

While the interventionalists' tactile feedback, fluoroscopy and 2D echocardiography (such as 2D TEE and ICE) have been used for many years to guide transseptal puncture with a good safety record,[10] real time 3D TEE provides distinct advantages that may enhance both the safety of the puncture procedure and the success of the subsequent percutaneous intervention in the left heart.

Among the several modalities of 3D TEE, biplane and 3D zoom imaging are particularly useful in guiding the transseptal puncture. The key imaging aspect of guiding a transseptal puncture is to demonstrate the exact location of septal tenting prior to actual puncture. Only after proper location of tenting is confirmed by imaging, the Brockenbrough needle is advanced and the transseptal puncture is performed.[11] Biplane 3D TEE imaging assures that transseptal puncture is confined to the true interatrial septum while preventing piercing of the aorta, superior vena cava (SVC), and other cardiac structures such as the so-called lipomatous hypertrophy of the interatrial septum (Figs 28.1A to D; Movie clip 28.1A and B).

The true interatrial septum is essentially confined to the floor of the fossa ovalis (Latin for "egg-shaped dugout"); the floor is derived from the septum primum. The fossa ovalis is surrounded by the rim (also referred to in Latin as the limbus), which is formed by the septum secundum.[12] The location, size, and shape of the fossa ovalis varies widely among individuals.[13] The fossa ovalis is readily distinguished on en face views of the right atrial aspect of the interatrial septum as a lighter colored ovoid crater. In contrast, the region of fossa ovalis cannot be readily recognized on the rather featureless left atrial aspect of the interatrial septum when standard image gain settings are used.[14] However, at low gain setting, the area of fossa ovalis (which is thinner than the surrounding atrial walls) can be identified as an ovoid area of dropout especially in patients with a concomitant atrial septal aneurysm

(ASA; Figs 28.2A to D and Movie clip 28.2). In individuals with PFO, the opening in the floor of the fossa ovalis is present along the antero-superior rim of fossa ovalis. In such individuals, transseptal puncture needle is often directed through the PFO opening.

On 3D TEE imaging can also readily characterize the size and the shape of the ASA, defined arbitrarily as a ≥ 10 mm sway of the interatrial septum in either direction from the midline.[15] Anatomically, ASA is characterized by redundancy and floppiness of a typically enlarged fossa ovalis floor. The knowledge of an ASA is important to interventionalists; ASA may make transseptal puncture more difficult by requiring septal stretching and/or increased force to traverse the septum.[16] These maneuvers may increase the risk for cardiac perforation during transseptal puncture.[17]

It is important to emphasize that the term lipomatous hypertrophy of the interatrial septum is actually a misnomer as the fat accumulates not in the interatrial septum per se but rather outside of the heart in the groove between the muscular walls of the right and left atrium (Figs 28.3A to C and Movie clip 28.3). The groove is known to surgeons as either the Waterston's or Søndergaard's groove.[18,19] Puncturing of the lipomatous hypertrophy area is dangerous as the needle exits the heart into the epicardial space.

En face 3D zoom views of the interatrial septum from the right and left atrial perspective during tenting allows for better selection of the puncture site. Often transseptal puncture across the foramen ovale is the preferred route; however, for some procedures a puncture of a different portion of the interatrial septum may be more desirable (as, for instance, during closures of mitral paraprosthetic leaks).

VALVULAR DISEASE

Mitral Stenosis: Percutaneous Mitral Balloon Valvuloplasty

Rheumatic heart disease remains the leading cause of mitral stenosis worldwide. Rheumatic mitral stenosis is the most common form of valvular disease in developing parts of the world. In contrast, rheumatic mitral stenosis in Japan, North America, and Northern and Western Europe is typically seen among immigrants from less developed parts of the world. Rheumatic MV disease is a progressive lifelong autoimmune-like disorder triggered by and further exacerbated by recurrent group A streptococcal infections (typically pharyngitis).[20]
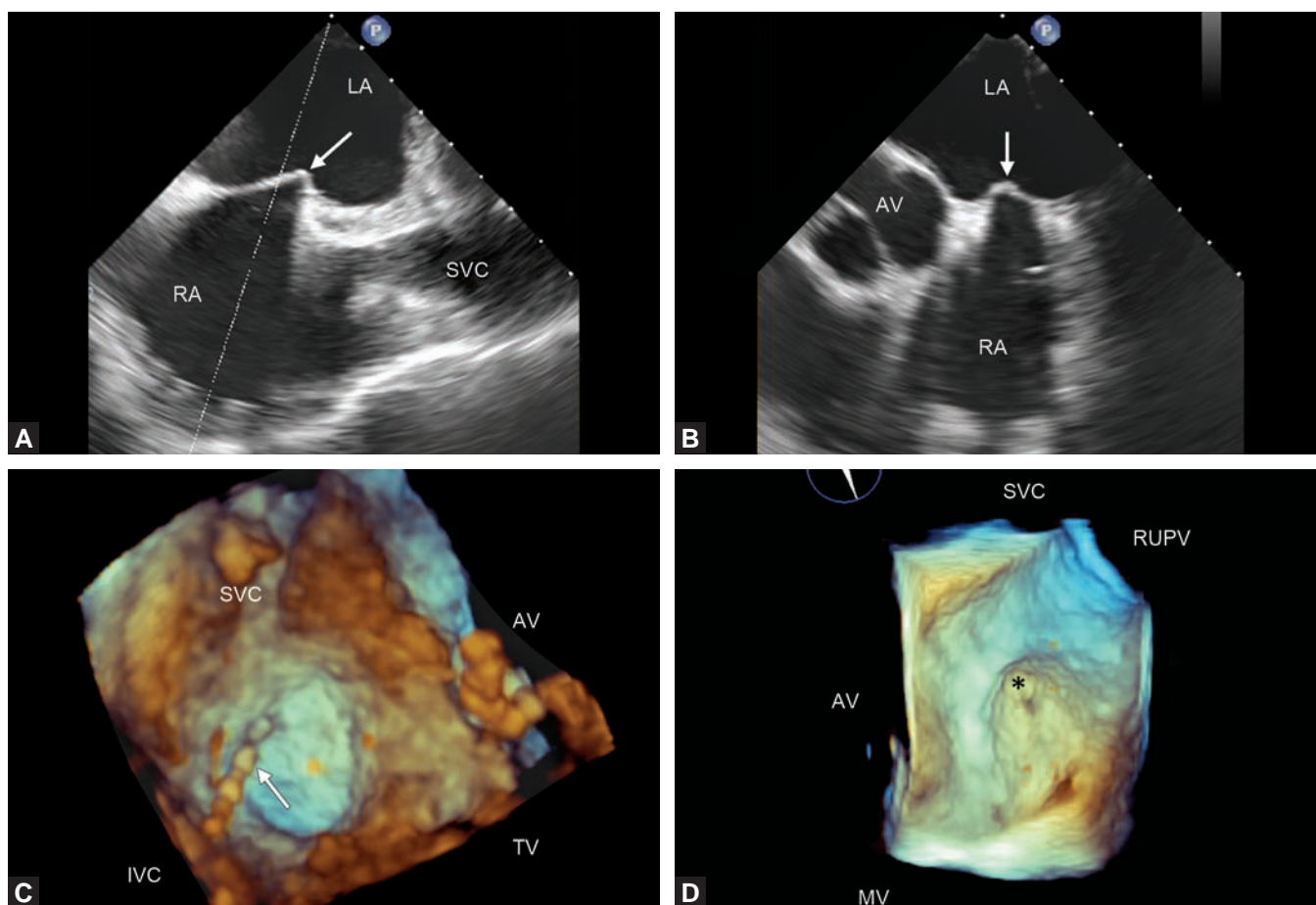
Figs 28.1A to D: 3D TEE guidance of trans-septal puncture. (A and B) Biplane imaging of the interatrial septum demonstrates tenting of the interatrial septum (arrows) by the catheter containing the Brockenbrough needle. Note that the tenting occurs in the central region of the interatrial septum and away from SVC and the aortic valve. Movie clip 28.1B corresponds to this figure; (C) 3D TEE zoom image demonstrates the en face view of the right atrial aspect of the interatrial septum. The dashed line follows the limbus of the fossa ovalis. Note the location of trans-septal puncture (arrow) in the superior portion of the fossa ovalis; (D) 3D TEE zoom image demonstrates the en face view of the left atrial aspect of the interatrial septum. Note the evagination of the interatrial septum into the cavity of the left atrium caused by the Brockenbrough needle assembly (asterisk). Movie clip 28.1A corresponds to this figure. (AV: Aortic valve; IVC: Inferior vena cava; LA: Left atrium; MV: Mitral valve; RA: Right atrium; RUPV: Right upper pulmonary vein; SVC: Superior vena cava; TV: Tricuspid valve).

Probably the very first description of rheumatic mitral stenosis anatomy was provided in 1668 by the British physician John Mayow (1641–1679), who recorded an "extreme constriction of the mitral orifice in a young man".[21] In 1715, Raymond Vieussens (1635–1715), a French physician, published the first comprehensive description of mitral stenosis.[22] Rheumatic mitral stenosis is notable for several "firsts" in the history of medicine: it was the first valvular heart disease to be treated surgically; it was the first heart disease to be diagnosed by echocardiography and it was the first valvular disease to be treated with balloon valvuloplasty.[23]

In the 1920s, Elliot Cutler (1888–1947)[24] and Sir Henry Souttar (1875–1964)[25] working at the Brigham and Women's Hospital in Boston were the first to attempt surgical relief of rheumatic mitral stenosis using procedures that they termed "valvulotomy" and "finger dilation," respectively. In the late 1940s, soon after World War II, techniques of rheumatic mitral stenosis surgery were rediscovered and improved by Charles Bailey and Dwight Harken, who also coined the procedural terms that are still used today.[26] Bailey called his procedure "commissurotomy" while Harken coined the term "valvuloplasty."[27]

In the 1950s, rheumatic mitral stenosis was the first heart disease visualized echocardiographically by Ingle Edler (1911–2001) and Carl Hertz (1920–1990), inventors of echocardiography.[28] In the 1960s, rheumatic mitral stenosis was the first valvular disease to be treated with
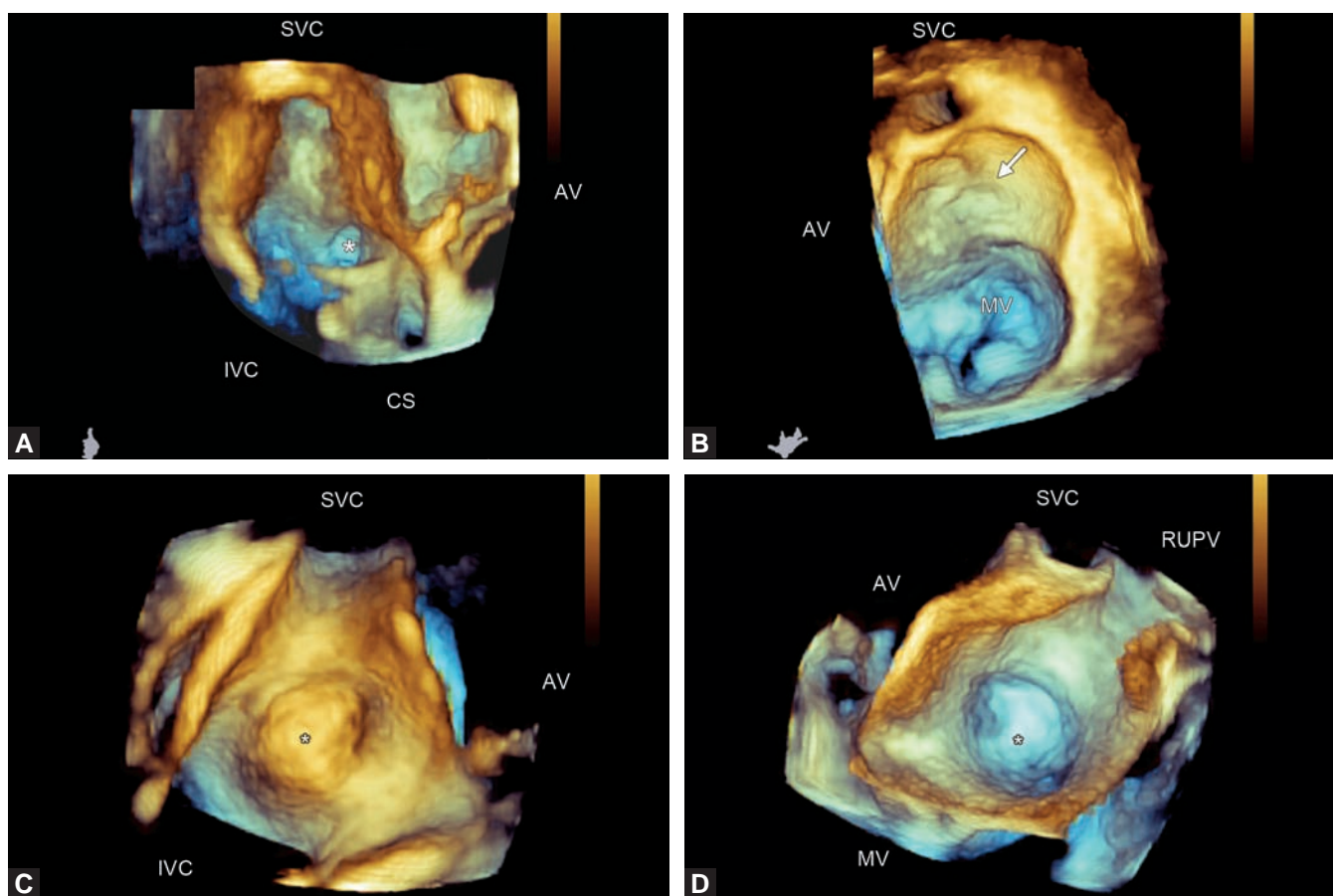
Figs 28.2A to D: Anatomy of fossa ovalis. There is a large variability in the size, shape and location of the fossa ovalis in humans. In addition, the floor of the fossa ovalis (derived from the septum primum) can be either firm or floppy. A floppy septum leads to formation of an atrial septal aneurysm. These 3D TEE zoom images were obtained from two different patients. (A and B) Images obtained from a patient with a small fossa ovalis (asterisk). (A) demonstrates the right atrial and; (B) the left atrial aspect of the interatrial septum. Note that the fossa ovalis, with a pale floor and its darker rims, is easily recognized on the right atrial aspect of the interatrial septum. In contrast, the location of the fossa ovalis (arrow) is less evident on the rather featureless left atrial aspect of the interatrial septum; (C and D) Images obtained from a patient with a large fossa ovalis and an ASA (C) demonstrates the right atrial and (D) the left atrial aspect of the interatrial septum. In contrast to the patient from (A and B), the location of the fossa ovalis in now easily recognized on the left atrial aspect of the interatrial septum when the ASA protrudes away from the left atrium and into the right atrium as shown in (D). Movie clip 28.2 demonstrates the ASA from the posterior aspect of the left atrium. (AV: Aortic valve; CS: Coronary sinus; IVC: Inferior vena cava; MV: Mitral valve; RUPV: Right upper pulmonary vein; SVC: Superior vena cava).

a mechanical MV by Albert Starr (born 1926) and Lowell Edwards (1898–1982).[29] Finally, in the 1980s, Kanji Inoue of Japan developed the ingenious balloon [Inoue balloon, Toray Industries (America) Inc., San Mateo, CA] and the technique of percutaneous mitral balloon valvuloplasty (PMBV), which remains the preferred treatment for the relief of rheumatic mitral stenosis in eligible patients.[30]

In the absence of contraindications, PMBV is recommended in following instances:

- Symptomatic patients with moderate or severe mitral stenosis.
- In asymptomatic patients with moderate or severe mitral stenosis, PMBV is indicated when there is pulmonary artery systolic pressure is > 50 mm Hg at rest or > 60 mm Hg with exercise, or when there is new onset atrial fibrillation.
- PMBV may also be considered in symptomatic patient with mild mitral stenosis (valve area > 1.5 cm^2) when pulmonary artery systolic pressure greater > 60 mm Hg, pulmonary artery wedge pressure > 25 mm Hg, or mean MV gradient > 15 mm Hg during exercise.

Contraindication for PMBV include unfavorable MV Wilkins score (greater than or equal to 10; see below), more than moderate mitral regurgitation and the presence of intracardiac thrombus.[31]
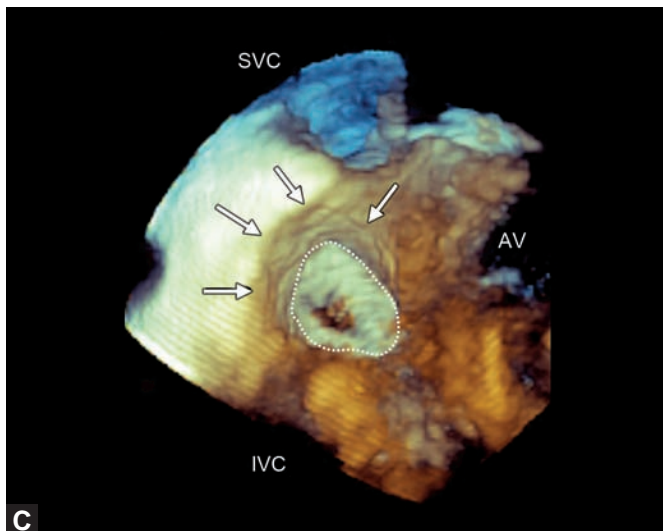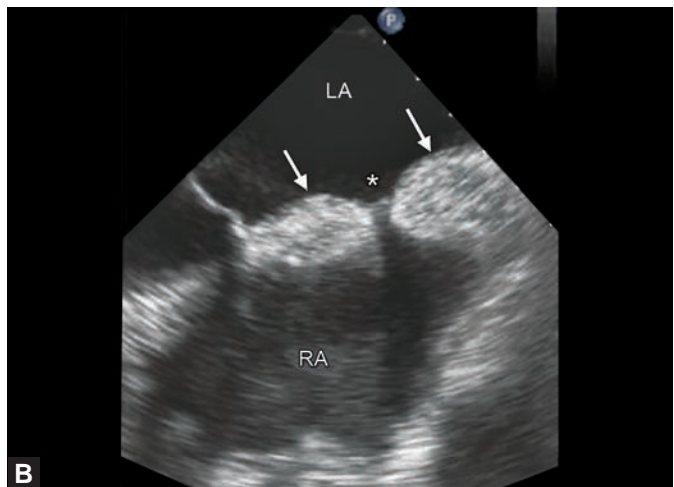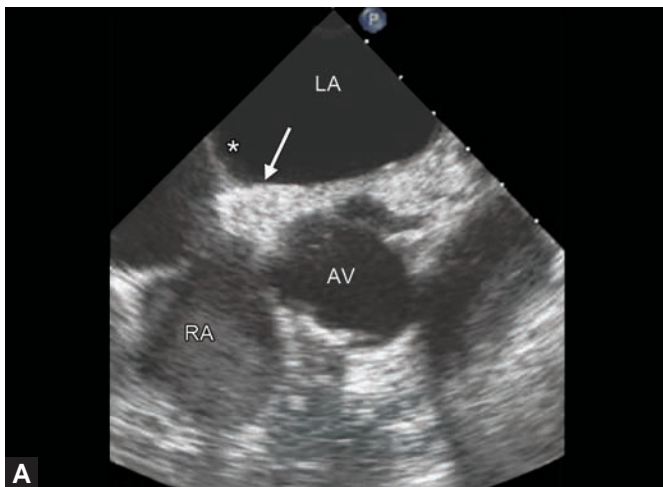
Figs 28.3A to C: Lipomatous hypertrophy of the interatrial septum. Lipomatous hypertrophy of the interatrial septum (also referred to as lipomatous atrial septal hypertrophy, LASH) is an important finding that should be communicated to the interventionalist performing the trans-septal puncture. LASH represents accumulation of epicardial fat in the interatrial fold and not in the true interatrial septum. Thus, in LASH the fossa ovalis remains thin but its rims appear unusually thick. When there is LASH, the trans-septal puncture should be performed through the fossa ovalis and not through the accumulated fat. (A and B) Biplane 3D TEE image from a patient with marked LASH. Note the dumbbell appearance of the interatrial septum. The fossa ovalis has a thin floor (asterisk); its rims are demarcated by epicardial fat accumulation (arrows). Movie clip 28.3 corresponds to this figure; (B and C) 3D TEE zoom image of the right atrial aspect of the interatrial septum from a patient with LASH. Note how the fossa ovalis (white dashed line) is surrounded by unusually tall rims (arrows). These raised rims are due to accumulation of epicardial fat. (AV: Aortic valve; IVC,: Inferior vena cava; LA: Left atrium; RA: Right atrium; SVC: Superior vena cava).

The role of 3D TEE in PMBV is threefold: confirmation of the diagnosis of mitral stenosis, possible refinement of the MV Wilkins score and guidance of PMBV per se.[32]

MV planimetry by 3D transthoracic or transesophageal echocardiography is becoming the gold standard for the anatomic assessment of the severity of mitral stenosis.[33] The MV is funnel shaped with its narrowest area located in the left ventricle and often in a plane that is not parallel with standard imaging planes of 2D echocardiography. Using 3D echocardiography (3DE) techniques of multiplane reconstructions one can overcome the limitations of 2D planimetry and measure the area of at the very tip of the MV funnel. MV area can also be measured on zoomed en face views of the MV either semiquantitatively using calibrated grids or even quantitatively using newer software techniques of on-image planimetry (Figs 28.4A to D and Movie clip 28.4).

3D TEE may also help in calculating the MV Wilkins's score, an essential prerequisite for PMBV. The Wilkins's score was originally developed in the late 1980s using 2D transthoracic echocardiography and is based on mitral leaflet thickness, calcifications, and mobility as well as the thickness of the subvalvular apparatus.[34] Each of the four categories is graded on a scale of 0 (normal) to 4 (severely abnormal). A normal MV, thus, has a score of 0. The most unfavorable score is 16. PMBV is contraindicated when mitral score is > 10. Significant thickening, calcifications, and immobility of mitral leaflets and well as significant thickening of the mitral subvalvular apparatus predispose MV to leaflet tear, a known complication of PMBV that may lead to significant de novo mitral regurgitation. 3D TEE may enhance the scoring through its superior ability to visualize leaflet mobility and the details of the subvalvular mitral apparatus.
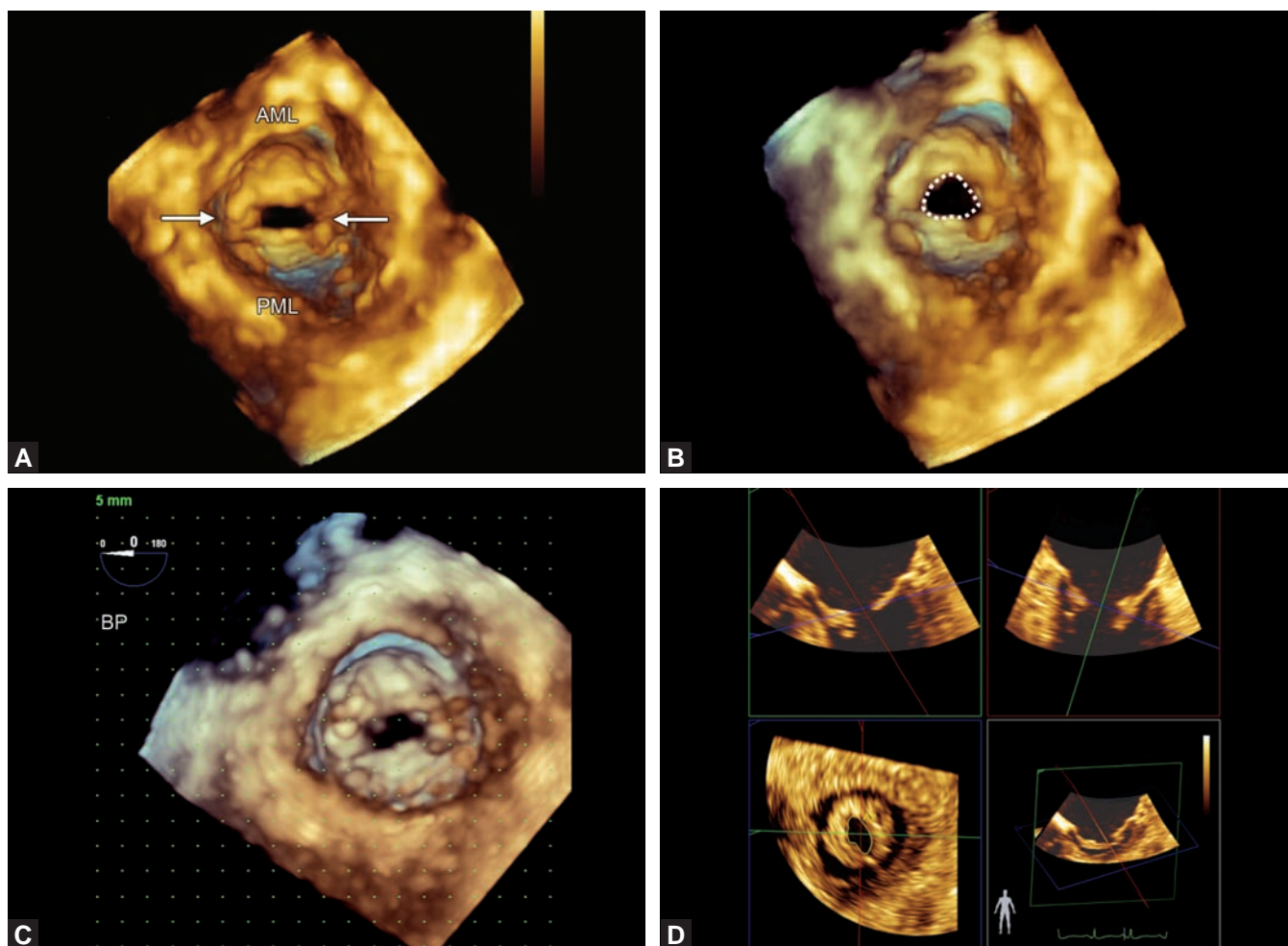
Figs 28.4A to D: 3D TEE diagnosis of mitral stenosis. 3D TEE images obtained from a 53-year-old woman with rheumatic mitral stenosis who grew up in the former Soviet Union. (A), (B) and (C) demonstrate 3D TEE zoom images of the MV from the left ventricular perspective; (D) is a multiplane reconstruction image. (A) 3D TEE image demonstrates typical features of rheumatic mitral stenosis: commissural fusions (arrows) and the doming of the anterior mitral leaflet (AML). On the accompanying Movie clip 28.4 there is also diminished mobility of the posterior mitral leaflet (PML); (B), (C) and (D) demonstrates various 3D TEE methods of calculating the MV area: quantitative on-image planimetry (A), semiquantitative method using a 5 mm grid (B), and the multiplane reconstruction method (C). By all three methods, the patient has severe mitral stenosis with a MV area of approximately 0.6 cm^2.

3D TEE provides guidance throughout the PMBV procedure which is performed in the following fashion. After obtained venous access (typically using the femoral vein), transseptal puncture of the interatrial septum is performed as described earlier in this chapter. Subsequently a deflated Inoue valvuloplasty balloon is brought into the left atrium through the transseptal puncture. Given its ability to visualize the left atrial aspect of the MV en face, 3D TEE can precisely guide positioning of the valvuloplasty balloon across the MV. Once positioned across the MV, the balloon is inflated under 3D TEE and fluoroscopy guidance with the intent to separate the two leaflets of the MV along the commissures fused by the rheumatic process (Figs 28.5A to D and Movie clip 28.5A to C).

The outcome of PMBV can be assessed in real time by 3D TEE; en face views of the left ventricular (LV) side of the MV are particularly useful. The desired outcome is a controlled commissural tear that enlarges the MV orifice and does not create de novo or worsens preexisting mitral regurgitation. 3D TEE can also visualize the mechanism of unfavorable outcome, namely a noncommissural leaflet tear often leading to significant de novo acute mitral regurgitation (Figs 28.6A to D and Movie clip 28.6).
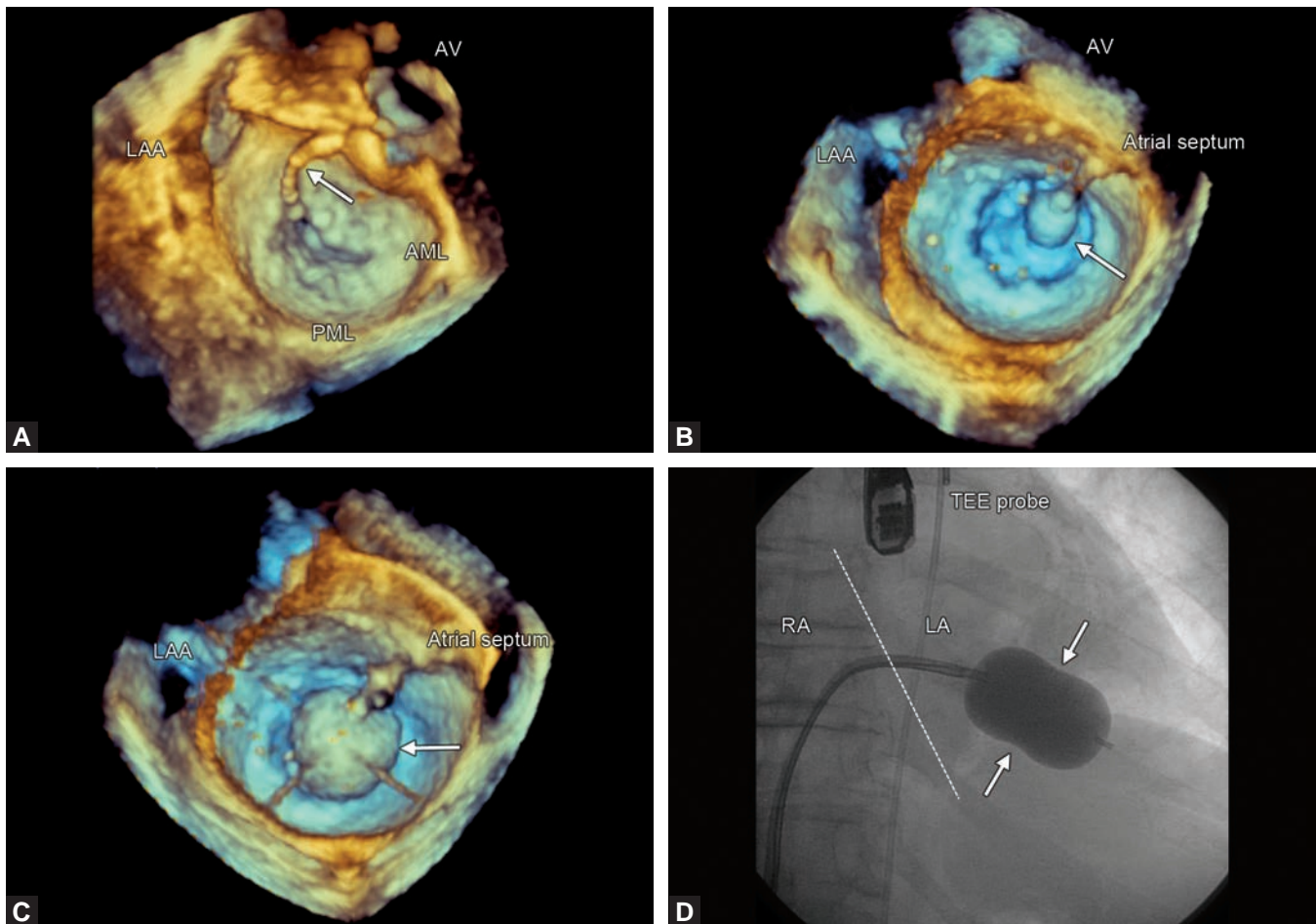
Figs 28.5A to D: Guidance of percutaneous mitral balloon valvuloplasty. Percutaneous mitral balloon valvuloplasty (PMBV) is the preferred method for alleviating mitral stenosis in appropriate patients. 3D TEE in conjunction with fluoroscopy provides excellent PMBV guidance. (A), (B), and (C) demonstrate 3D TEE zoom images of MV from the left atrial perspective; (D) is a fluoroscopy image. (A) Following the trans-septal puncture, 3D TEE is used to guide the deflated Inoue valvuloplasty Inoue balloon into the orifice of the MV. Movie clip 28.5C corresponds to this figure; (B) In the next step, the balloon (arrow) is advanced through the mitral orifice and partly inflated; (C) In the final step, the balloon (arrow) is fully inflated in an attempt to relieve the mitral stenosis. Movie clip 28.5B corresponds to this figure; (D) Fully inflated Inoue balloon seen on a fluoroscopy image in the anteroposterior projection. Arrows point to the balloon's waist which should be in the plane of the mitral orifice. Movie clip 28.5A corresponds to this figure. (AML: Anterior mitral leaflet; AV: Aortic valve; LAA: Left atrial appendage; PML: Posterior mitral leaflet).

Mitral Regurgitation: MV Clipping

Medical management improves symptoms but does not alter the natural progression of mitral regurgitation. Current guidelines recommend surgical correction of moderate-to-severe or severe mitral regurgitation in patients with symptoms and/or evidence of LV dysfunction.[31]

In general, surgical MV repair is preferable over surgical valve replacement for correction of mitral regurgitation with lower hospital mortality, longer survival, better preservation of ventricular function, fewer thromboembolic complications, and reduced risk of endocarditis.[35,36] To date, there are no commercially available techniques of percutaneous valve replacements for native MV disease. In contract, there is a commercially available alternative to surgical MV repair, namely MV clipping to treat selected forms of native MV regurgitation.

The techniques of MV repair have been pioneered in the 1970s by the French surgeon Alain Carpentier.[37] (He also coined the term "bioprosthesis" and was instrumental in developing bioprosthetic valves a few years earlier).[38] Most MV repair techniques rely on leaflet reduction, chordal alteration, and annuloplasty ring insertion. These complete repairs cannot be replicated
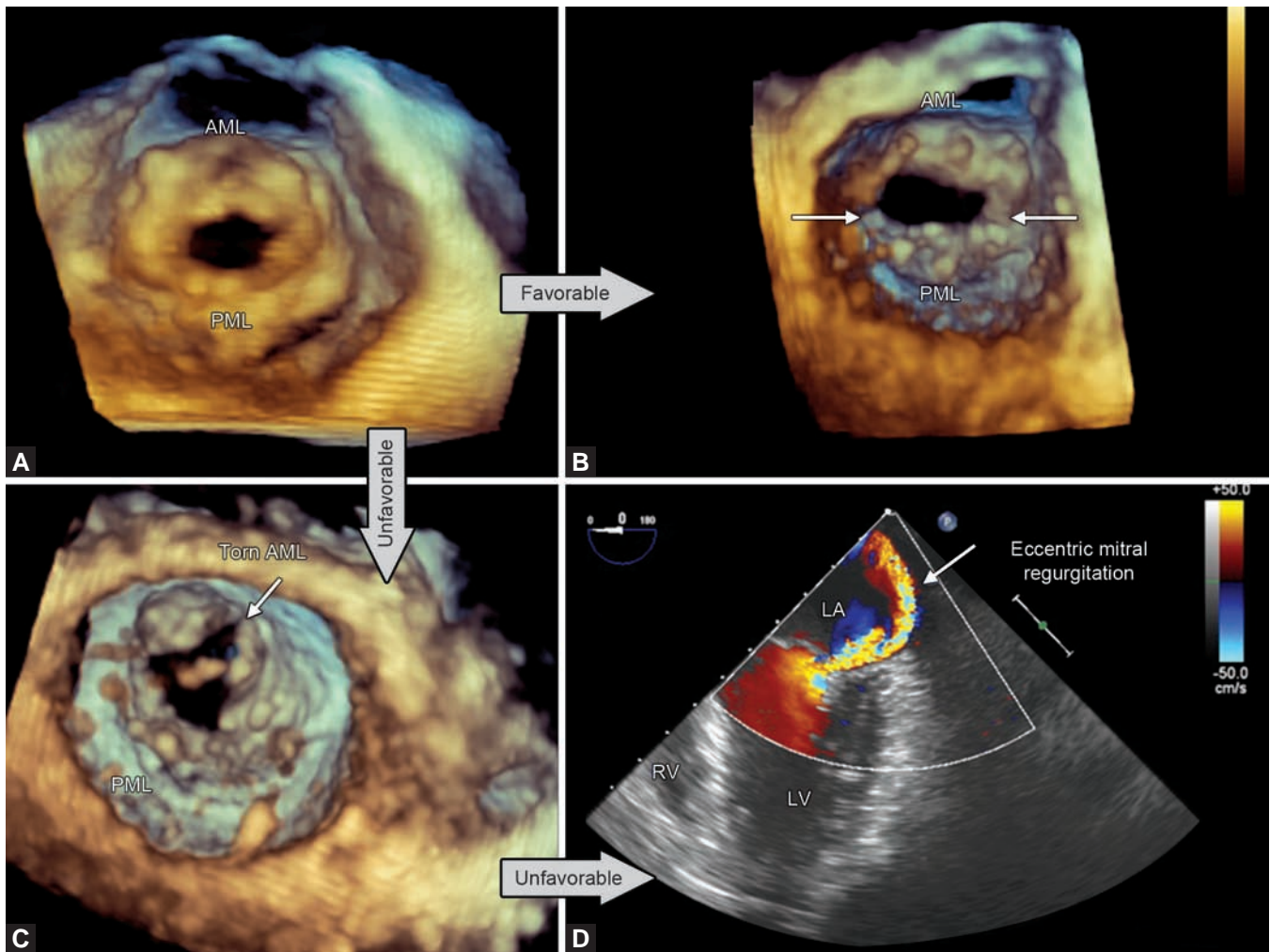
Figs 28.6A to D: Outcomes of percutaneous mitral balloon valvuloplasty. 3D TEE zoom images from patients with rheumatic mitral stenosis demonstrate the left ventricular aspect of the MV. (A) demonstrates severe mitral stenosis before percutaneous mitral balloon valvuloplasty (PMBV); (B) demonstrates the result of a successful PMBV. Note the increase in the MV area due to separation of commissures of the MV (arrows); (C) demonstrates torn AML (arrow), an unfavorable outcome of PMBV which resulted in severe de novo mitral regurgitation seen in figure D. Movie clip 28.6 which corresponds to figure D shows that the jet of mitral regurgitation is eccentric and directed laterally. (AML: Anterior mitral leaflet; LA: Left atrium; LV: Left ventricle; PML: Posterior mitral leaflet RV: Right ventricle).

yet with current commercially available percutaneous techniques although many are in development.[39]

In the 1990s the Italian surgeon Ottavio Alfieri developed a simple technique for surgical correction of MV regurgitation that entails placement of a surgical stitch to approximate the free edges of the leaflets at the site of regurgitant jet origin. Typically, the stitch is placed centrally between A2 and P2 scallops of the MV that results in a double orifice MV. Alfieri called his technique "edge-to-edge repair" but the technique has since become known colloquially as the Alfieri stitch.[40,41]

MV clipping is essentially the percutaneous version of the edge-to-edge surgical repair. MV clipping using the MitraClip® device (Abbott Vascular, Abbott Park, IL) is approved for general use in Europe and is undergoing clinical trials in the United States. In the randomized Endovascular Valve Edge-to-Edge Repair Study (EVEREST II) trial, mitral clipping using the MitralClip® device was associated with superior safety and similar improvements in clinical outcomes but was less effective at reducing mitral regurgitation compared to conventional surgery.[42]

Echocardiography, including 3D TEE, is essential in selecting appropriate patients for MV clipping, guiding of the procedure, and assessing the success of the procedure.

Selection of Patient Eligible for MV Clipping

All eligible patients should have the following:
- Chronic moderate-to-severe or severe mitral regurgitation originating centrally between A2 and P2 scallops of the MV.
- Mitral regurgitation may be functional (due to LV dysfunction) or degenerative (due to prolapsed or flail mitral leaflet) with certain anatomic limitations (for degenerative mitral regurgitation: flail gap < 10 mm; flail width < 15 mm; for functional mitral regurgitation: coaptation depth < 11 mm; coaptation length > 2 mm).[43]
- Either symptomatic with a left ventricular ejection fraction (LVEF) of more than 25% or asymptomatic with at least one of the following: an LVEF of 25–60%, a LV end-systolic diameter of 40–55 mm, new atrial fibrillation, or pulmonary hypertension.

Details of echocardiographic diagnosis of MV prolapse[44] or degenerative mitral regurgitation is discussed elsewhere in this textbook. It suffices to say here that 3D TEE (especially its en face views) allow for detailed evaluation of MV anatomy and precise establishment of the mechanism of mitral regurgitation.

3D TEE Guidance of MV Clipping

The MitraClip device is a 4 mm-wide polyester-covered cobalt–chromium implant with two arms mounted on a sophisticated catheter-based delivery system. After obtaining femoral venous access and using standard transseptal approach over a guide wire and tapered dilator, the clip delivery system is brought into the left atrium through a guide catheter.[45]

Echocardiographic guidance for transseptal puncture is provided in a standard fashion as described earlier in the chapter but with an important modification regarding the location of trans-septal puncture. The site of transseptal puncture is extremely important for the success of MV clipping. In general, a more posterior and superior puncture site is preferred. A distance of at least 4 cm between the site of puncture and the clip landing site on the MV is recommended.[46] In particular, passage across

PFO—the route commonly used in other percutaneous procedures in the left heart—should be always avoided during MV clipping. Passage through a PFO usually results in a position that is too inferior and anterior. Furthermore, tunnel-type PFOs may impede free movement of the clip delivery system.

Following successful transseptal puncture, the clip with its arms closed and attached to the delivery system is brought into the left atrium through the guide catheter. After the clip delivery system emerges into the left atrium through the guide catheter, its tip is then bent toward the MV. The arms of the clip are opened and subsequently oriented perpendicular to the leaflet coaptation line. 3D TEE guidance is absolutely essential in guiding this orthogonal clip orientation (Figs 28.7A to D and Movie clip 28.7).

In the next step, the open clip is advanced below the mitral leaflet tips into the left ventricle. The arms of the clip are then partially closed and the delivery system is pulled back until the mitral leaflets are captured in the arms of the clip. Using 3D TEE and color Doppler, the position and the degree of residual mitral regurgitation are assessed as the arms of the clip are gradually closed to complete the edge-to-edge repair and form a double-orifice MV. Occasionally, placement of a second clip may be necessary to treat residual mitral regurgitation. However, this increases the chance of procedure-related mitral stenosis (Figs 28.8 to D and Movie clip 28.8).

Aortic Stenosis: Transcatheter Aortic Valve Replacement

Calcification of a seemingly normal trileaflet or a congenital bicuspid valve resulting from an atherosclerosis-like process is the most common form of acquire aortic stenosis. Rheumatic aortic stenosis is rare in the United States and other developed countries. It results from commissural fusion and leaflet calcifications, and is invariable associated with concomitant rheumatic MV disease.[47] Once severe aortic stenosis becomes symptomatic, the survival is dismal (only a few years)[48] and not much different from many metastatic cancers.[49]

No medical therapy has ever been shown to alter the natural history of aortic stenosis; aortic valve replacement is the only effective therapy. Surgical aortic valve replacement (SAVR) has been shown to improve symptoms and is generally accepted to prolong survival based on
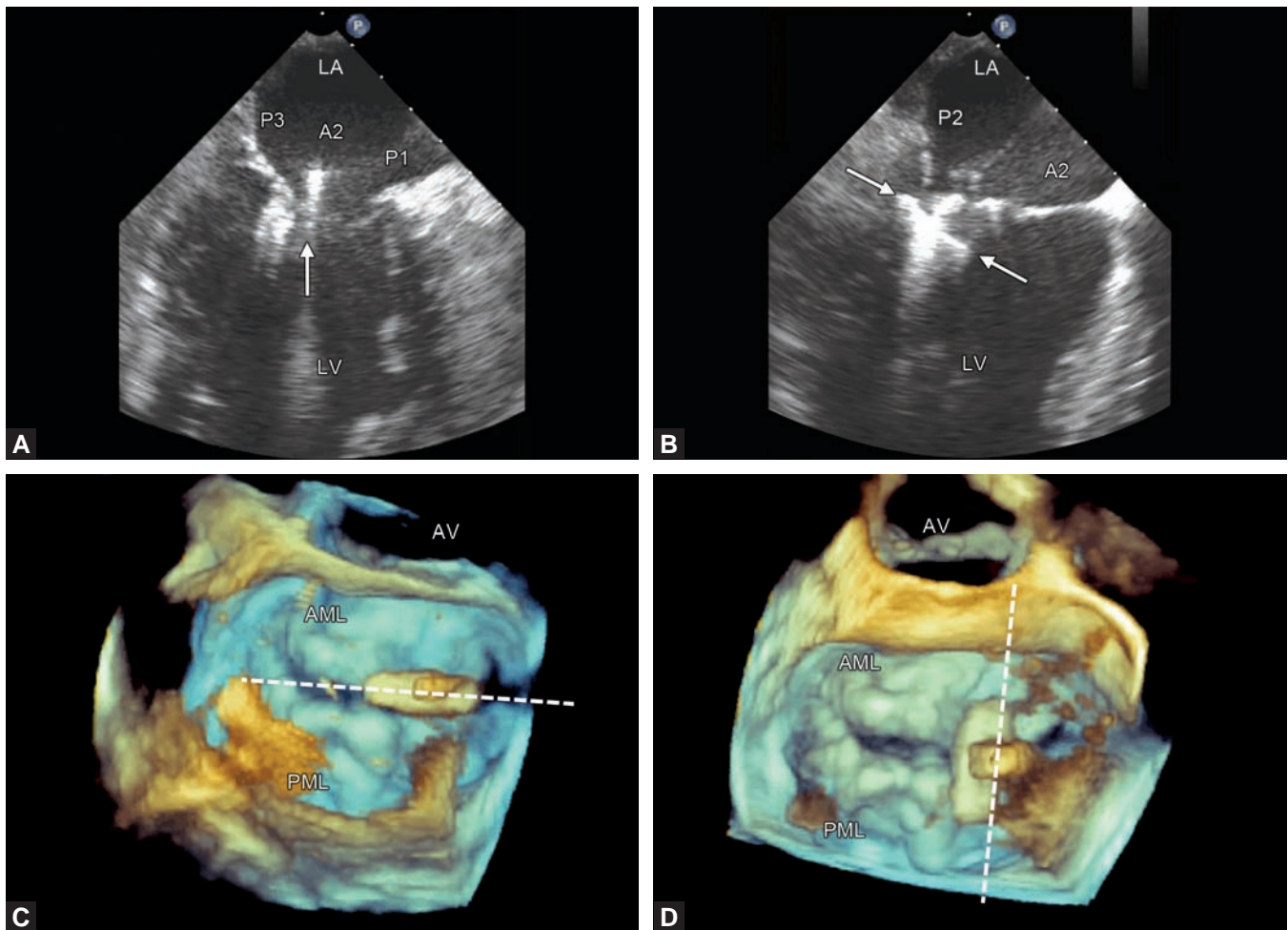
Figs 28.7A to D: Guidance of MV clipping. (A and B) Biplane 3D TEE image demonstrates proper positioning of the mitral clip (arrows) prior to clip closure. The clip should be perpendicular to the MV closure line and placed in the region of A2 and P2 scallops of the MV. Movie clip 28.7. corresponds to this figure; (C and D) 3D TEE zoom image of the MV from the left atrial perspective; (C) demonstrates improper clip positioning (clip is parallel to the mitral coaptation line); (D) demonstrates proper clip positioning (clip is perpendicular to the mitral coaptation line). (AML: Anterior mitral leaflet; AV: Aortic valve; LA: Left atrium; LV: Left ventricle; PML: Posterior mitral leaflet).

historical comparisons and extensive experience over the past 50 years.[50] The first orthotopic SAVR, albeit for aortic insufficiency, was performed in 1960 by the American surgeon Dwight Harken.[51] Currently, about 13,000 SAVR are performed annually in the United States for relief of aortic stenosis.[52]

Historically, two percutaneous alternatives to SAVR have been proposed: aortic balloon valvuloplasty (ABV) and transcatheter aortic valve replacement (TAVR) also referred to at transcatheter aortic valve implantation (TAVI). BAV was first performed in 1986 by Alain Cribier in France.[53] In contrast to PMBV (which is the treatment of choice for relief of mitral stenosis with good long-term outcomes), percutaneous ABV is used primarily as a

bridge to aortic valve replacement; used alone ABV has high restenosis and complication rates.[54]

The first TAVR in a human was performed in 2002 by Alain Cribier in France[55] using a balloon expandable valve similar in design to the one tested in animals by Danish inventors a decade earlier.[56] TAVR is the only intervention for aortic stenosis shown to prolong survival in a randomized trial.[57] It is currently indicted for patients with severe aortic stenosis who are at high risk or unsuitable for SAVR.

Currently, there are two TAVR valves with or near market approval in various parts of the world: (1) balloon expandable Sapien® valve (Edwards Lifesciences Inc., Irvine, CA); and (2) self-expandable CoreValve® (Medtronic
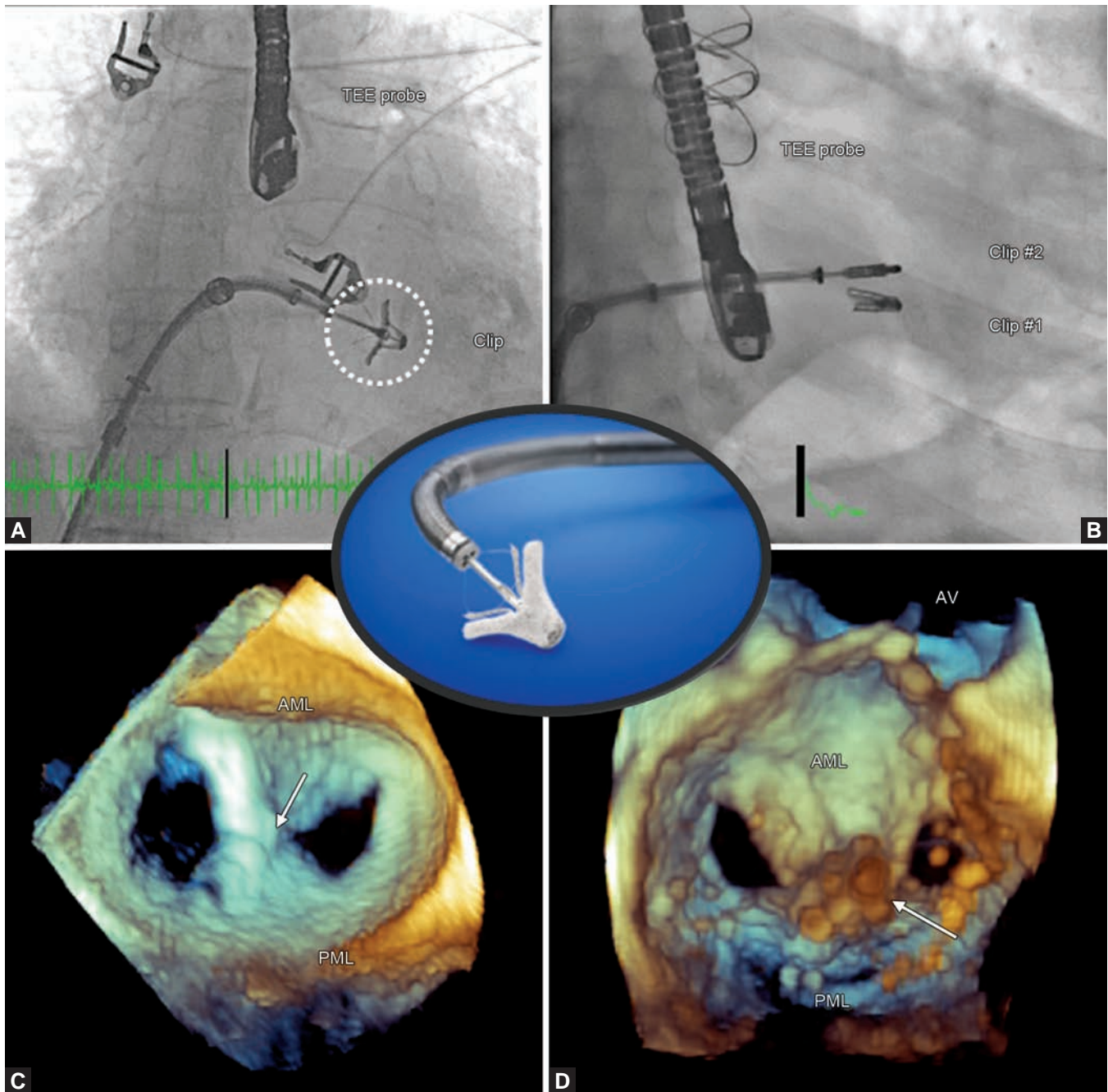
Figs 28.8A to D: Delivery of mitral clip. (A and B) Fluoroscopy images of mitral clips. In (A), the mitral clip is still attached to its delivery catheter and is being opened in preparation for grasping of mitral leaflets; In (B) obtained from a different patient, one mitral clip is already deployed (Clip #1), the other is being deployed (Clip #2). (C and D) 3D TEE zoom images of the MV during diastole with one clip (arrows) fully deployed; (C) demonstrates the left atrial aspect and (D) demonstrates the left ventricular aspect of the MV. Note that clip deployment creates a double-orifice MV. Movie clip 28.8 corresponds to (C). (AML: Anterior mitral leaflet; AV: Aortic valve; PML: Posterior mitral leaflet).

Inc., Minneapolis, MN). Echocardiographers should be familiar with the basic design and mode of delivery of these two valves. Both are bioprosthetic pericardial valves suspended on a metal frame (Figs 28.9A and B).

Sapien® valve is currently made of bovine pericardium suspended on a chrome–cobalt alloy frame. A collapsed Sapien® valve is mounted on a deflated balloon in a similar fashion used for coronary stents. Upon delivery,
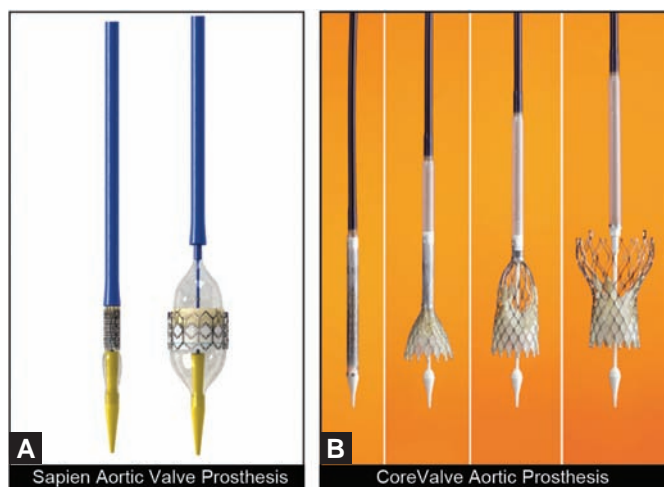
Figs 28.9A and B: Transcatheter aortic valve prostheses. (A) Sapien™ aortic valve is a balloon expandable prosthesis placed across the aortic annulus; (B) CoreValve™ is a self-expanding aortic valve prosthesis. A deployed CoreValve™ prosthesis extends from the LVOT to the ascending aorta.
Source: (A) Image is courtesy of Edwards Lifesciences, Irvine, CA.
Source: (B) Image is courtesy of Medtronic Inc., Minneapolis, MN.

the Sapien® valve is balloon expanded across the stenosed native aortic valve. In contrast, CoreValve® is made of porcine pericardium suspended on a nitinol alloy frame. Prior to CoreValve® implantation, balloon valvuloplasty of the native aortic valve is performed. Subsequently, a collapsed CoreValve® is brought into the ascending aorta that then self-expends across the stenosed native valve after it emerges from the delivery sheath. Both valves can be implanted using various arterial access points: the femoral artery, LV apex, or ascending aorta.[58]

The role of echocardiography including 3D TEE is twofold: to identify appropriate patients and to provide intraprocedural monitoring.

Selection of Patient Eligible for TAVR

Echocardiography is essential in establishing the presence of the only currently approved indication for TAVR: severe acquired calcific stenosis of a trileaflet valve (senile calcific aortic stenosis). TAVR is currently not indicated for aortic stenosis of a bicuspid aortic valve although, as mentioned earlier, the very first TAVR performed by Alain Cribier was in a patient with severe bicuspid aortic valve stenosis.[53]

Can 3DE improve on standard techniques of assessing aortic stenosis severity discussed elsewhere in this chapter? Using the multiplane reconstruction techniques,

3D TEE can provide accurate measurements of the left ventricular outflow tract (LVOT), aortic annulus and the aortic annulus-to-left coronary artery ostium distance.

Calculation of the aortic valve area (AVA) by continuity equation is the principal echocardiographic method of assessing anatomic severity of aortic stenosis. The major source of error in AVA calculation by continuity equation is miscalculation of the cross sectional area of the LVOT due to mismeasurement of the LVOT diameter and/or faulty geometric assumption of a circular LVOT shape.[59] Using multiplane reconstruction techniques of either CT or 3DE (Figs 28.10A to D) one can demonstrate that LVOT is typically ovoid rather than circular in shape.[60,61] In addition, it can also be demonstrated that the LVOT "diameter" measured by 2DE is often a geometric chord rather than a true diameter. Since a chord (a line connecting two points on the circumference that does not cross the center) is by definition shorter than a diameter, 2DE will often underestimated the size of LVOT area and thus overestimate the severity of aortic stenosis.

The size of the aortic annulus is another measurement that is important for TAVR as the size of the replacement valve is based on the patient's annular size. 2DE systematically underestimates the annular size compared to CT or MRI.[62] In contrast, 3D TEE sizing of the annular size (Figs 28.11A to D) are superior to 2D TEE and may be used when good CT data are unavailable for TAVR sizing.[63]

Prior to Sapien® valve placement, the annular to left coronary artery ostium height is important as well in selecting appropriate replacement valve size. Echocardiographically, this height cannot be measured by 2D TEE; however, such a measurement is possible with multiplane reconstruction techniques of 3D TEE (Figs 28.12A to D).[64]

Theoretically, AVA can also be measured by 3D planimetry. However, aortic valve calcifications create image dropout making this measurement imprecise.

TAVR: Intra- and Postprocedural Monitoring by 2D/3D TEE

Both 2D and 3D TEE are used during TAVR to help guide the valve insertion, monitor for intraprocedural complications, and assess postimplantation success.

In contrast to MV procedures where 3D TEE plays the principal role in guidance, TAVR placement is performed primarily under fluoroscopic and CT guidance. Nonetheless, 2D and 3D TEE is used to provide important
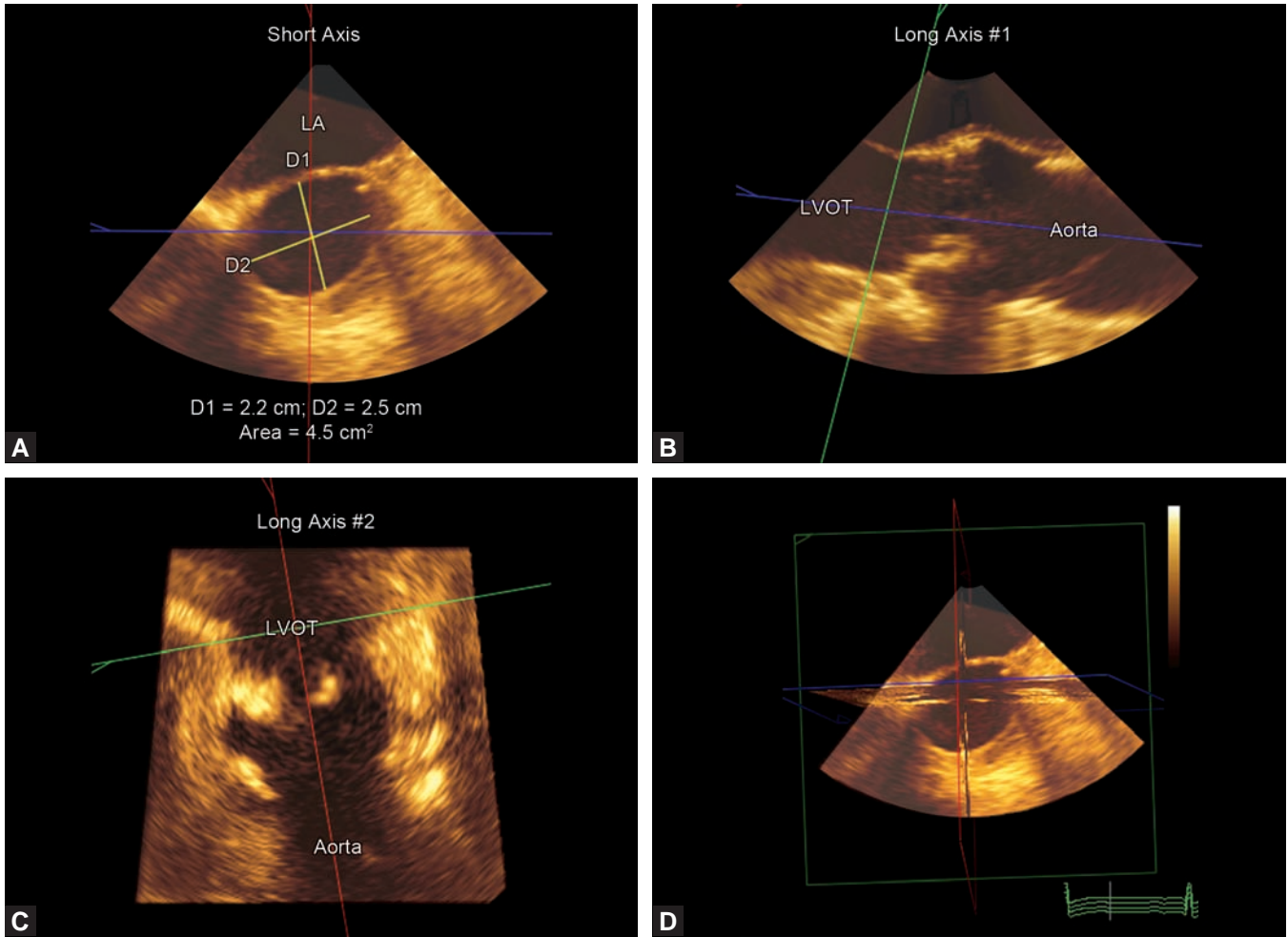
Figs 28.10A to D: 3D TEE assessment of the LVOT. Multiplane reconstruction 3D TEE imaging of the LVOT in a patient prior to CoreValve placement demonstrates an ovoid-shaped LVOT measuring 2.2 × 2.5 cm in diameters and having an area of 4.5 cm². (LA: Left atrium; LVOT: Left ventricular outflow tract).
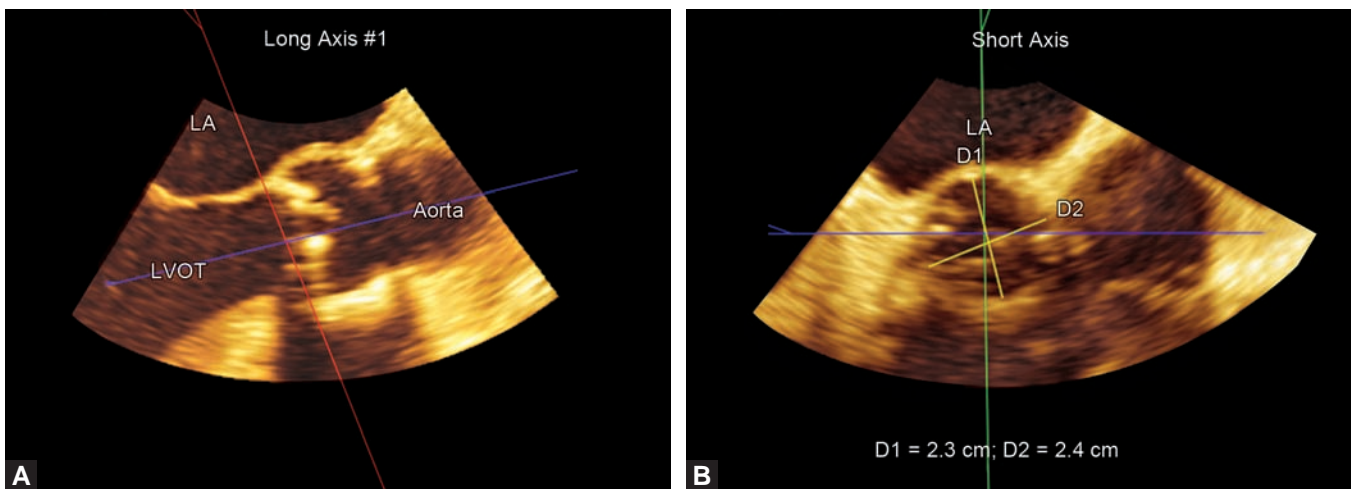

Figs 28.11A and B
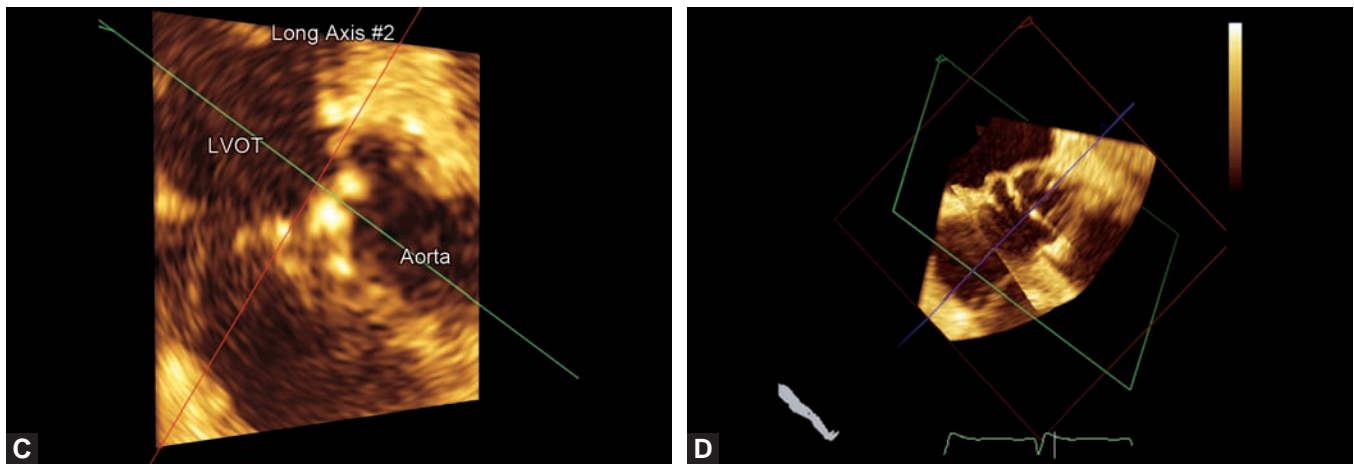
Figs 28.11A to D: 3D TEE assessment of the aortic annulus. Multiplane reconstruction 3D TEE imaging of the aortic annulus in a patient prior to CoreValve placement demonstrates a near-circular aortic annulus measuring 2.3 × 2.4 cm in diameters. (LA: Left atrium; LVOT: Left ventricular outflow tract).
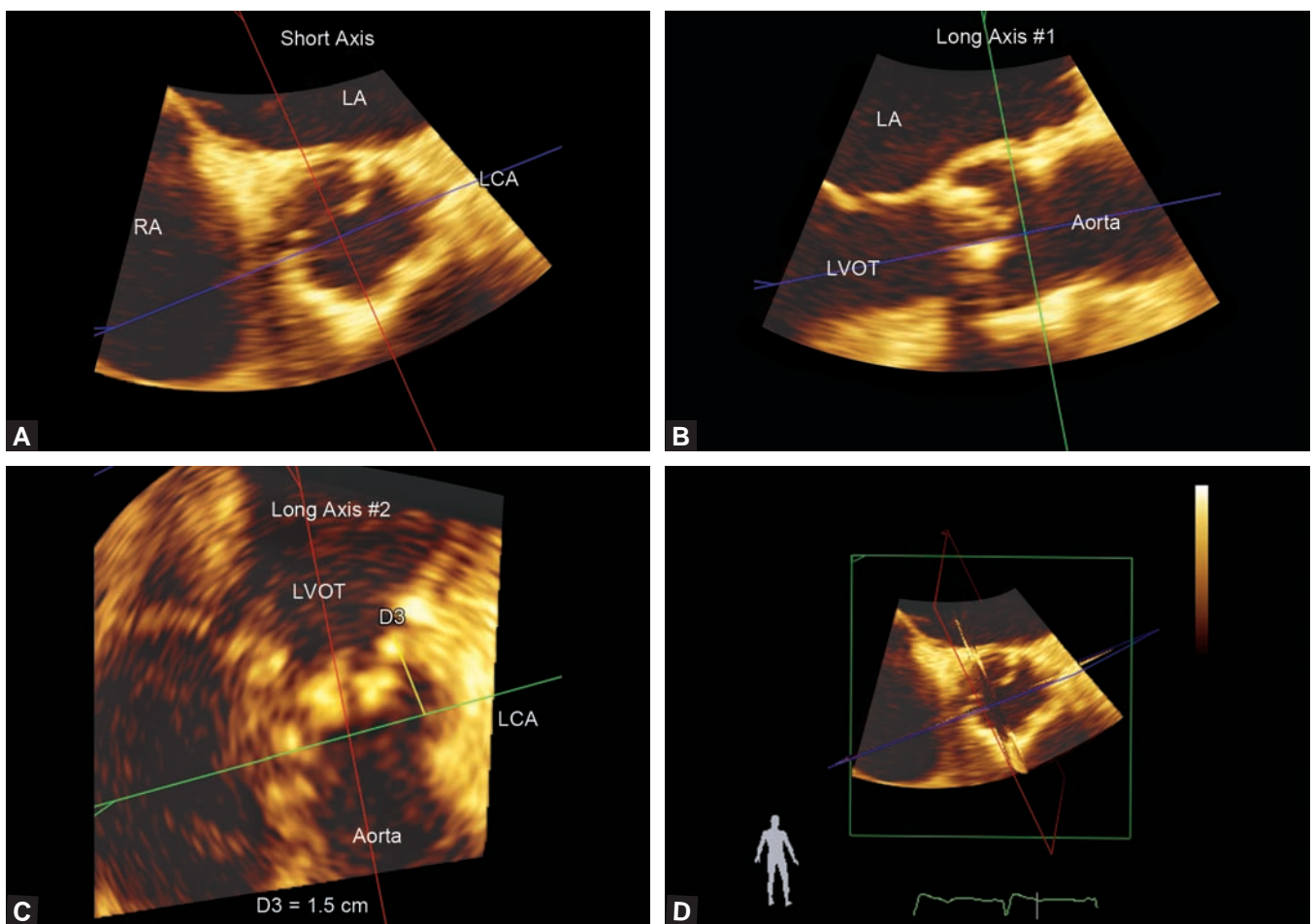
Figs 28.12A to D: 3D TEE assessment of the annulo-ostial distance. Multiplane reconstruction 3D TEE imaging of the aortic annulus in a patient prior to Sapien valve placement demonstrates how to measure the distance between the aortic annulus and the left main coronary artery (annulo-ostial distance). Note that the ostium of the left main coronary artery is first localized in the short axis and the distance is then measured in the corresponding long-axis (in this case, Long Axis #2). (LA: Left atrium; LCA: Left main coronary artery; LVOT: Left ventricular outflow tract; RA: Right atrium).
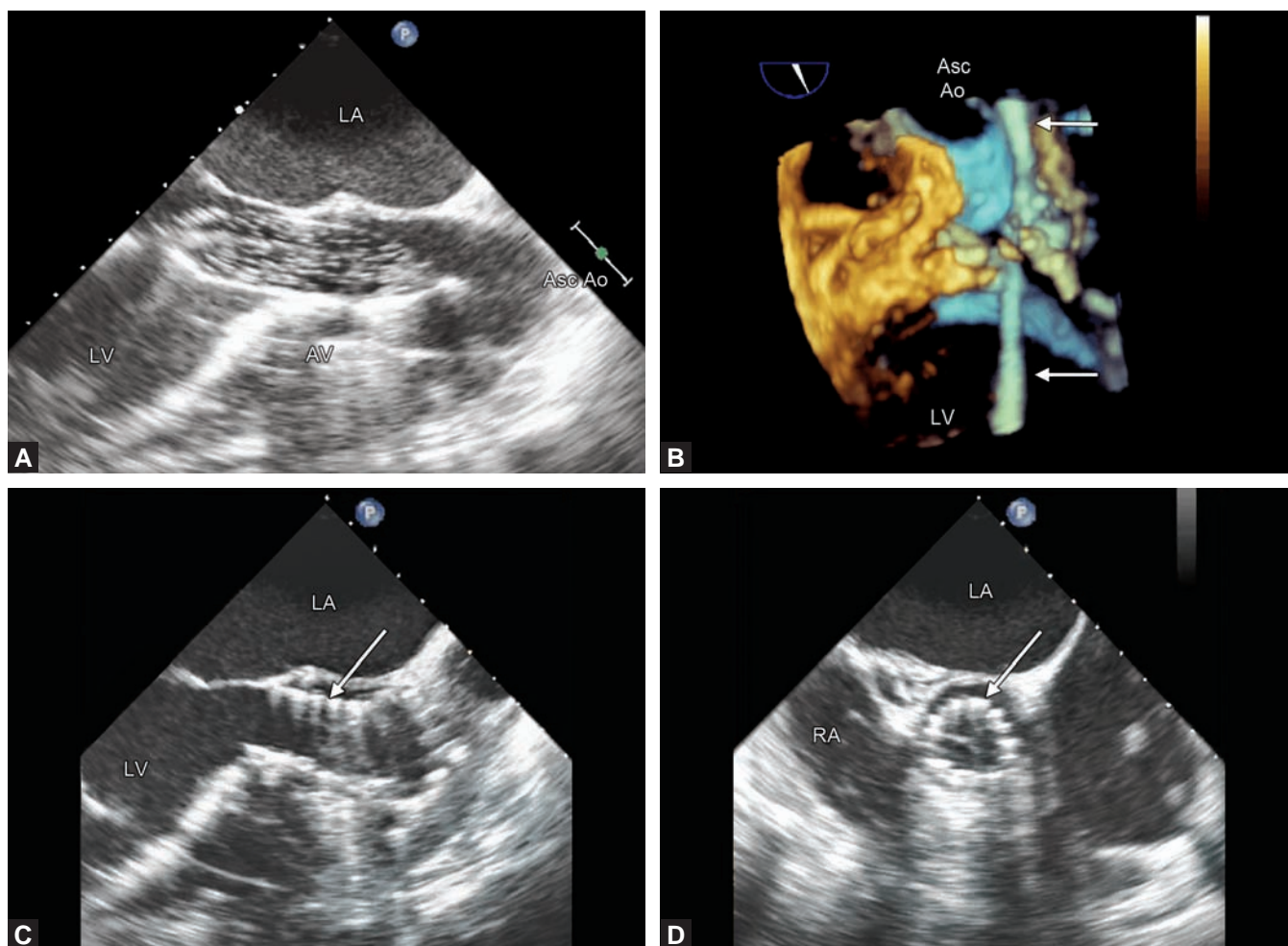
Figs 28.13A to D: TEE guidance of transcutaneous aortic valve replacement. (A) Prior to percutaneous aortic valve replacement, balloon valvuloplasty (arrow) of the native aortic valve is performed; (B) 3D TEE zoom image demonstrates a catheter (arrow) crossing the native aortic valve in preparation for percutaneous aortic valve replacement; (C and D) 3D TEE biplane image of the newly placed CoreValve (arrows) during diastole. In the right portion of this figure, one can seen closed prosthetic leaflets in the short-axis of the valve. (Asc Ao: Ascending aorta; LA: Left atrium; LV: Left ventricle; RA: Right atrium).

real time information regarding aortic valve anatomy and function, and to observe for complications such as pericardial effusion or ventricular dysfunction. Moreover, guide wires, catheters, valvuloplasty balloons and the replacement valve (Figs 28.13A to D) can continuously be observed by echocardiography; in this respect 3D TEE is often superior to 2D TEE.

Immediately post TAVR, Doppler echocardiography plays crucial role is assessing the success of the procedure. Color Doppler is used to assess for paravalvular regurgitation (Figs 28.14A to D), which may be present in at least 10% of TAVR patients and which portends poorer prognosis.[65] Spectral Doppler reordered from transgastric windows in used to assess the gradients across the newly implanted TAVR (Figs 28.15A to C).

Closure of Paravalvular Prosthetic Leaks

The reported prevalence of clinically important paravalvular leaks (PVL) due to valve dehiscence ranges between 3% and 12.5% of all surgically implanted prosthetic valves.[66] In the early postsurgical period, prosthetic valve dehiscence is typically due to procedural mishaps (e.g. a loose suture in a patient with calcified native annulus).
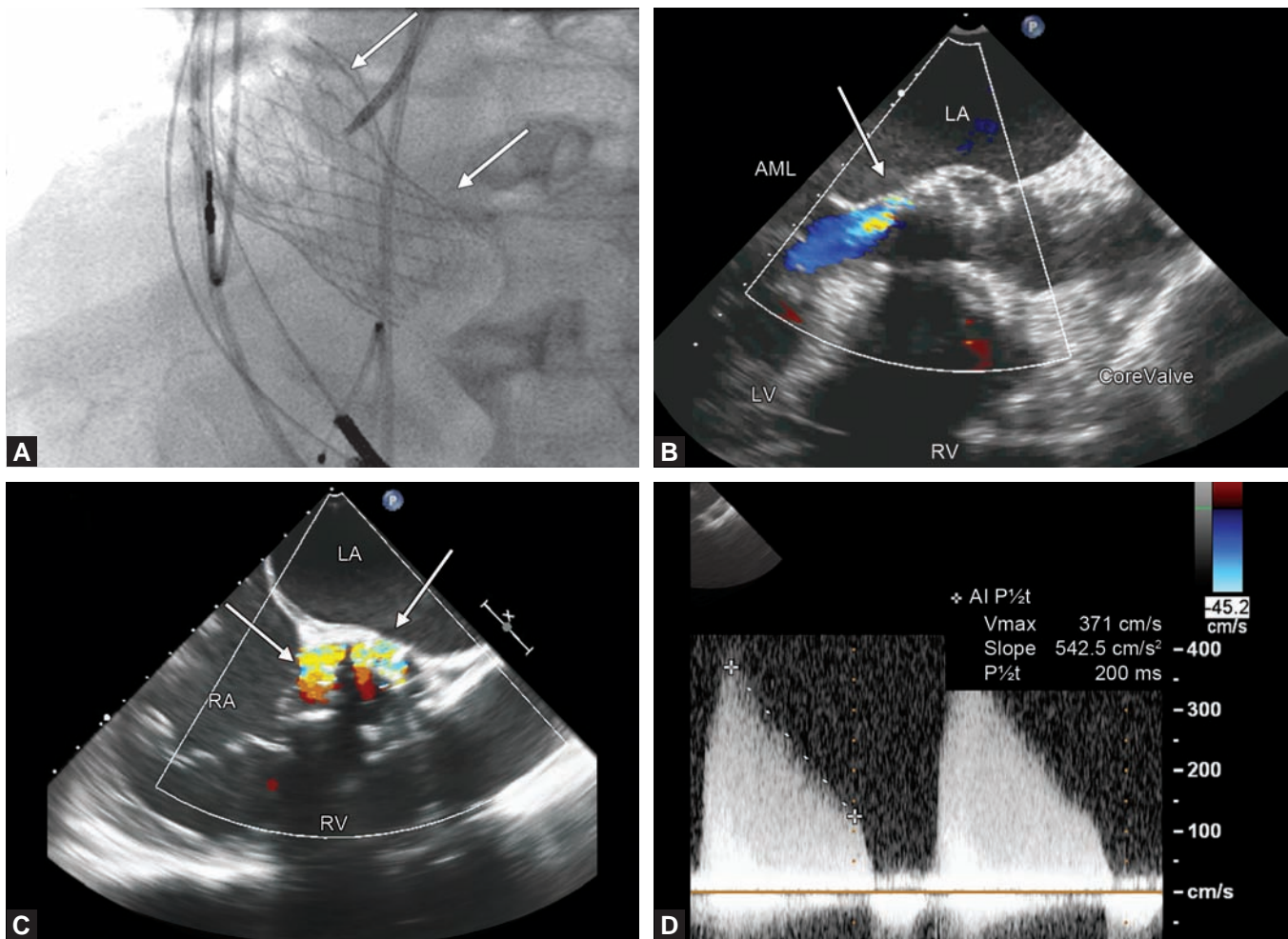
Figs 28.14A to D: Assessment of paravalvular aortic regurgitation post-transcutaneous aortic valve replacement. (A) Implanted CoreValve (arrows) seen on fluoroscopy; (B) Mild paravalvular regurgitation (arrow) in a patient with CoreValve. Frequently the paravalvular leak is located adjacent to the AML; (C) Severe paravalvular regurgitation (arrows) in another patient with CoreValve. Note the large amount of color flow along the entire posterior aspect of the prosthetic valve. After placement of another CoreValve using the valve-in-valve technique, the severe aortic regurgitation disappeared; (D) Spectral Doppler of severe paravalvular regurgitation seen in (C). Note the rapid deceleration slope of the aortic regurgitant jet (pressure half-time of 200 ms). (AML: Anterior mitral leaflet. LA: Left atrium; LV: Left ventricle; RA: Right atrium; RV: Right ventricle).

Late-onset prosthetic dehiscence is usually due to infective endocarditis. Irrespective of its cause, prosthetic valve dehiscence leads to paravalvular regurgitation and hemolytic anemia. The magnitude of hemolytic anemia does not necessarily correlates with the severity of paravalvular regurgitation.[67]

Heart failure and transfusion-dependent anemia are major indications for PVL closure. Until recently, redo open heart surgery was the only means of closing clinically significant PVLs. However, reoperation is associated with high morbidity and mortality, with reported in-hospital mortality rates of 13%, 15%, and 37% for the first, second, and third reoperations, respectively.[68]

It appears that in 1987 the first percutaneous PVL closure was performed.[69] Percutaneous closure of PVLs is emerging as an alternative to redo surgery.[70] Most initial experience has been with closure of mitral PVLs[71] but techniques are being developed for PVLs of prosthetic aortic valves as well.[72] Percutaneous closure is becoming the treatment of choice for most clinically significant PVLs; surgery is still reserved for very large PVLs (involving more than 25% of the prosthetic ring circumference) or PVLs related to active endocarditis.[73] At present, there are no closure devices that are specifically designed for PVL closure; instead either vascular plugs or occluders designed for ASD, VSD, or PDA closure are used off label.
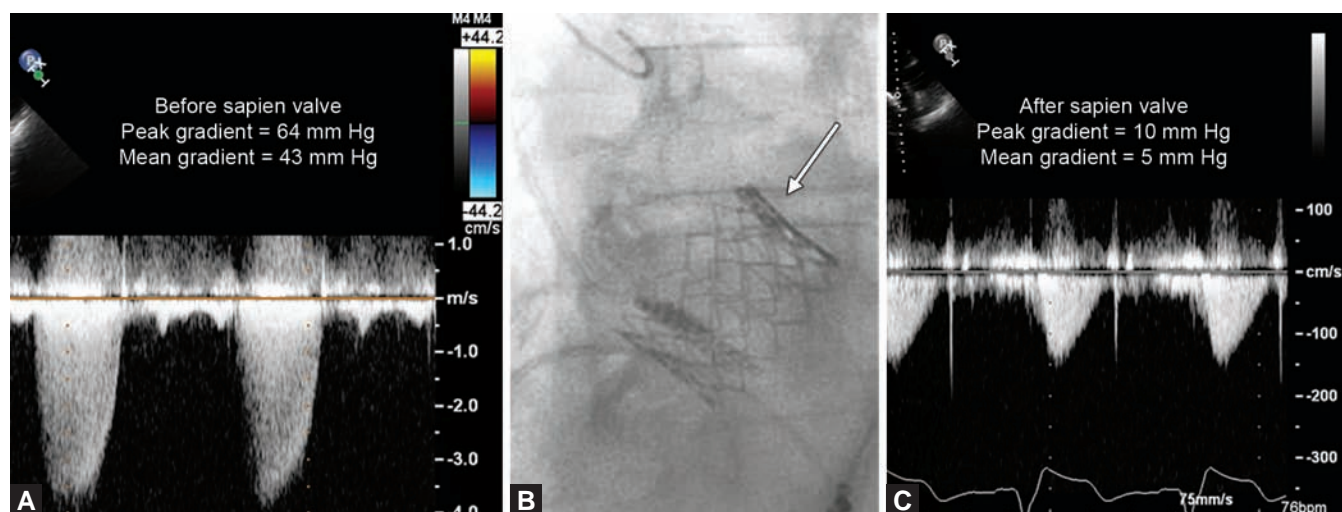
Figs 28.15A to C: Assessment of aortic valve gradients before and after transcutaneous aortic valve replacement. Aortic valve gradients before (A) and after (C) percutaneous implantation of the Sapien aortic valve; the valve is seen on fluoroscopy in (B).

Depending of PVL size, one or more devices may be needed to successfully close the leak.[74]

Improvements in 3D TEE imaging are the major driving force behind the development of percutaneous PLV closures. 3D TEE is important both for establishing the precise diagnosis of PVL and for monitoring of percutaneous closure.

3D TEE Diagnosis of PVL

The diagnosis of a PVL can be established by 2DE. However, 3D TEE provides incremental information regarding the exact location, size, and shape of a PVL (Figs 28.16A and B). This information is crucial for the success of PVL closure procedure. With its ability to provide en face views of the entire MV, 3D TEE demonstrates PVLs in an intuitive and accurate. It is essential to use color Doppler to confirm the location of PVLs and to avoid mischaracterization of periprosthetic image dropouts as PVLs. In summary, 3D TEE can accurate identify patients with suitable anatomy for percutaneous PVL closure.

3D TEE Monitoring of Percutaneous PVL Closure

For percutaneous closure of mitral PVLs, standard transs-eptal approach is used. 3D TEE is instrumental in guiding transseptal puncture as discussed earlier in this chapter. Occasionally, transaortic or transapical approach may be used. Irrespective of the approach used, 3D TEE is used

intraprocedurally to guide placement of wires, catheters, and closure devices (Fig. 28.17). Without 3D TEE guidance many PVL closure procedures would be either impossible to perform using fluoroscopy alone or would expose the patient significant radiation. Postprocedurally, 2DE and 3DE is used to assess for residual regurgitation and to evaluate for possible prosthetic valve malfunction due to closure device impingement. In general, closure of mitral PVL located laterally (Figs 28.17A to D) is technically easier than the closure of those located medially (Figs 28.18A to C).

DEVICE CLOSURE OF CARDIAC SHUNTS

Surgical closure of cardiac shunt predates many other forms of cardiac surgery and was practiced well before the advent of cardiopulmonary bypass in the 1960s. Percutaneous closure has become the treatment of choice for many cardiac shunts including PDA, secundum ASDs, and muscular VSDs with surgery typically being reserved for complex cases.

Closure of PDAs

Ductus arteriosus is an arterial communication between the left pulmonary artery and the proximal descending thoracic aorta that develops embryologically from the left sixth aortic arch. Ductus arteriosus is an essential component of the normal fetal circulation; it directs
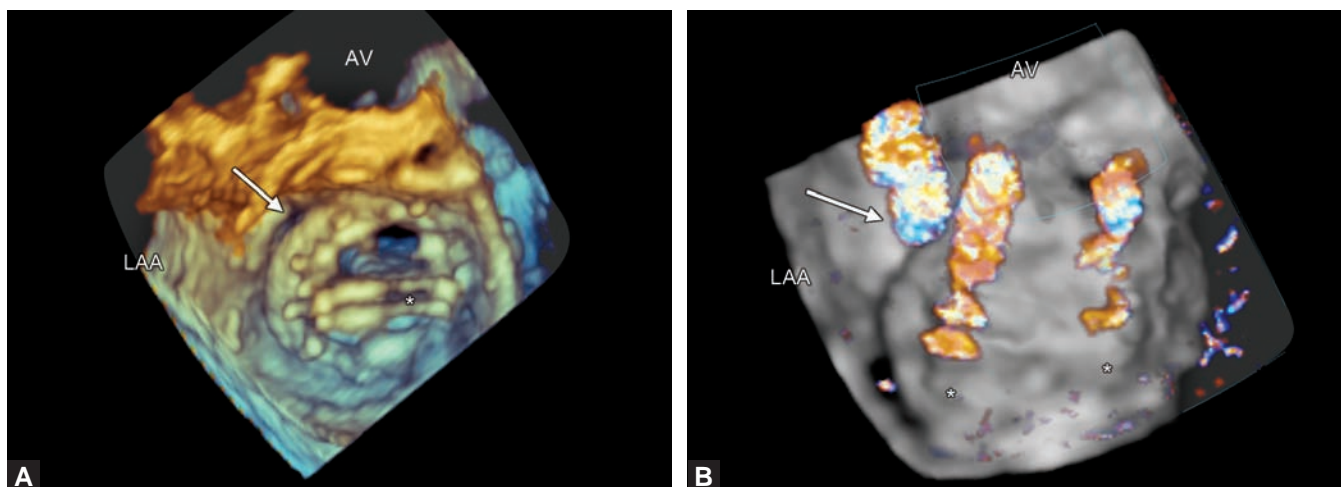
Figs 28.16A and B: 3D TEE diagnosis of paravalvular mitral regurgitation. (A) 3D TEE en face zoom view of the St Jude mechanical mitral prosthesis; prosthetic leaflets in the open position during ventricular diastole (asterisk) are seen. Arrow points to the location of the paravalvular leak between the aortic valve and the LAA; (B) 3D TEE color Doppler of the St Jude mechanical prosthesis visualized in the same orientation as in figure A. Note the location, size and the shape of the paravalvular leak (arrow). Also note the physiologic ('washing') jets inside the prosthetic valve (asterisks). (AV: Aortic valve; LAA: Left atrial appendage).

the blood away from the very high-resistance fetal pulmonic circulation of the collapsed lungs to the lower resistance systemic circulation (physiologic right-to-left shunt). During fetal life, ductus arteriosus is kept open by vasodilators such as prostaglandin PGE2, which is believed to be produced both locally in the ductus and by the placenta.

Soon after delivery, pulmonary vascular resistance drops below the systemic vascular resistance leading to shunt reversal; this left-to-right shunt is transient in most infants. The high oxygen content of ductal blood activates an oxygen-sensitive potassium channel that leads to contraction of the ductal muscular layers and cessation of ductal flow. In the majority of infants scarring completely obliterates ductus arteriosus by the end of the neonatal period.[75]

PDA results from the failure of physiologic closure of ductus arteriosus past the first year of life. It can be isolated or may be associated with a variety of other forms of congenital heart disease. Typically, PDAs presents with a left-to-right shunt; however, shunt reversal can occur if pulmonary vascular resistance rises above the systemic vascular resistance.

PDA is the first congenital heart defect to be closed successfully by surgery and was the first congenital heart defect to be closed percutaneously. The first successful ligation of a PDA was performed in 1938 by Robert E Gross, then the chief surgical resident, and John P Hubbard

at Boston Children's Hospital.[76] The first successful percutaneous closure of a PDA was reported by Werner Portsmann and colleagues working at Charité Hospital located in what was then East Germany.[77]

*Percutaneously or surgically closure of a PDA is indicated for the following*:[78]
- Left atrial and/or LV enlargement or if pulmonary arterial hypertension is present, or in the presence of net left-to-right shunt
- Prior endarteritis
- It is reasonable to close an asymptomatic small PDA by catheter device.

Surgical repair by a surgeon experienced in congenital heart disease is recommended when:
- PDA is too large for device closure
- Distorted ductal anatomy precludes device closure.

PDA closure is contraindicated in patients with pulmonary arterial hypertension and net right-to-left shunt.

General aspects of PDA diagnosis are discussed elsewhere in this textbook. From the percutaneous or surgical point of view, the role of imaging is to establish the general anatomy of a PDA. Typically, PDAs have a conical shape with the wider opening at the aortic side and the smaller one at the pulmonary artery side. However, a variety of shapes have been described.[79] There are limited data on the use of 3DE in the diagnosis of PDA[80] and for guidance of PDA closure (Figs 28.19A to D).[81,82] In general,
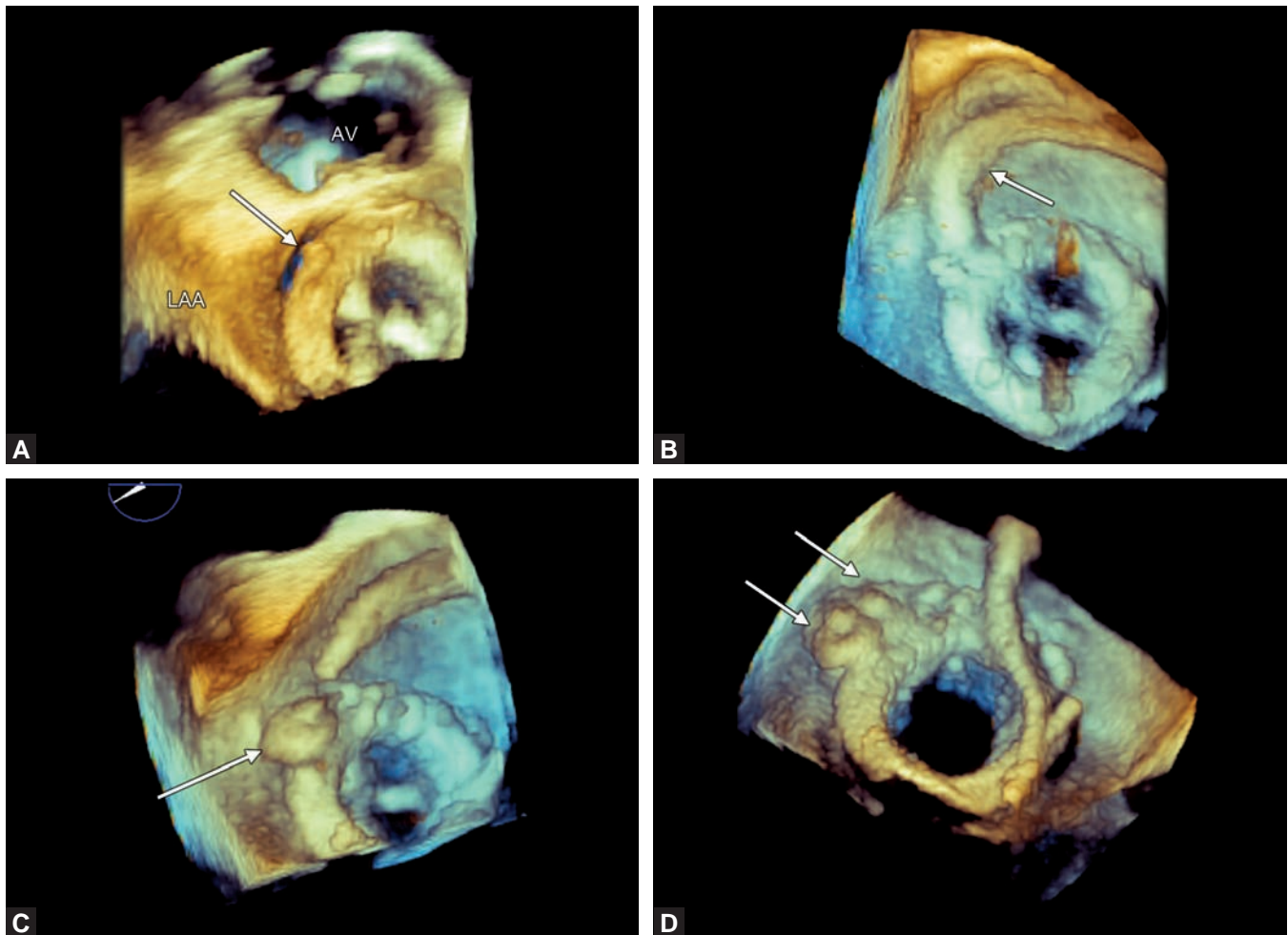
Figs 28.17A to D: 3D TEE guidance of a lateral mitral paravalvular leak closure. 3D TEE en face zoom view of the mitral bioprosthetic valve is seen from the same perspective in all four figures. (A) Arrow points to the location of the lateral paravalvular leak at approximately 10 o'clock (arrow) on the standard surgical view of the MV located between the LAA and the native aortic valve (AV); (B) 3D TEE imaging is used to guide the transseptal catheter (arrow) to the paravalvular leak; (C) A vascular plug (arrow) is placed in the paravalvular leak; (D) Because leak closure was incomplete after first plug placement, another plug is delivered adjacent to the first plug. The two plugs (arrows) were able to close the leak successfully.

TEE allows for continuous monitoring of PDA flow during percutaneous closure; this minimizes X-ray exposure of concomitant fluoroscopy (Figs 28.20A and B).[83]

Closure of ASDs

There are at least four different types of ASDs in the descending order of prevalence: secundum ASD, primum ASD, sinus venosus ASD (which may be of the superior or inferior vena cava type), and unroofed coronary sinus. Following bicuspid aortic valve, ASD is the most common congenital anomaly in adults occurring in approximately 1 out of 1,000 individuals.[84]

Successful surgical closure of ASDs predates the advent of cardiopulmonary bypass. In 1952, closure of an ASD in a 5-year-old girl by F John Lewis was the first successful open heart operation (performed under general hypothermia and inflow occlusion) at the University of Minnesota.[85] In 1953, ASD closure by John Gibbon in Philadelphia was the very first successful cardiac surgery using cardiopulmonary bypass.[86] The first percutaneous closure of an ASD was performed in 1975 by King and Mills at Ochsner Medical Center in New Orleans, LA.[87] At present, closure of secundum ASDs is the only approved indication for current percutaneous closure devices.

Major indications for surgical or percutaneous ASD closure are as follows:[78]

- Right atrial and right ventricular enlargement with or without symptoms
- Closure of an ASD is reasonable in the presence of paradoxical embolism or orthodeoxia-platypnea.

Closure of an ASD is contraindicated in patients with severe irreversible pulmonary hypertension and no evidence of a left-to-right shunt.

3D TEE is instrumental in both the diagnosis of an ASD and guidance of percutaneous ASD closure.

3D TEE Diagnosis of ASDs

Appropriate patient selection is of utmost importance for the success of percutaneous ASD closure.[88] One should first establish the diagnosis of a secundum ASD, the only ASD type amenable to percutaneous closure at present.[89] After obtaining 3D TEE images of the interatrial septum, we use the so-called TUPLE (tilt up then left) maneuver to obtain en face images of the interatrial septum in anatomically correct orientations (Figs 28.21A to C and Movie clip 28.21A and Movie clip 28.21B). Briefly, the TUPLE maneuver is a
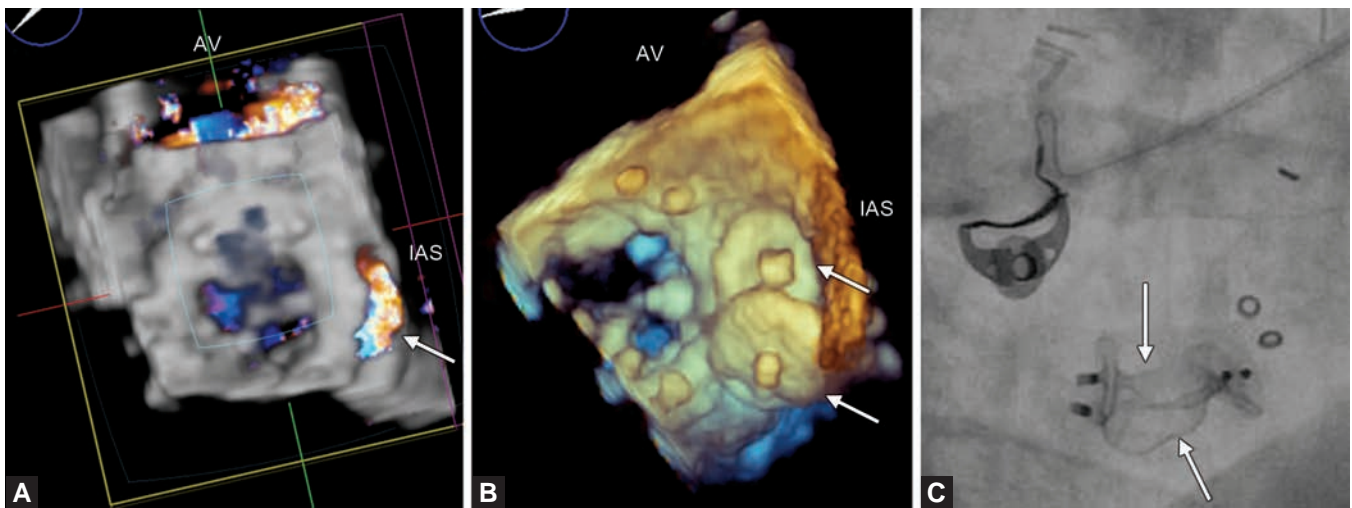

Figs 28.18A to C: 3D TEE guidance of a medial mitral paravalvular leak closure. (A) 3D TEE color Doppler en face zoom view of the mitral bioprosthetic valve demonstrates a medial paravalvular leak at approximately 3 o'clock (arrow) on the standard surgical view of the MV. The leak is located adjacent to the interatrial septum (IAS) and away from the aortic valve (AV); (B) 3D TEE en face zoom view of the mitral bioprosthesis demonstrates two vascular plugs (arrows) used to close the medial paravalvular leak successfully; (C) The appearance of the two vascular plugs on fluoroscopic image in the cranially angulated right anterior oblique projection.
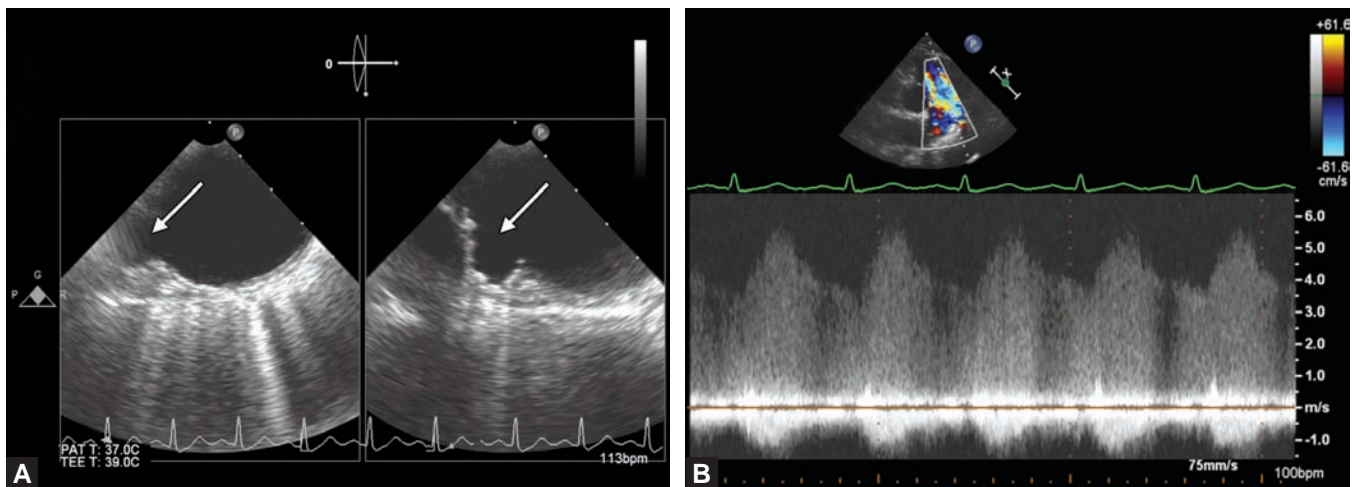
Figs 28.19A and B
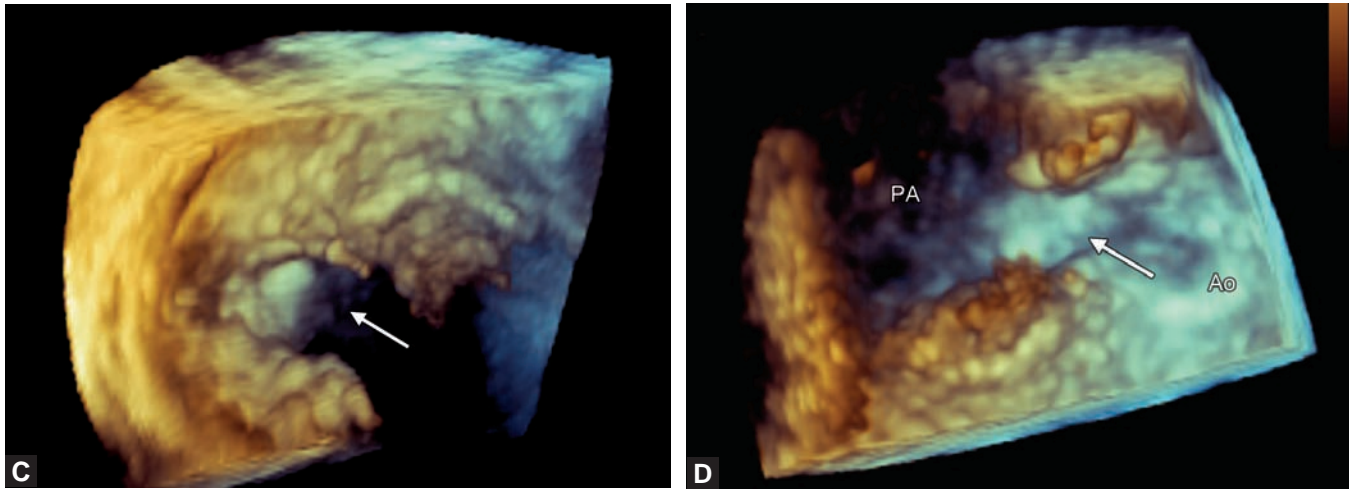
Figs 28.19A to D: 2D/3D TEE diagnosis of PDA. (A) 3D TEE biplane image demonstrating the aortic side (arrows) of a PDA; (B) Spectral Doppler tracings demonstrate flow velocity pattern typical of a PDA with a left-to-right shunt and normal pulmonary artery pressures. There is high pressure gradient between the aorta and the pulmonary artery throughout the cardiac cycles (higher in systole than in diastole); (C) 3D TEE en face zoom view of the aortic orifice of the PDA (arrow); (D) 3D TEE zoom view demonstrates the PDA in its long axis. The PDA appears as a tube between the aorta (Ao) and the pulmonary artery (PA).
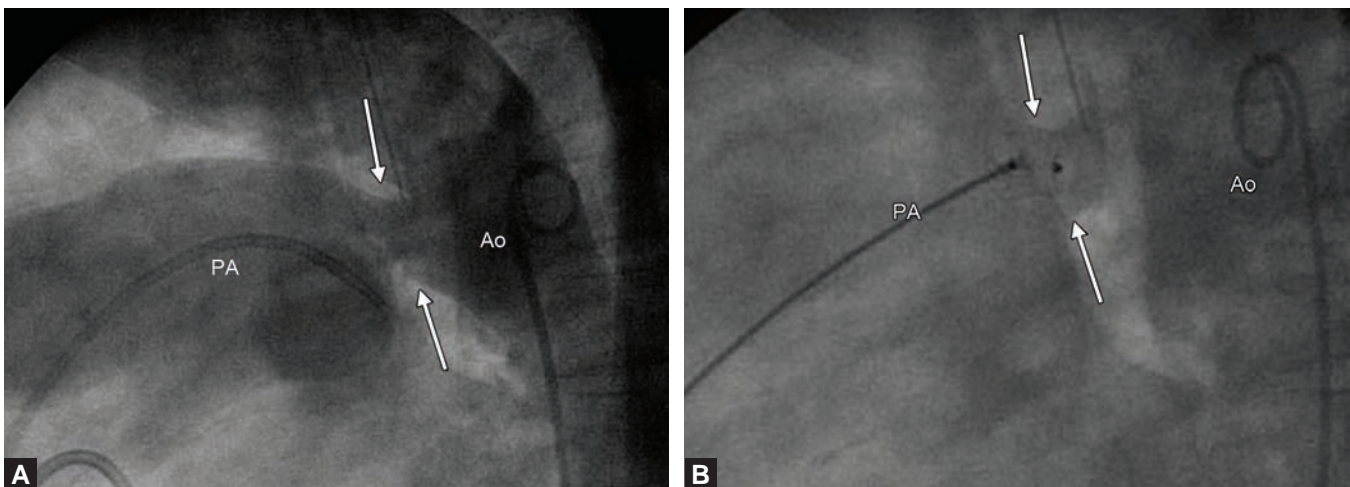

Figs 28.20A and B: Fluoroscopy during PDA closure. (A) Prior to PDA closure, PDA is imaged using contrast injection into the descending aorta. The contrast exits the aorta (Ao) into the pulmonary artery (PA) via the PDA (arrows); (B) A PDA closure device (arrows) is being deployed into the PDA. The device is still attached to its delivery cable seen in the pulmonary artery (PA).

three-step process in which the initial 3D zoom image of the interatrial septum is tilted up to reveal the right atrial aspect of the interatrial septum. The image is then rotated counterclockwise in the Z-axis until the SVC is located at 12 o'clock. Finally, the image is then rotated to the left to reveal the left atrial aspect of the interatrial septum.[90] After using the TUPLE maneuver one can easily determine ASD type, location, shape, and size.

Secundum ASDs (Figs 28.22A to D) are located in the fossa ovalis and come in a variety of shapes (circular, ovoid, triangular).[91] They may contain fenestrations (cribriform ASD) or may be associated with an atrial septal aneurysm.[92] Sizing of an ASD involves measuring of ASD diameters and determining the size of surrounding ASD rims; these data are essential for choosing an appropriate closure device. The three most commonly used ASD closure devices (Figs 28.23A to C) are as follows:

- Amplatzer™ atrial septal occluder (St Jude Medical, St Paul, MN). It consists of two discs (the left atrial disc being larger than the right atrial disc) connected
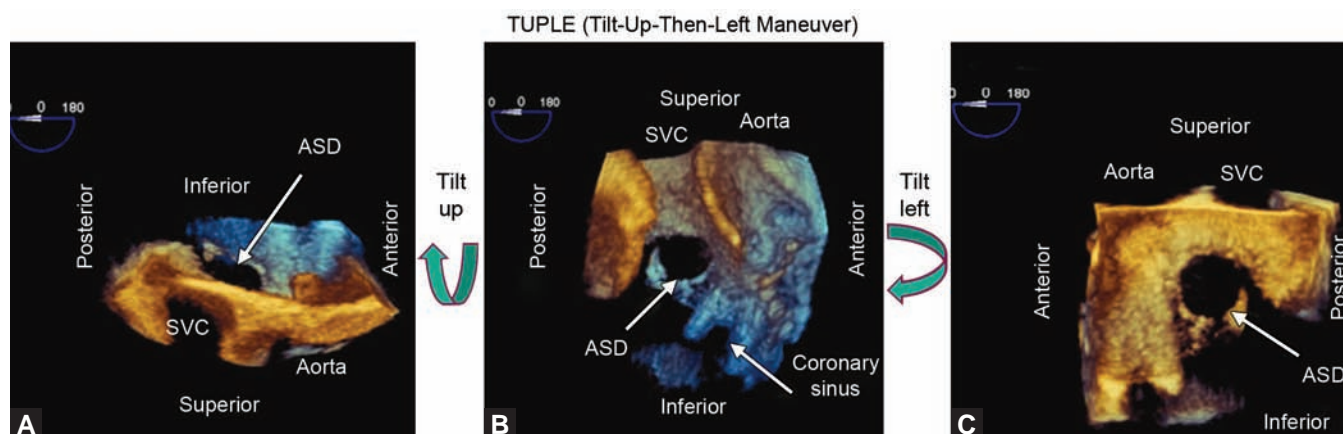
Figs 28.21A to C: TUPLE maneuver for orienting the interatrial septum. TUPLE (Tilt-Up-Then-Left) is a simple maneuver for orienting the interatrial septum into an anatomically correct orientation. (A) Interatrial septum is first visualized on 2D TEE at 0°. Then the corresponding 3D TEE zoom image of the interatrial septum is obtained; (B) The 3D TEE image is tilted up to reveal the right atrial aspect of the interatrial septum. Note that the superior vena cave is located at 12 o'clock; (C) The 3D TEE image is then rotated to the left to reveal the left atrial side of the interatrial septum. Movie clip 28.21A corresponds to this Figure.
Note: If the 2D TEE image is obtained at any angle other than 0° the 3D TEE image is figure 2 is not only tilted up but also rotated counterclockwise until the SVC is at 12 o'clock. Movie clip 28.21B demonstrates this modification of the TUPLE maneuver. (ASD: Atrial septal defect; SVC: Superior vena cava).

by a waist; it comes in a variety of sizes based on waist diameter (from 4 mm to 38 mm). Device selection is based on the measured diameter of the defect, which should correspond to the waist diameter of the device. This device is used to close nonfenestrated secundum ASDs.

- Amplatzer™ multifenestrated septal occluder (St Jude Medical, St Paul, MN) is used to close fenestrated (cribriform) secundum ASDs. It contains two discs of equal diameter connected by a thin shaft; it comes in a variety of size based on the diameter of the left atrial disc (from 18 mm to 35 mm). Device selection is ultimately based on the measured diameter of the defect, which should be proportional to the disc diameter of the device.
- Gore-Helex atrial septal occluder (W L Gore & Associates, Inc., Flagstaff, AZ) contains two equal-sized discs mounted on a spiral shaft; it comes in a variety sizes based on the disc diameter (from 15 mm to 35 mm). The occluder size selected for the defect should achieve at least a 2:1 ratio between disc diameter and defect diameter.

When selecting an ASD closure device, the maximum diameter of a secundum ASD cannot exceed device-specific cutoff value and there should be sufficient ASD rim to anchor the device. Historically, the device size was selected based on an invasive measurement of ASD diameter using sizing balloons placed across an ASD (Figs 28.24A and B) and gradually inflated until no color Doppler flow across the ASD is seen on 2D TEE (so-called stop-flow diameter). More recently, device selection is based on direct ASD diameter measurements by 3D TEE (Figs 28.25A to C). The maximum ASD diameter amenable to closure with an Amplatzer™ atrial septal occluder is 38 mm; for a Gore-Helex device the maximum ASD diameter is 18 mm.

3D TEE imaging is also important in measuring rims that surround a secundum ASD (Figs 28.26A and B). There are several different nomenclatures of ASD rims; we prefer the system that labels rims based on the surrounding structure (e.g. aortic rim)[93] rather than on their anatomic orientation (e.g. antero-superior rim).[94] In general, there are five distinct ASD rims listed in a clockwise direction: SVC rim, aortic room (adjacent to the aortic valve), atrioventricular rim (adjacent to the tricuspid and MV), inferior vena cava (IVC) rim, and posterior rim (the rim opposite the aortic rim).

In general, the rims should be "sufficient"—that is, they have to exceed certain minimum distance. This minimum rim size is device specific. For instance, for the Amplatzer™ septal occluder the rims should be at least 5 mm. For the Amplatzer™ multifenestrated septal occluder, the SVC and the aortic rim should be at least 9 mm. Absence of the inferior vena cava rim is considered a contraindication for device closure of a secundum ASD.
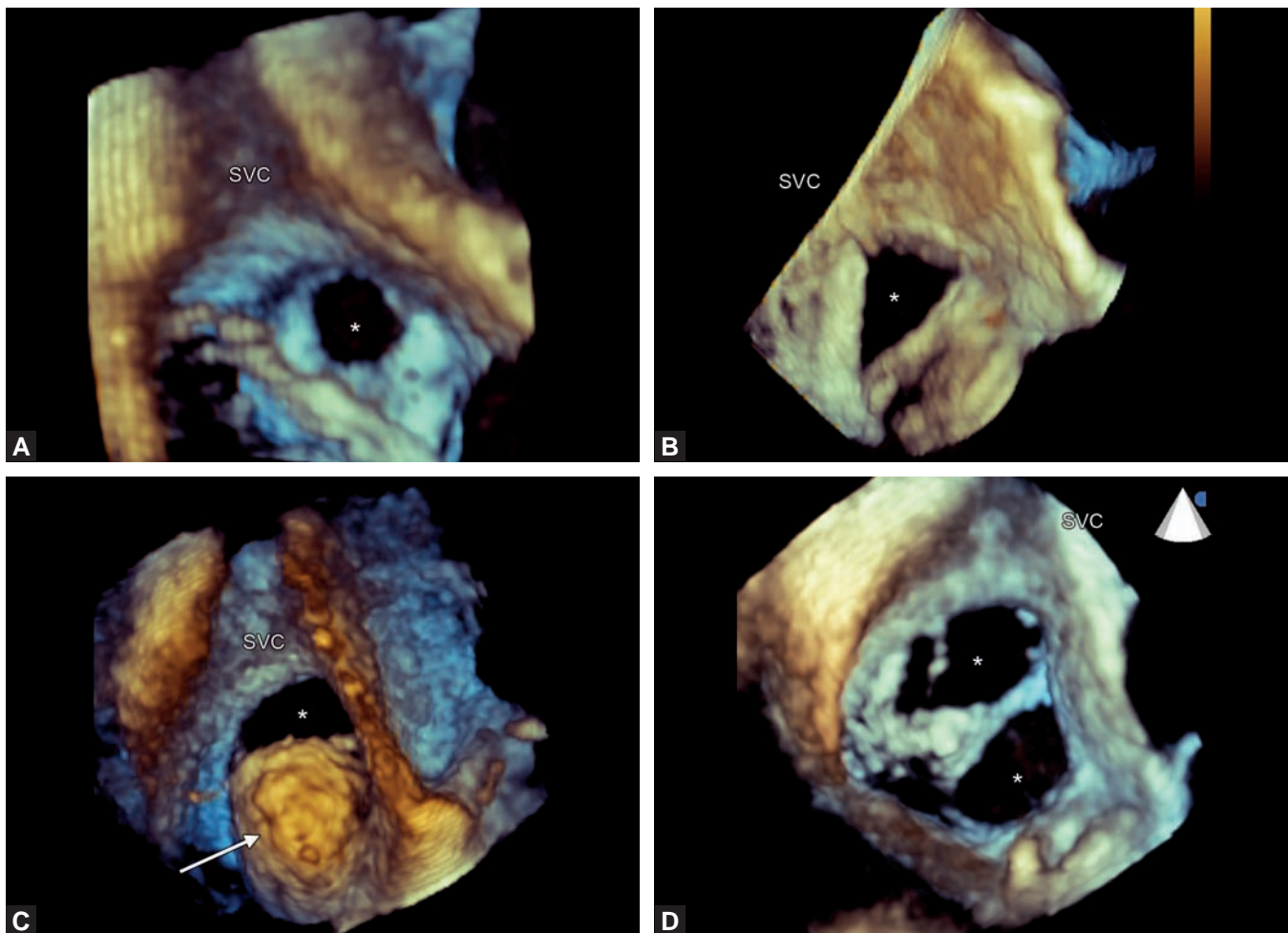
Figs 28.22A to D: Anatomic variations of secundum ASDs. 3D TEE zoom images of the right atrial side of the interatrial septum demonstrate variations in the size, shape and location of secundum ASDs. In each image the SVC is located at approximately 12 o'clock. (A) Secundum ASD asterisk) has a near circular shape; (B) Secundum ASD (asterisk) has a triangular shape; (C) Secundum ASD (asterisk) has an ovoid shape and is located in the superior portion of the fossa ovalis. The inferior portion of the fossa ovalis floor is aneurismal (arrow); (D) Fenestrated secundum ASD with multiple holes (asterisks) separated by remnants of the fossa ovalis floor.

3D TEE Monitoring of Percutaneous ASD Closure

3D TEE allows for continuous visualization of the tip of the guiding catheter, as well as of the closure device as it is being delivered. After the secundum ASD is sized and deemed amenable to percutaneous repair by 3D TEE, the interventionalist may decide to confirm the ASD size using a balloon. Color Doppler echocardiography is used during balloon inflation. When no flow between the balloon and ASD margins is seen by color Doppler, the interventionalist measures the ASD diameter on fluoroscopy image (stop-flow diameter).

Subsequently, a delivery catheter is brought into the left atrium across the ASD using a transvenous approach (typically via the femoral vein). A collapsed ASD closure device is advanced through the catheter into the left atrium. The left atrial disc is opened first and apposed against the left atrial side of the defect. The right atrial disc is then opened and maneuvered until the device is firmly attached to the rims of the ASD. 3D TEE imaging is used to ascertain proper positioning of the closure device. Both discs can be visualized by 3D TEE although right atrial disc may be more difficult to visualize than left atrial disc. This is due to the fact that relative to the TEE probe located in the esophagus the right atrial disc in the far field and partly shadowed by the left atrial disc (Figs 28.27 and 28.28).

In addition, 3D TEE helps determine if sufficient tissue rim is caught in between the two plates of the device. When
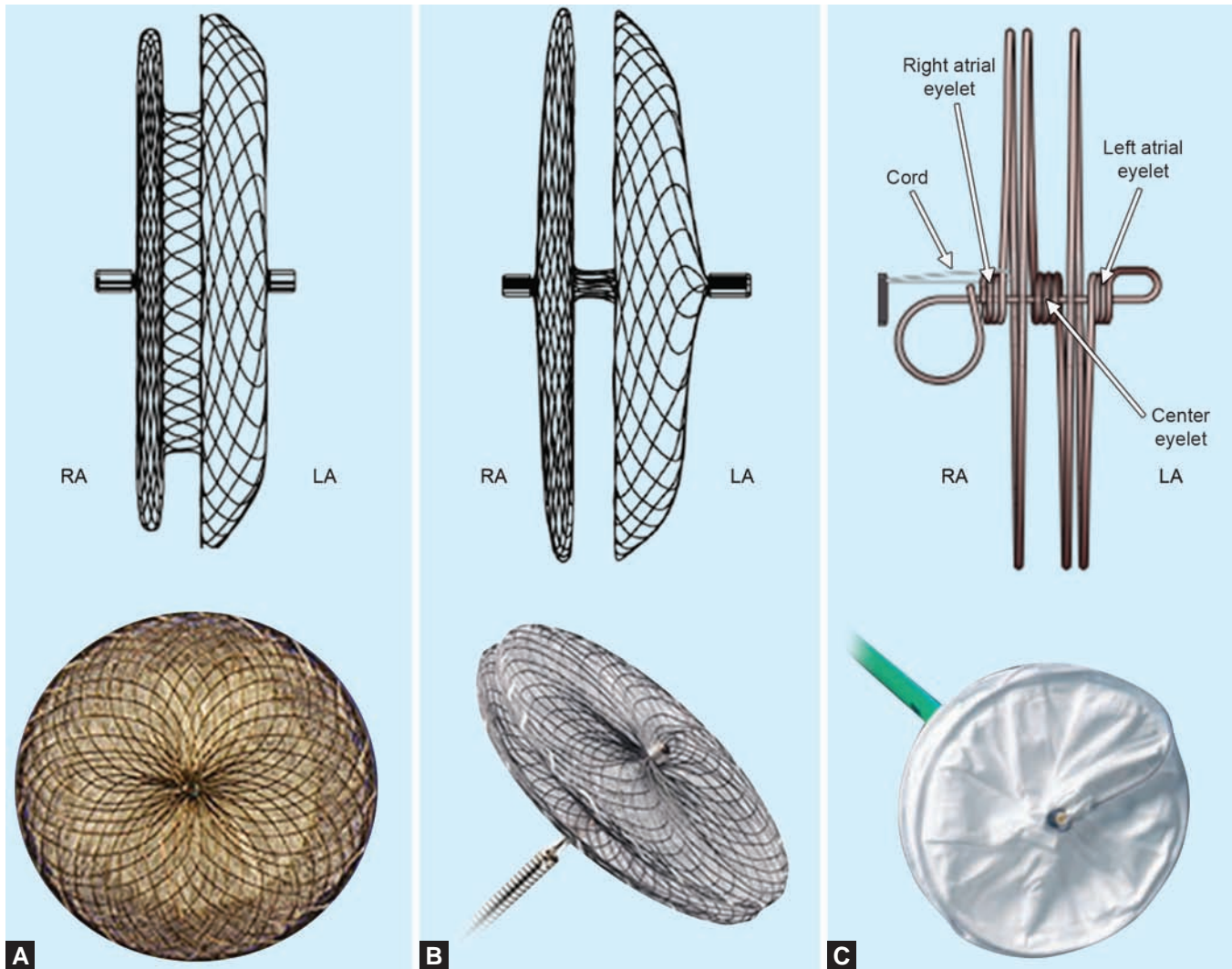
Figs 28.23A to C: ASD closure devices. (A) Amplatzer™ atrial septal occluder (St Jude Medical, St Paul, MN); (B) Amplatzer™ multifenestrated septal occluder (St Jude Medical, St Paul, MN); (C) Gore-Helex atrial septal occluder (W L Gore & Associates, Inc., Flagstaff, AZ).

rim capture is insufficient, 3D TEE can be used to guide repositioning of the device. At the end of the procedure, the device is fully deployed after its release from the delivery shaft. 2D- and 3D TEE color Doppler imaging is crucial for assessing the success of percutaneous ASD closure. On color Doppler, ideally there should be no residual para-device leak (i.e. flow around the device between ASD rims and the edge of the device); the absence of such a leak is indicative of a complete ASD closure. Small amounts of color Doppler flow across rather than around the device may be normal; such flows will cease upon endothelialization of the device.

ICE is an alternative to 3D TEE for monitoring of ASD closure (Figs 28.29A to C).

Closure of PFOs

Foramen ovale, a communication between the right and left atrium at the level of fossa ovalis, is an essential part of fetal circulation. It allows for shunting of oxygen-rich blood (arriving into the right atrium via umbilical veins) to systemic circulation. After birth, the communication closes in the majority of children but remains open in about a quarter of adult population.[95] The persistence of this communication is referred to as PFO.

PFO has been implicated in the pathogenesis of cryptogenic stroke[96] and its surgical or percutaneous closure has been advocated in prevention of recurrent systemic embolism. The role of 3D TEE in percutaneous PFO closure is similar to that described for ASD closure.
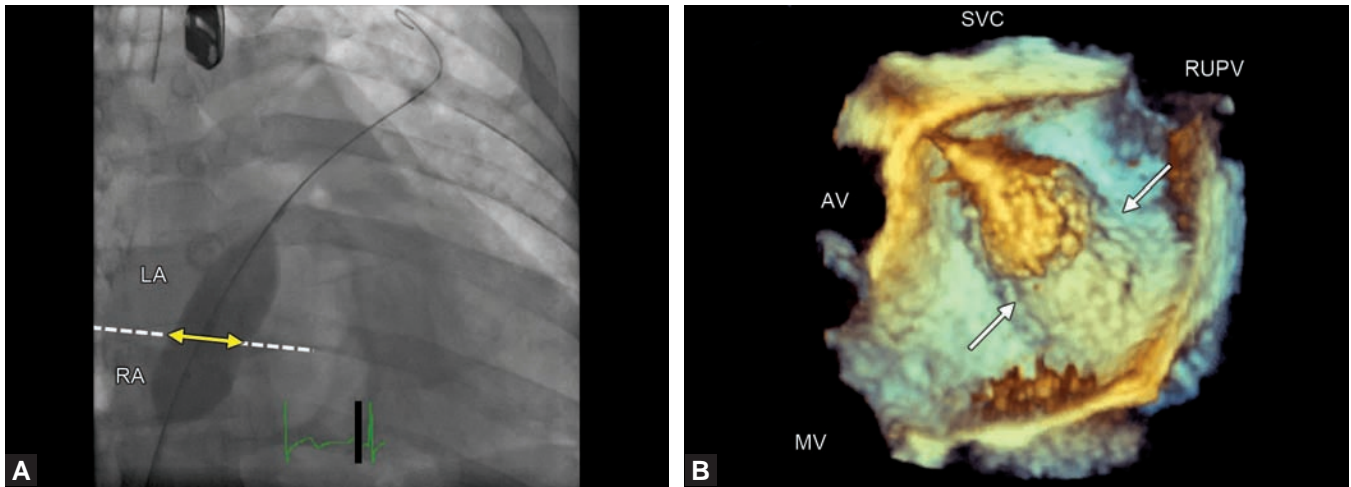
Figs 28.24A and B: ASD sizing balloon. (A) ASD sizing balloon seen on fluoroscopy extending from the right atrium (RA) to the left atrium (LA). Note that the central portion of the balloon (waist) is located in the ASD. The balloon is inflated gradually until color flow across the ASD ceases on TEE imaging. At that moment, the waist diameter is measured; it represents the so-called stop-flow diameter and is used to choose appropriate ASD closure device size; (B) 3D TEE zoom image demonstrates the left atrial aspect of the sizing balloon. (AV: Aortic valve; MV: Mitral valve; RUPV: Right upper pulmonary vein; SVC: Superior vena cava).
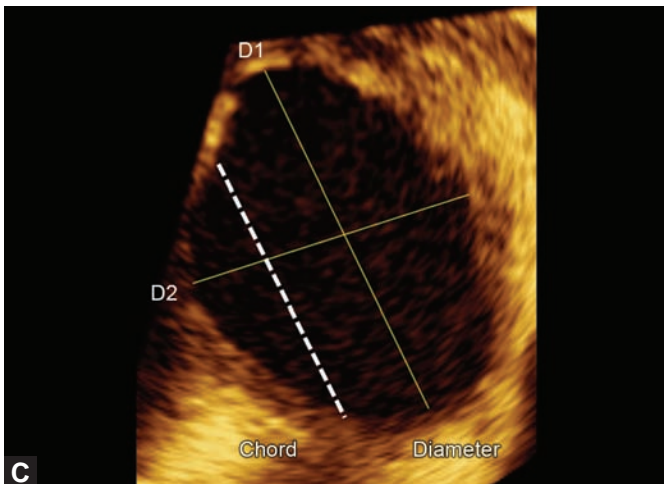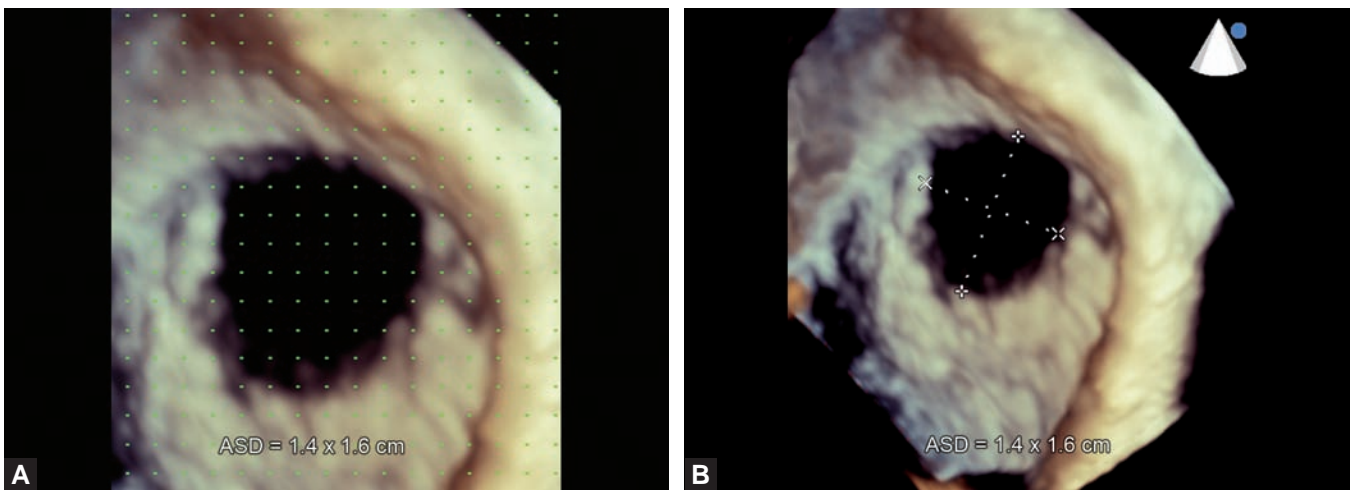

Figs 28.25A to C: 3D TEE sizing of ASDs. ASDs can be sized on 3D TEE using a variety of methods. In this figure the ASD is seen from the right atrial perspective. (A) ASD sizing using an overlay grid; in this instance the distance between the dots is 2 mm; (B) ASD sizing using direct on-image calipers; (C) ASD sizing using the multiplane reconstruction method. Also note the difference between the true ASD diameters and a chord. Distances presumed to be diameters on 2D TEE are frequently chords rather than true diameters.
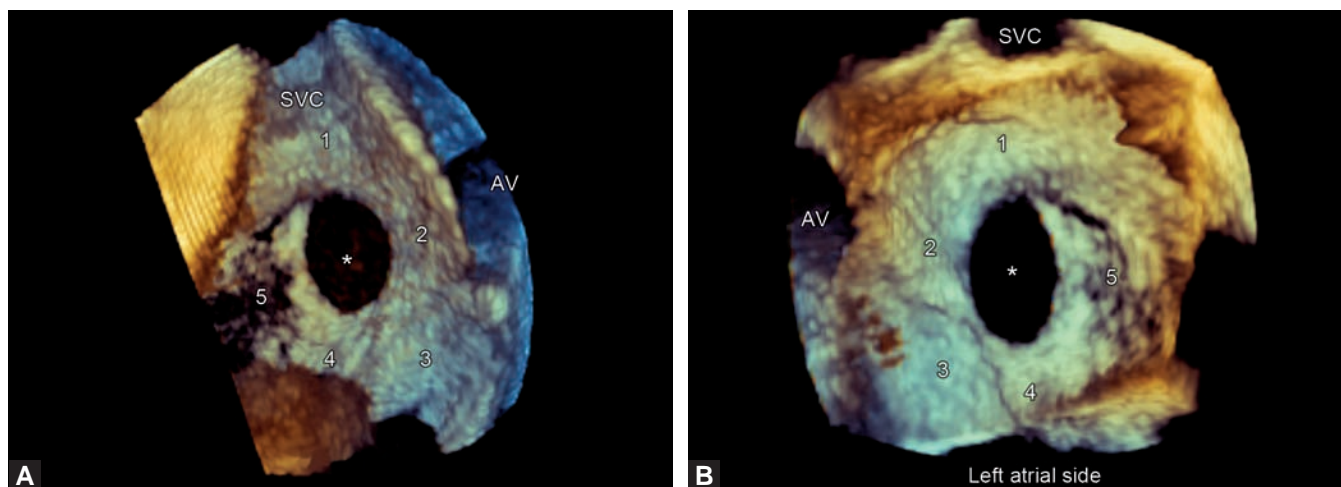
Figs 28.26A and B: 3D TEE visualization of ASD rims. 3D TEE zoom view of the interatrial septum and surrounding structures from the right atrial (A) and left atrial perspective (B). Five ASD rims are depicted in each figure: (1) SVC rim; (2) aortic rim next to the aortic valve (AV); (3) atrioventricular rim next to the tricuspid and mitral valve; (4) IVC rim; and (5) posterior rim.
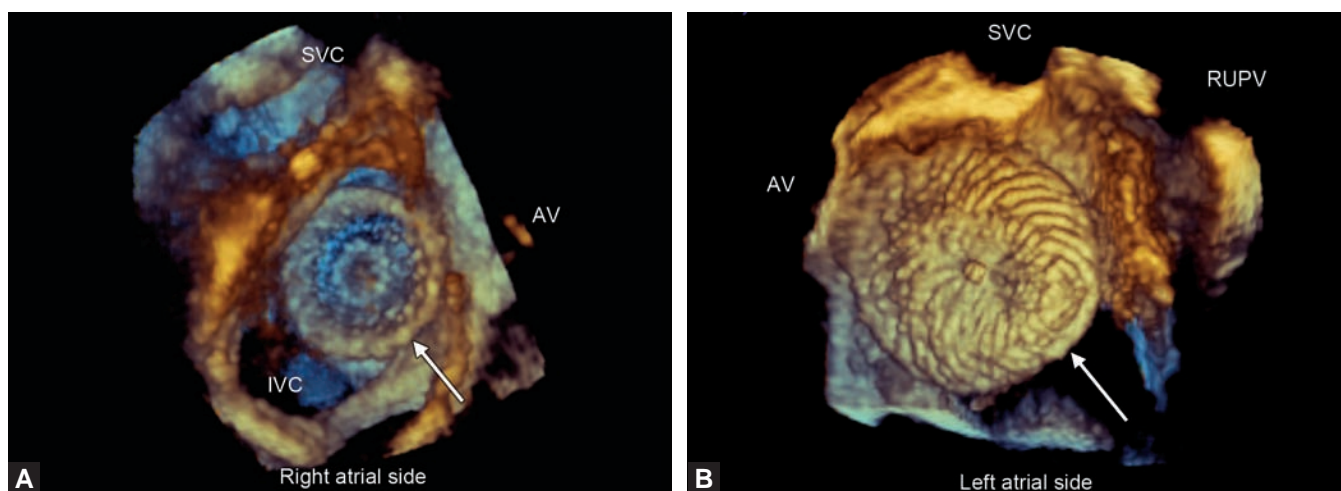

Figs 28.27A and B: 3D TEE appearance of Amplatzer ASD occluder. Amplatzer ASD occluder (arrow) is well visualized from the right atrial side (A) and the left atrial side (B). (AV: Aortic valve; IVC: Inferior vena cava; RUPV: Right upper pulmonary vein; SVC: Superior vena cava).

PFOs are typically closed percutaneously with devices that are specifically designed for PFO closure (Figs 28.28A to C) such as the STARFlex occluder (previously referred to as CardioSEAL device; NMT Medical, Boston, MA) and Amplatzer PFO Occluder (St Jude Medical, St Paul, MN). Percutaneous PFO closure was first reported in 1992 using the Bard Clamshell Septal Occluder, a predecessor of the STARFlex device.[97] Randomized trials have thus far failed to demonstrate clear benefit of PFO closure with either STARFlex or Amplatzer PFO Occluder.[98,99]

Closure of VSDs

There are several types of VSDs: perimembranous (infracristal); muscular (further subdivided into inlet, trabecular and infundibular, or supracristal); and atrioventricular defect (a communication between the left ventricle and the right atrium).[100] Perimembranous VSDs often have a windsock appearance due to evagination of the membranous septum.[101]

Colloquially, the term "muscular VSD" if often used synonymously with the trabecular VSD. Muscular VSD
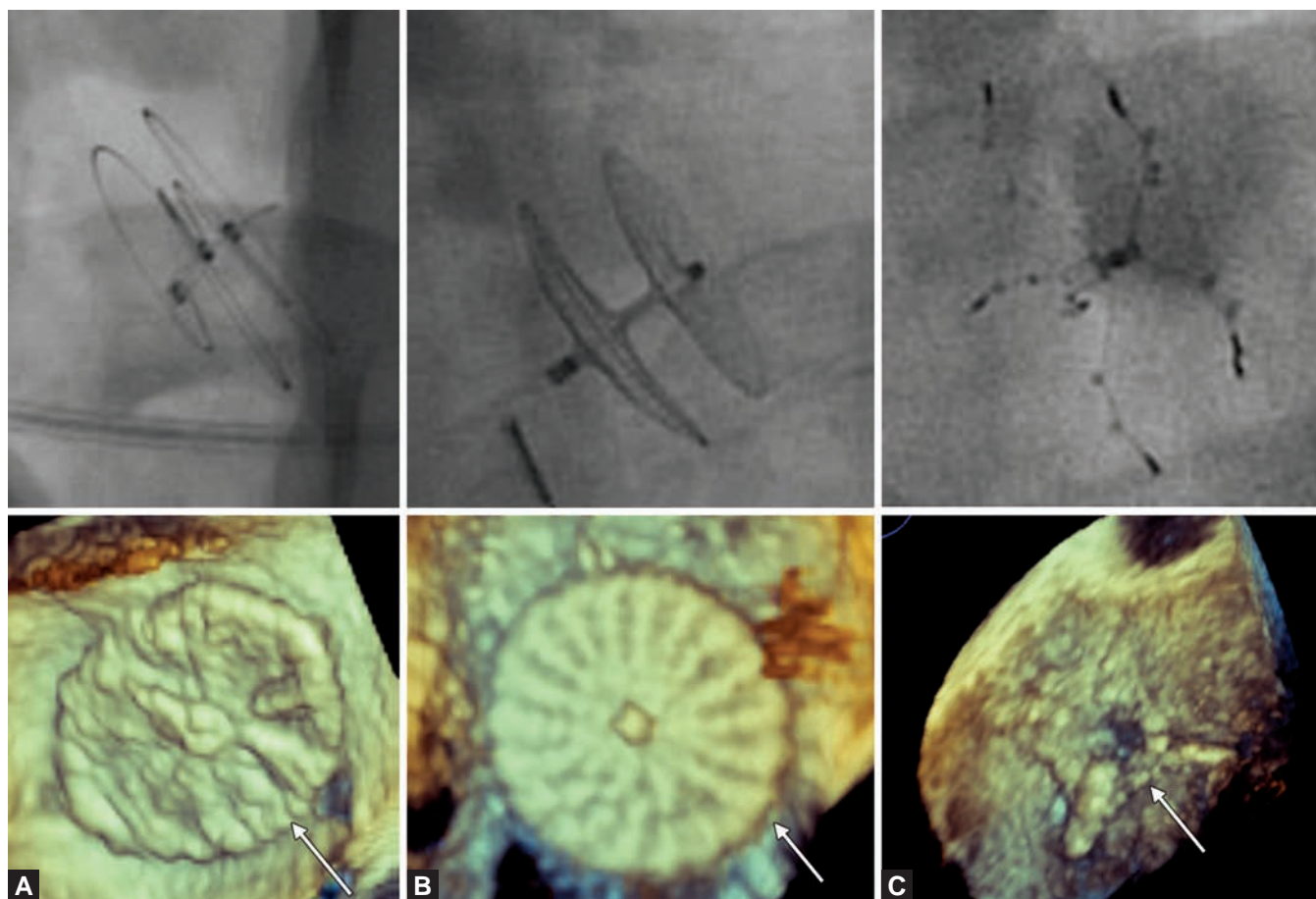
Figs 28.28A to C: 3D TEE and fluoroscopic appearance of ASD and PFO closure devices. (A) Gore-Helex atrial septal occluder (W L Gore & Associates, Inc., Flagstaff, AZ); (B) Amplatzer™ multifenestrated ("cribriform") septal occluder (St Jude Medical, St Paul, MN); (C) STARFlex occluder (previously referred to as CardioSEAL device; (NMT Medical, Boston, MA).

may be congenital or acquired (e.g. following myocardial infarction or trauma).[102] Closure of a VSD should be considered if one of the following criteria is present:

- Qp/Qs (pulmonary-to-systemic blood flow ratio) ≥ 2.0 and clinical evidence of LV volume overload.
- History of infective endocarditis
  Closure of a VSD may also be considered if:
- Qp/Qs > 1.5 with pulmonary artery pressure less than two thirds of systemic pressure and pulmonary vascular resistance less than two-thirds of systemic vascular resistance.
- Net left-to-right shunting is present at Qp/Qs > 1.5 in the presence of LV systolic or diastolic failure.

Closure of a VSD is contraindicated in patients with severe irreversible pulmonary arterial hypertension (who typically present with pulmonary vascular resistance greater than two-thirds of systemic vascular resistance).

Percutaneous closure of a VSD was first performed in 1987 at Harvard Medical School.[103] At present, percutaneous closure devices in the United States are approved for use in patients who are at high risk for standard surgical VSD closure and whose VSD is not in the proximity of cardiac valves. Thus, percutaneous closure is primarily performed in patients with congenital muscular VSDs. Nonetheless, off-label use for percutaneous closure of postinfarction VSDs has been reported.[104]

One such device approved in the United States is the Amplatzer™ ventricular septal occluder (St Jude Medical, St. Paul, MN). It consists of two discs of equal diameter (a LV disc and a right ventricular disc) separated by a waist that fits within the VSD. Device comes in a variety of sizes based on the waist diameter (from 4 mm to 18 mm). Outside the United States, a specially designed device with eccentric discs is used to close perimembranous VSDs.[105]
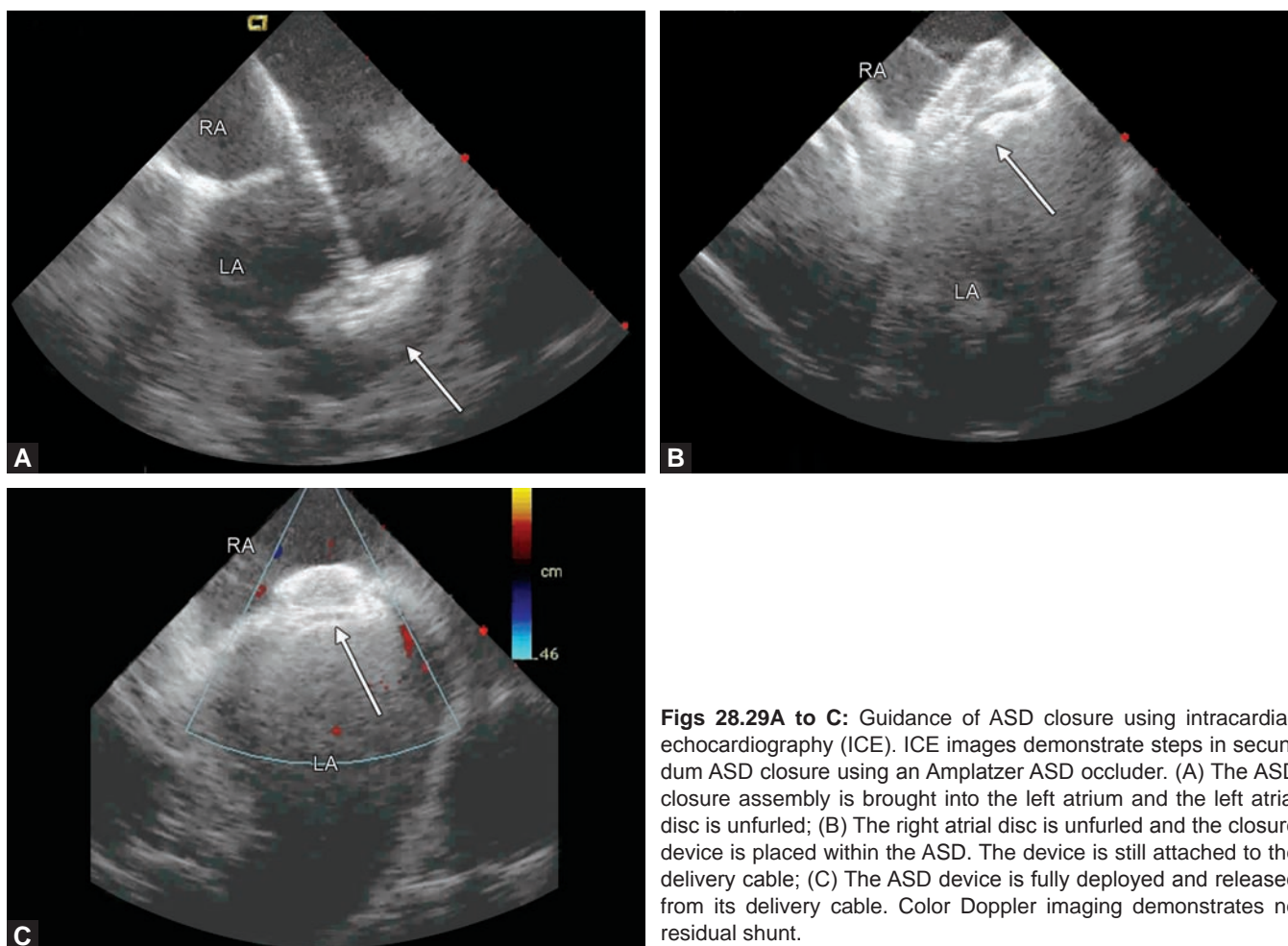
Figs 28.29A to C: Guidance of ASD closure using intracardiac echocardiography (ICE). ICE images demonstrate steps in secundum ASD closure using an Amplatzer ASD occluder. (A) The ASD closure assembly is brought into the left atrium and the left atrial disc is unfurled; (B) The right atrial disc is unfurled and the closure device is placed within the ASD. The device is still attached to the delivery cable; (C) The ASD device is fully deployed and released from its delivery cable. Color Doppler imaging demonstrates no residual shunt.

3D TEE is important for both the diagnosis and for guidance of percutaneous closure of a VSD.[106] With its unique ability to provide en face views, 3D TEE allows for accurate visualization of the VSD location, size, and shape (Figs 28.30A to E). The information is important in establishing the feasibility of device closure and selecting the proper size of the closure device.

During percutaneous VSD closure, the role of 3D TEE imaging is similar to that described for percutaneous ASD closures. 3D TEE visualization of intracardiac wires and catheters is helpful in guiding placement of a closure device into the defect. Postdeployment, 2D and 3D TEE color Doppler imaging is crucial for assessing whether VSD closure was successful or not (Figs 28.31A to D). With complete VSD closure there should be no residual para-device leak (i.e. flow around the device between VSD rims and the edge of the device) on color Doppler imaging. In contrast, small amounts of color Doppler flow across rather than around the device may be normal; such flows will disappear upon endothelialization of the device.

OCCLUSION OF THE LEFT ATRIAL APPENDAGE

Atrial fibrillation, the most common sustained cardiac arrhythmia, is a risk factor for intracardiac thrombus formation and thromboembolism; it accounts for approximately 15% of all ischemic strokes.[107] In nonvalvular atrial fibrillation, the LAA is the primary site of thrombus formation accounting for 91% of all atrial fibrillation-associated intracardiac thrombi. Even in valvular atrial fibrillation (which is related to rheumatic heart disease and this uncommon in high-income countries) LAA thrombi account for 57% of all thrombi.[108] Anticoagulation with warfarin or other oral agents is the standard of care
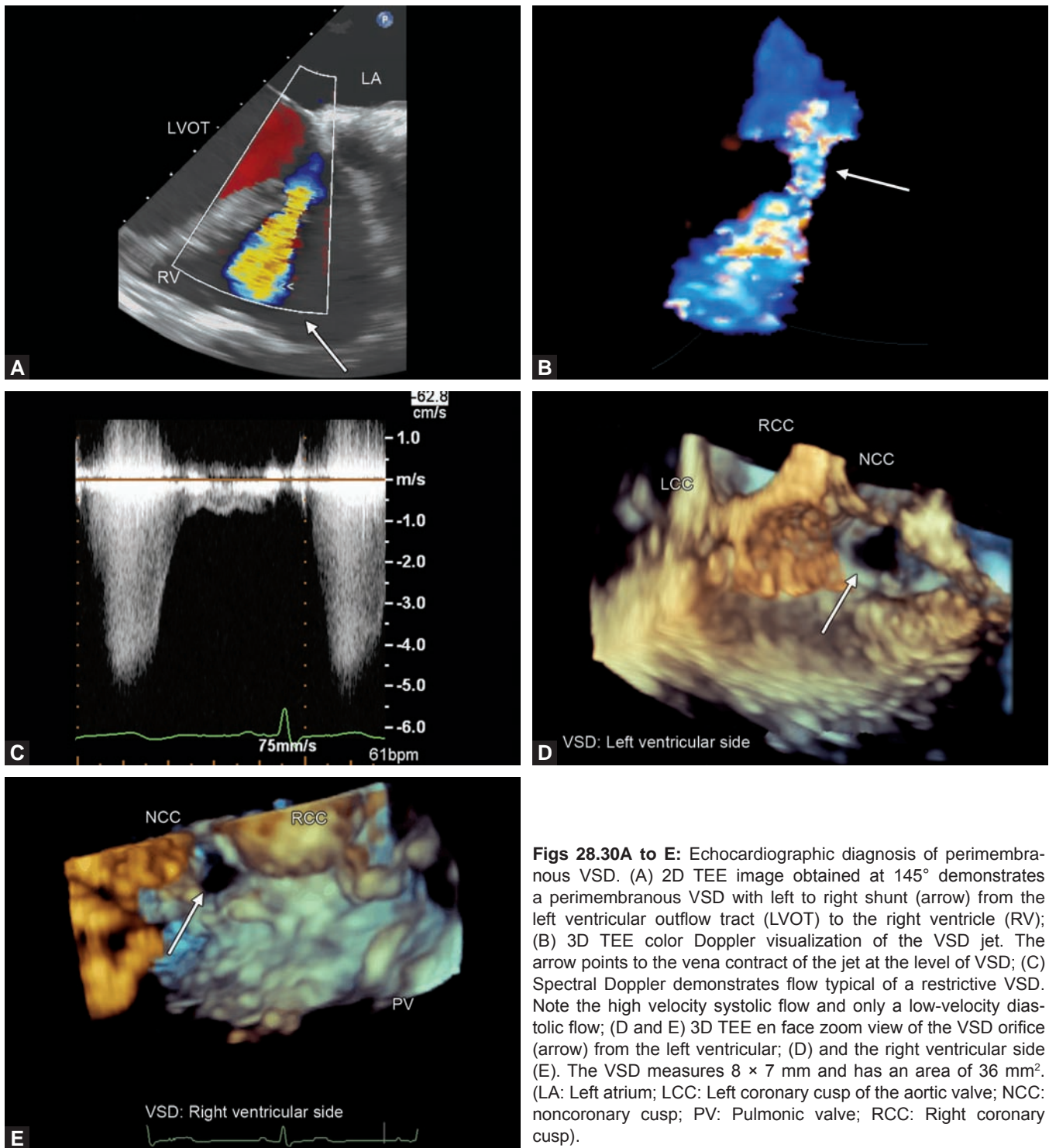
Figs 28.30A to E: Echocardiographic diagnosis of perimembranous VSD. (A) 2D TEE image obtained at 145° demonstrates a perimembranous VSD with left to right shunt (arrow) from the left ventricular outflow tract (LVOT) to the right ventricle (RV); (B) 3D TEE color Doppler visualization of the VSD jet. The arrow points to the vena contract of the jet at the level of VSD; (C) Spectral Doppler demonstrates flow typical of a restrictive VSD. Note the high velocity systolic flow and only a low-velocity diastolic flow; (D and E) 3D TEE en face zoom view of the VSD orifice (arrow) from the left ventricular; (D) and the right ventricular side (E). The VSD measures 8 × 7 mm and has an area of 36 mm². (LA: Left atrium; LCC: Left coronary cusp of the aortic valve; NCC: noncoronary cusp; PV: Pulmonic valve; RCC: Right coronary cusp).

for prevention of thromboembolism in atrial fibrillation. In patients who cannot take anticoagulant, exclusion of LAA from the body of the left atrium is an alternative for prevention of thromboembolism.

LAA exclusion can be achieved either surgically or percutaneously. Surgical techniques of LAA exclusion include LAA amputation,[109] clipping,[110] and ligation.[111] Surgical LAA exclusion is usually performed only as
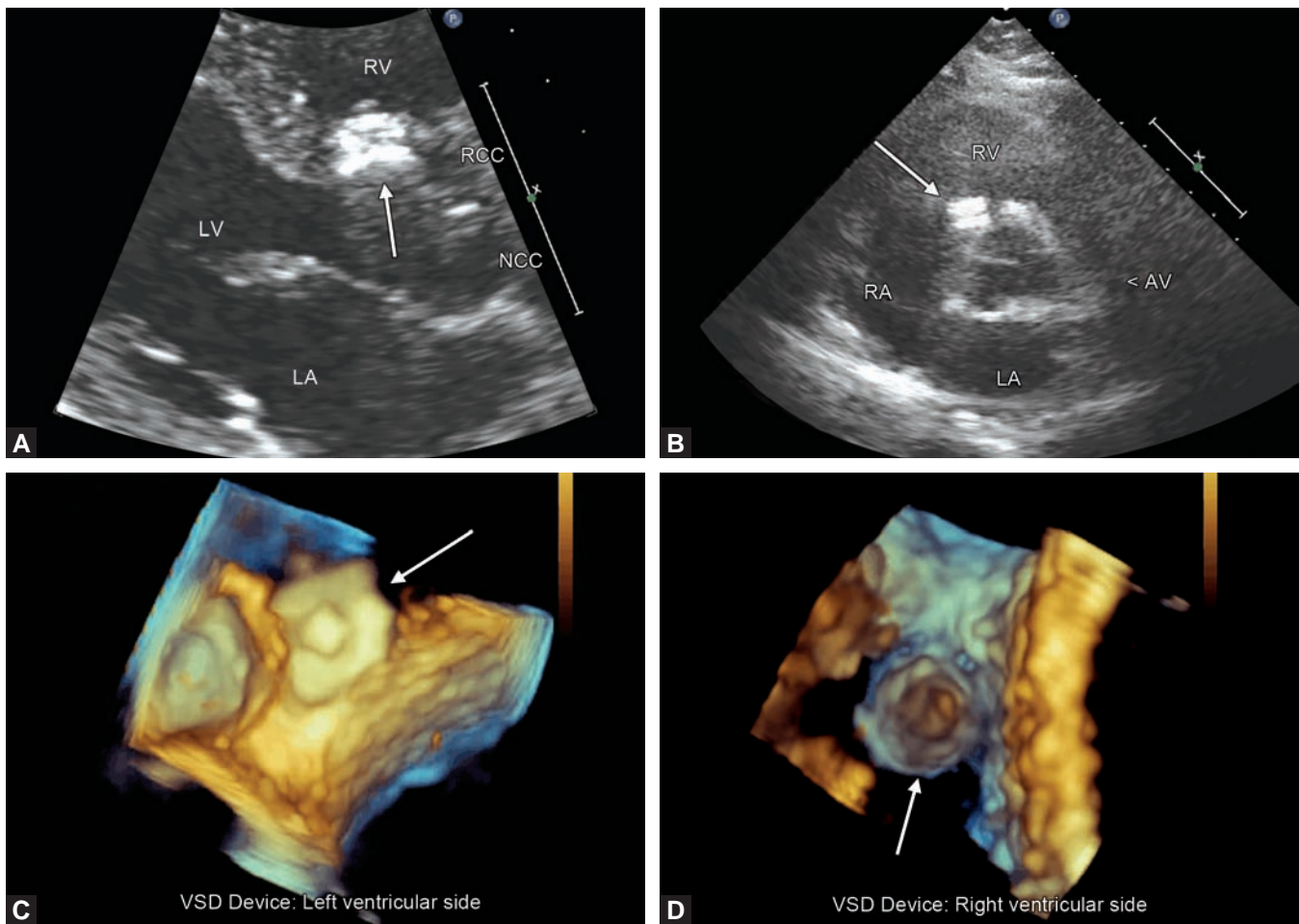
Figs 28.31A to D: Echocardiographic visualization of a VSD closure device. The patient underwent perimembranous VSD closure in China; such a procedure is not available in the United States unless part of an investigational study. (A and B) 2D transthoracic echocardiography demonstrates a closure device obliterating a perimembranous VSD in the parasternal long-axis (A) and the parasternal short-axis view (B); (C and D) 3D TEE en face zoom view of a VSD closure device (arrow) obliterating a perimembranous VSD seen from the left ventricular perspective (C) and the right ventricular perspective (D). (AV: Aortic valve; LA: Left atrium; LV: Left ventricle; NCC: Noncoronary cusp of the aortic valve; RA: Right atrium; RCC: Right coronary cusp; RV: Right ventricle).

an adjunct to another cardiac surgery (such coronary bypass grafting or valvular surgery) that limits the number of patients who could benefit from LAA exclusion. Furthermore, surgical LAA exclusion is frequently incomplete.[112] Percutaneous LAA exclusion can be achieved either by implantation of an endocardial occluder device or via transpericardial placement of an epicardial suture at the LAA ostium. 2D and 3D TEE imaging is important for patient selection and guidance of percutaneous LAA exclusion.[113]

Endocardial Device Closure of LAA

Although several occluders have been used, general principles of percutaneous closure of LAA using the endocardial approach are the same. Using a venous access (typically the femoral vein) and the previously described transseptal puncture, a delivery catheter is advanced through the venous system into the right atrium and then across the interatrial septum into the left atrium near the ostium of the LAA. Subsequently, the occluder is brought through the catheter into the LAA and deployed. LAA occluders consist of a nitinol wire frame covered with cloth. To date, they have only been approved for investigational use in the United States. Three LAA occluders have been evaluated in clinical trials: PLAATO, Watchman™, and Amplatzer™ cardiac plug (Figs 28.32A to C).[114]

PLAATO (Appriva Medical, Inc., Sunnyvale, CA) was the first device that was specifically designed for percutaneous LAA occlusion. Despite promising results,
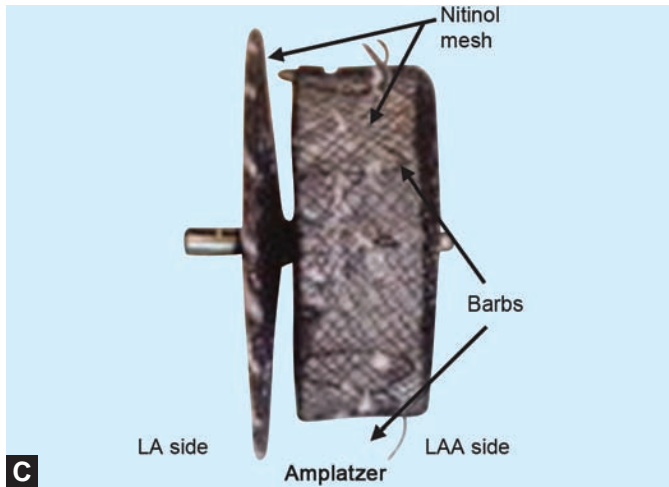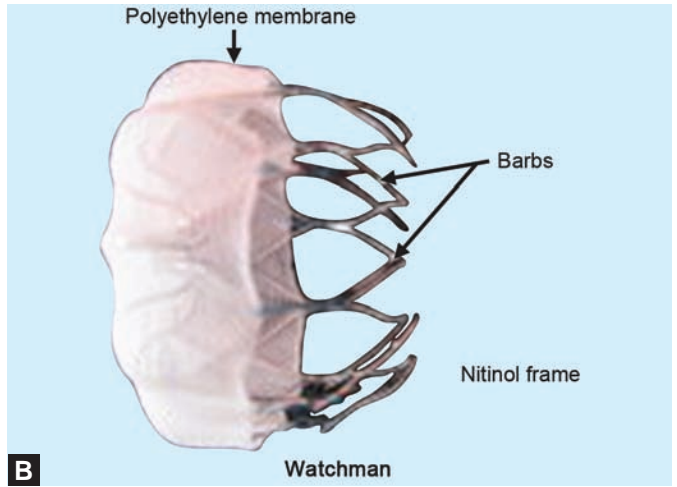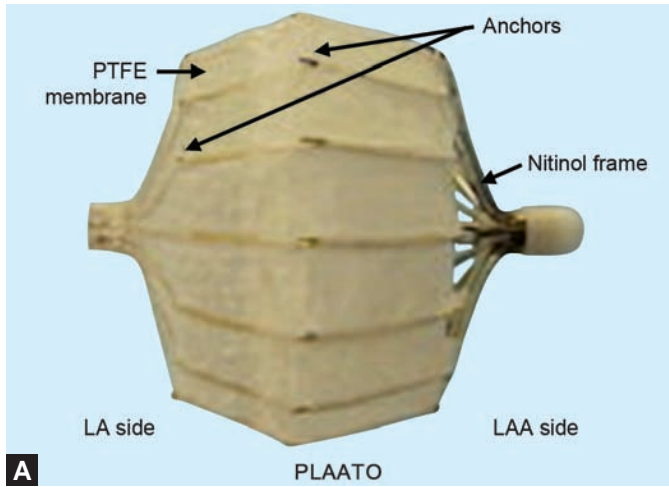
Figs 28.32A to C: Devices used for percutaneous closure of LAA. The greatest clinical experience to date is with the Watchman device. The PLAATO device is no longer available. The Amplatzer cardiac plug is currently in clinical trials in the United States.
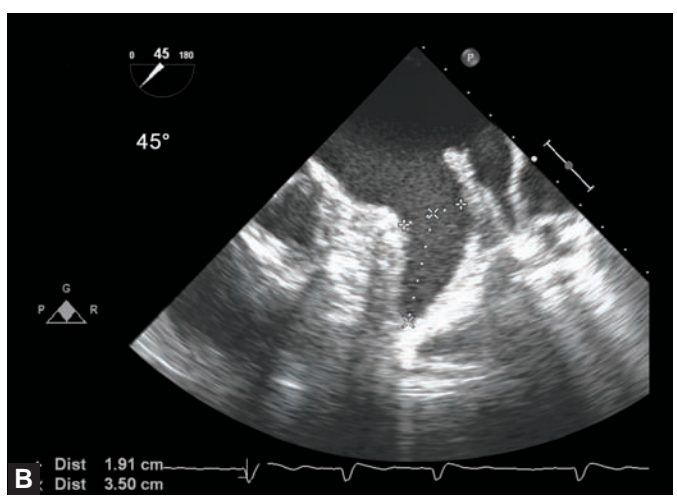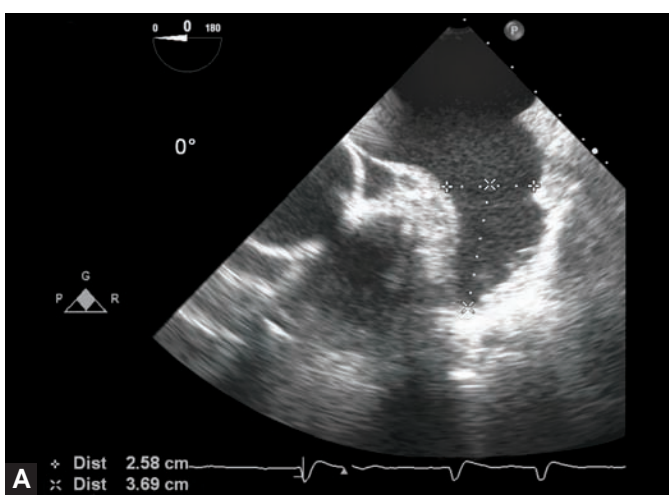
Figs 28.33A and B
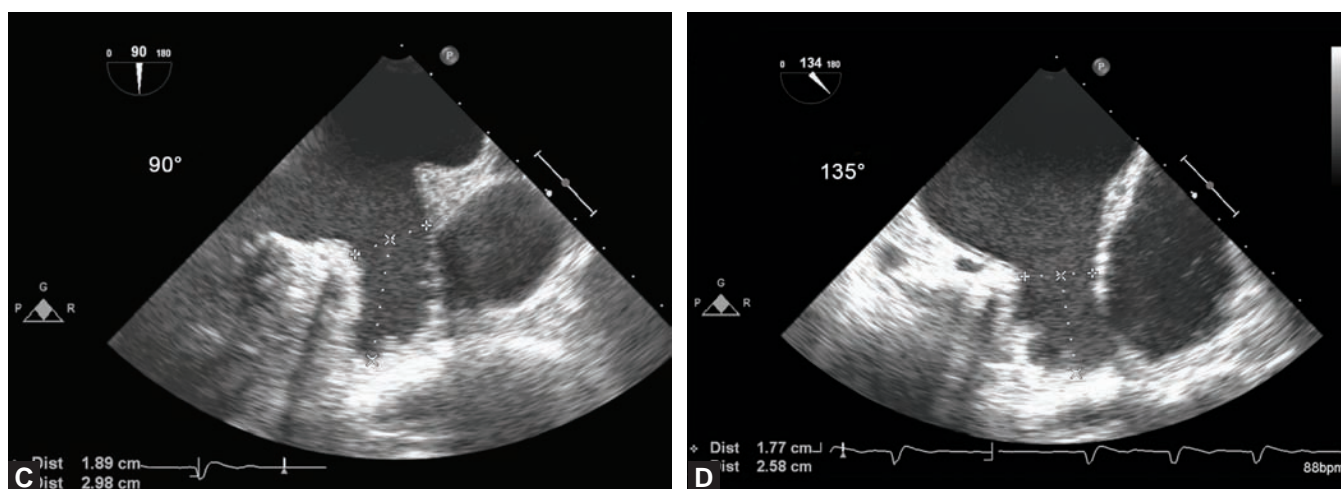
Figs 28.33A to D: Sizing of LAA by 2D TEE. On 2D TEE, LAA is visualized on multiple acquisition angles (typically 0°, 45°, 90° and 135°). Both the orifice diameter and the appendage depth are measured in each view.

PLAATO device has been discontinued. Enrollment for the Amplatzer™ cardiac plug (St Jude Medical, St Paul, MN) trial is in progress. Watchman™ (Boston Scientific, Natick, MA) is the only LAA occluder whose clinical trials have been completed. In the PROTECT-AF trial, LAA exclusion with a Watchman™ device was shown to be noninferior to warfarin therapy.[115] However, it is important to emphasize that all patients who received Watchman device were also treated with warfarin for 6 weeks and dual antiplatelet therapy (aspirin and clopidogrel) for 6 months postdevice implantation. Aspirin therapy was then continued for life.

2D- and 3D TEE in used for both patient selection and procedure guidance. TEE imaging can be used to accurately visualize the LAA prior to the procedure and to measure its size.[116] For device placement, both the orifice size and LAA length are important.

Historically, LAA was sized using 2D TEE imaging at various acquisition angles, typically at 0°, 45°, 90°, and 135° (Figs 28.33A to D). 3D TEE imaging allows for more precise sizing of the LAA; both 3D zoom and multiplane reconstruction imaging are helpful (Figs 28.34A to D).

On 3D TEE en face views, the LAA orifice is often ovoid rather than circular in shape. Using on-image calipers, the orifice diameters can be measured precisely. For proper device implantation, LAA must have a minimum length (the distance between the LAA orifice and LAA tip). This distance can be measured very accurately on multiplane reconstruction of 3D TEE images of LAA. Multiplane imaging allows for keeping the plane of the LAA orifice constant across imaging planes, something that is very difficult with 2D TEE imaging.

3D TEE is used in conjunction with fluoroscopy during LAA device closure (Figs 28.35A to C). 3D TEE allows for visualization of intracardiac trajectories of catheters and introducers, which helps with the transseptal puncture and deployment of an LAA occluder device (Figs 28.36A to D).

An LAA occluder device is properly placed when its long axis is parallel to the long-axis of the LAA. Improper off-angle positions of the occluder are much easier to demonstrate by 3D TEE than by 2D techniques. 2D and 3D color Doppler imaging is crucial for ascertaining that no significant residual communication between the LAA and the left atrium (para-device leak) persists after occluder device placement. For the Watchman™ device, the residual para-device jet should be either absent or at least no larger than 5 mm in width. If the device is placed improperly at first attempt, 3D TEE is used to guide recapture and redeployment of the device.

Epicardial Suturing of LAAs (Lariat Procedure)

The major downside of above described endocardial LAA occluders is the need for continued use of anticoagulation and antiplatelet therapy for several weeks postimpl-antation. In contrast, the Lariat procedure—in which LAA is occluded epicardially—does not require the use of postprocedural anticoagulation therapy. The Lariat procedure utilized both endocardial and epicardial access.

The endocardial portion of the procedure is conceptually similar to the Watchman procedure except
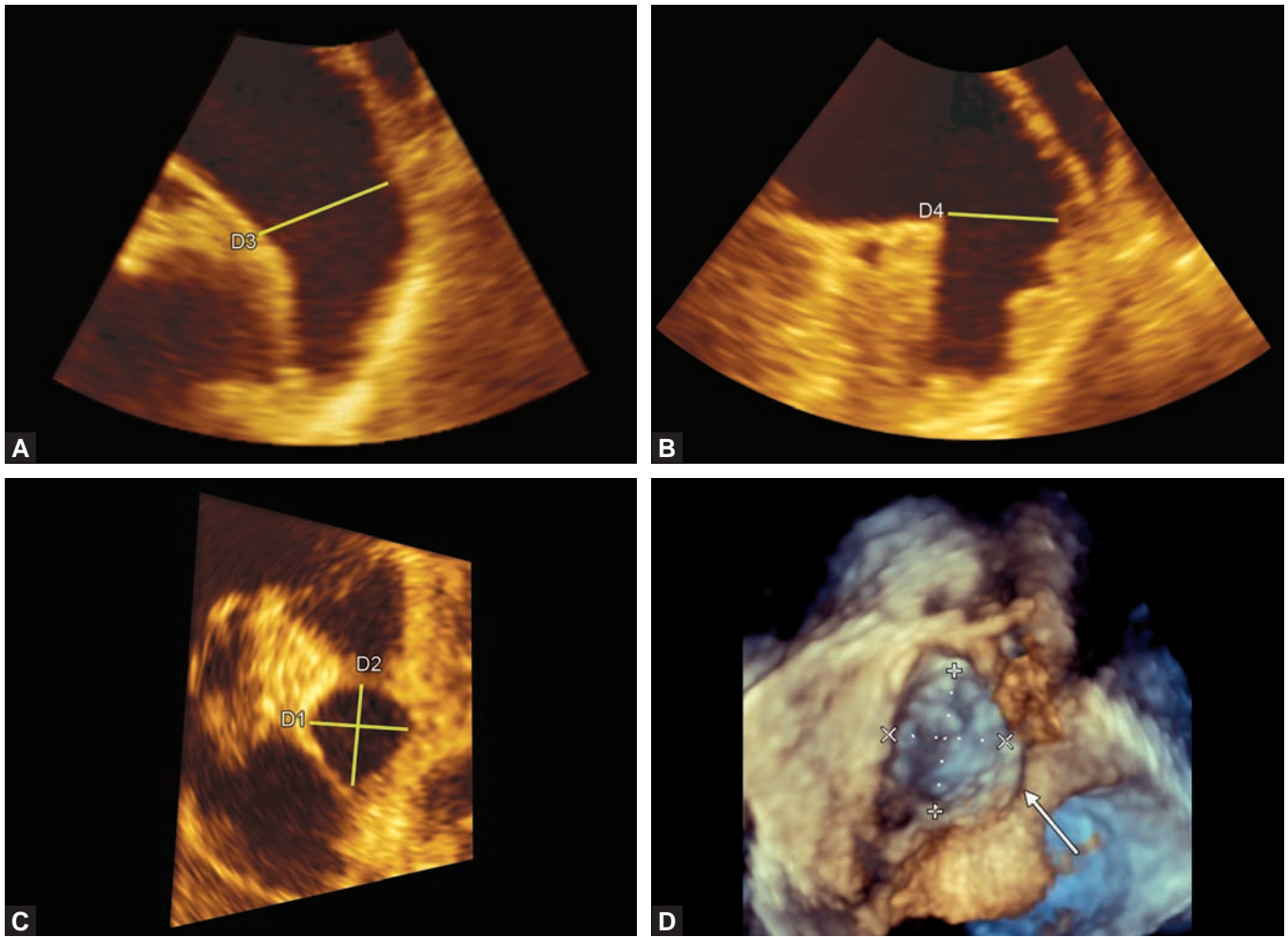
Figs 28.34A to D: Sizing of LAA by 3D TEE. 3D TEE provides for more precise sizing of the LAA using either the multiplane imaging (A, B and C) or 3D TEE en face zoom imaging and utilizing on-image calipers.
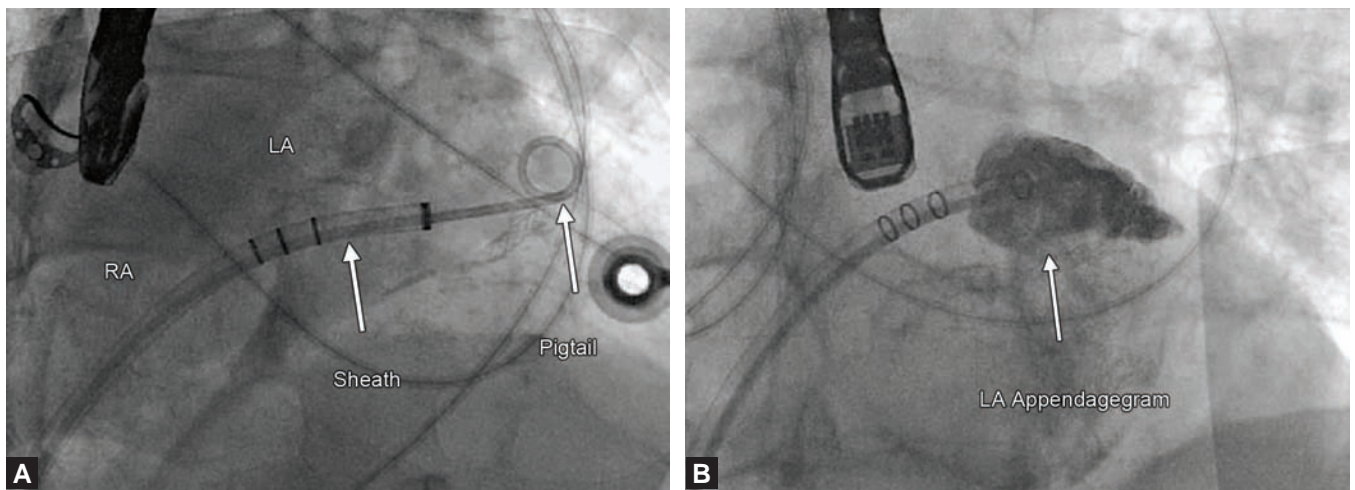
Figs 28.35A and B
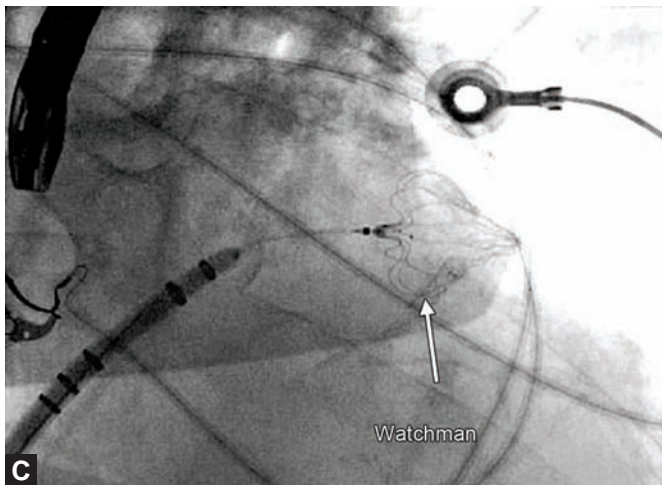
**Figs 28.35A to C:** Guidance of Watchman procedure by fluoroscopy. (A) After trans-septal puncture, a sheath is brought from the right atrium (RA) into the left atrium (LA) in preparation for the Watchman procedure. A pigtail catheter is advanced through the sheath and its tip is then placed into the LAA; (B) Iodinated contrast is then injected through the pigtail catheter to obtain the LAA gram; (C) In the final step the pigtail catheter is removed and the delivery catheter containing the Watchman device is advanced through the sheath and delivered into the LAA.
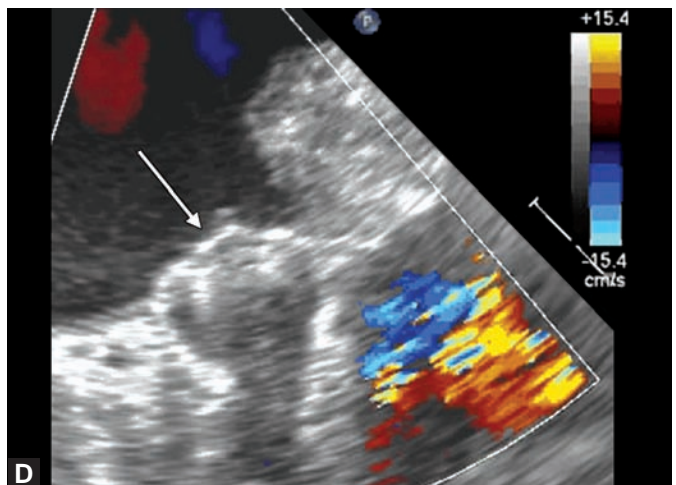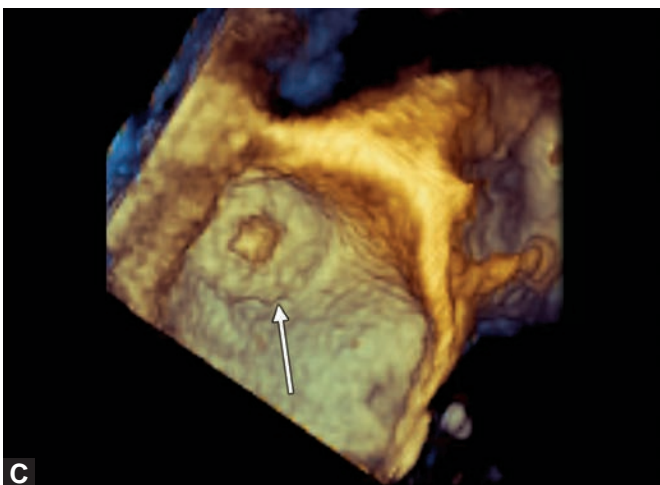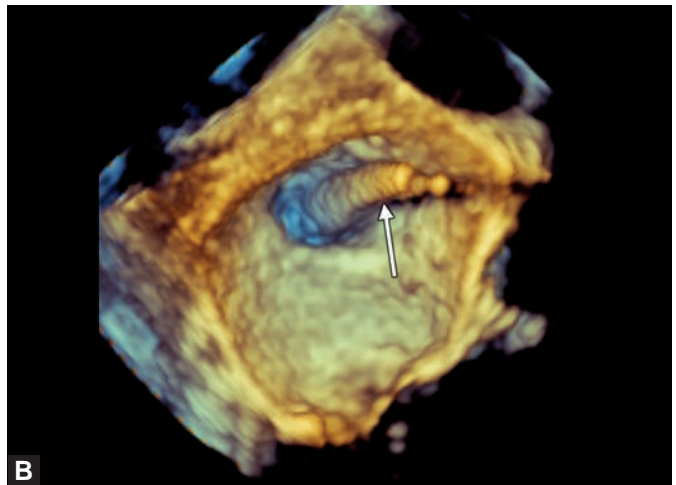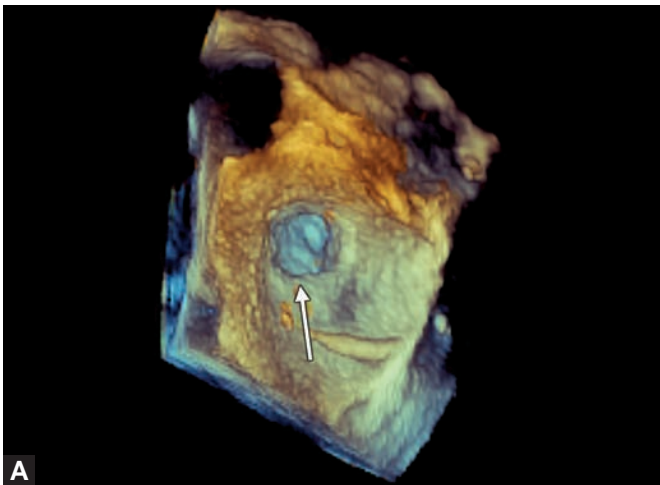
Figs 28.36A to D: Guidance of Watchman procedure by 2D/3D TEE. (A) LAA orifice (arrow) is visualized en face on 3D TEE; (B) 3D TEE aids in guiding the pigtail catheter (arrow) into the LAA; (C) 3D TEE is then used to guide deployment of the Watchman device. Arrow points to a fully deployed Watchman device obliterating the LA orifice; (D) On 2D TEE color Doppler imaging, no residual communication between the LA and LAA is seen indicative of a successful Watchman procedure.
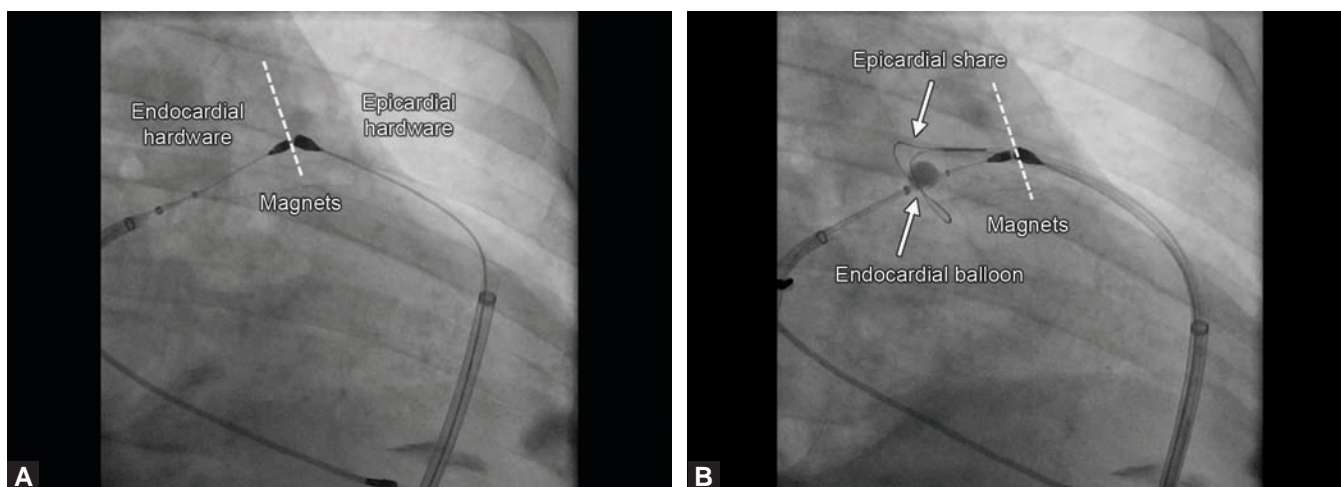
Figs 28.37A and B: Lariat procedure guidance by fluoroscopy. (A) Two magnet-tipped wires are seen connected to each other in preparation for Lariat-based obliteration of the LAA. On the left side is the endocardial wire with its tip in the apex of the LAA. This wire is deployed into the LAA transvenously after a transseptal puncture. On the right side is the epicardial wire which is advanced through the pericardial space until it meets the endocardial wire; (B) After the two wires are connected magnetically, a snare is placed over the orifice of the LAA epicardially. To prevent slippage of the snare, a balloon attached to the endocardial wire is inflated inside the LAA. Thereafter, the snare is tightened and a stitch is placed epicardially to complete exclusion of the LAA from the body of the left atrium.

that no occluder device is placed in the LAA. Using established transvenous and transseptal techniques, a magnet-tipped guide wire is threaded through the venous system, passed across the interatrial septum, and placed in the tip of the LAA. Another magnet-tipped guide wire is threaded epicardially through a pericardial access until it binds magnetically to the already placed LAA wire (Figs 28.37A and B).

Due to the need for this pericardial access, prior history of pericardial adhesions (such as due to pericardiotomy or pericarditis) is a contraindication for the Lariat procedure. In the next step, the Lariat™ Suture Delivery Device (SentreHEART, Inc.; Palo Alto, CA) is introduced into the pericardial space over the epicardial wire to deliver a pretied suture loop over the LAA. This delivery device was not specifically designed for LAA occlusion; it has been used for soft tissue closure in other organ systems.

As the suture loop is being lassoed over the LAA orifice, a balloon attached to the endocardial wire is inflated at the LAA orifice to prevent the suture from slipping away from the orifice. When the suture is nearly completely tied, the endocardial wire is removed from the LAA (Figs 28.38A to D).

At the end of the procedure, the suture is completely tied and the LAA is excluded from the body of the left atrium (Figs 28.39A and B). 2D and 3D color Doppler imaging is crucial for ascertaining that no significant residual communication between the LAA and the left atrium is present. In addition, TEE imaging is crucial in monitoring for possible procedure-related pericardial effusion.

The feasibility and safety of the Lariat procedure has been demonstrated in case series but the outcomes data are still lacking.[117] Specifically, there are no long-term data on the risk of pericardial injury related to pericardial access used in the Lariat procedure.

GUIDANCE OF ELECTROPHYSIOLOGY PROCEDURES

The role of TEE prior to or during electrophysiology procedures is well established. 2D- and 3D TEE is routinely used to exclude left heart thrombus prior to cardioversion[118] or to guide transseptal puncture. 3D TEE is valuable in visualizing the right atrial structures of special interest to electrophysiologists such as the cavotricuspid isthmus and crista terminalis.[119] In addition, 3D TEE is now being utilized to guide pulmonary vein isolation during atrial fibrillation ablation.

Pulmonary Vein Isolation for Atrial Fibrillation

As pointed out in the section on the LAA exclusion, atrial fibrillation is the most common sustained cardiac arrhythmia whose prevalence increases in age
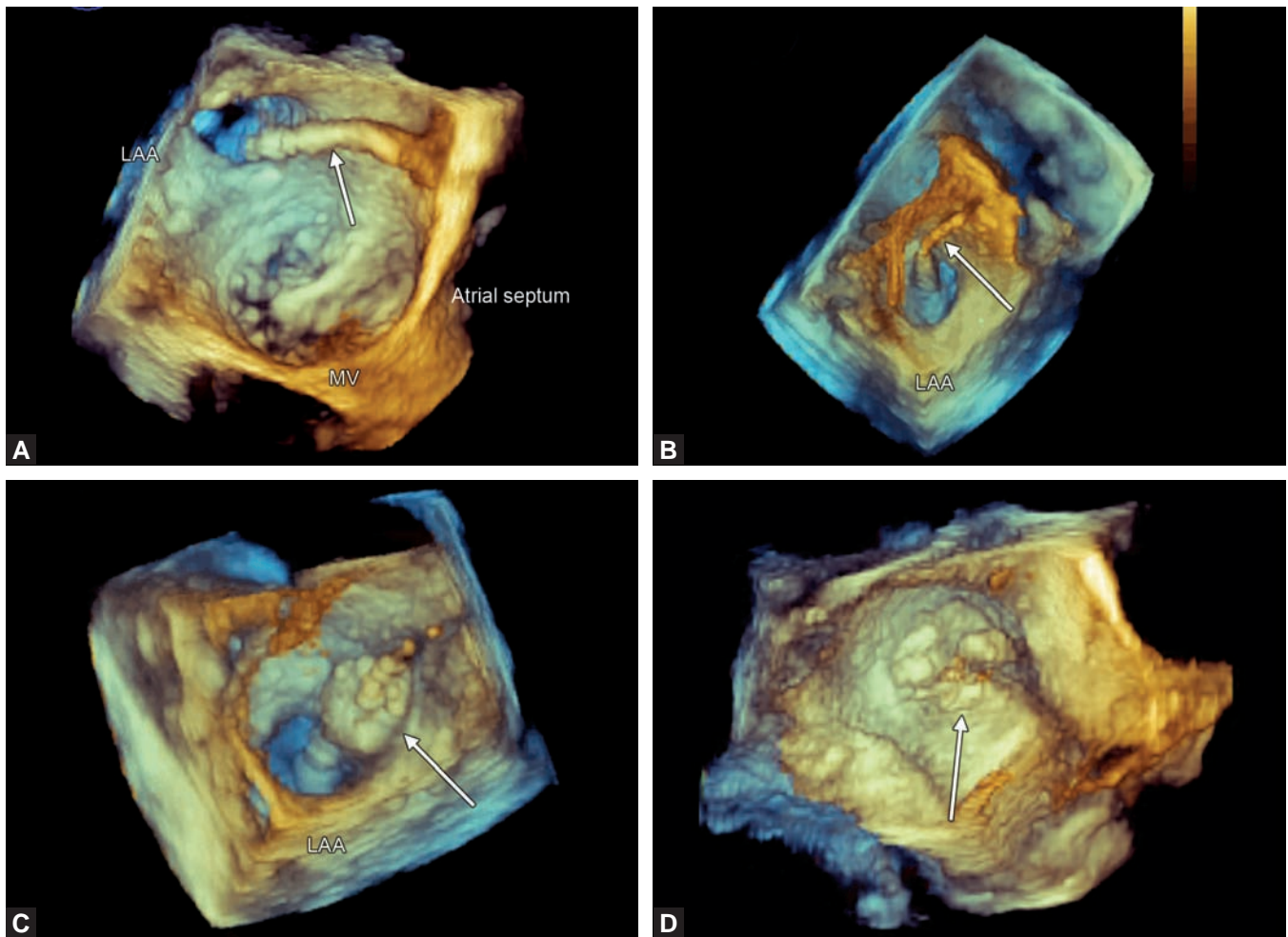
Figs 28.38A to D: Lariat procedure guidance by 3D TEE. (A) After a trans-septal puncture, the endocardial wire and its sheath (arrow) are guided toward the orifice of the LAA (LAA); (B) The endocardial wire (arrow) is seen entering the LAA; (C) In preparation for snaring of the LAA from the epicardial side, a balloon attached to the endocardial wire (arrow) is inflated at the orifice of the LAA; (D) 3D TEE en face zoom image of the ligated LAA orifice (arrow) after completion of the Lariat procedure. (MV: Mitral valve).
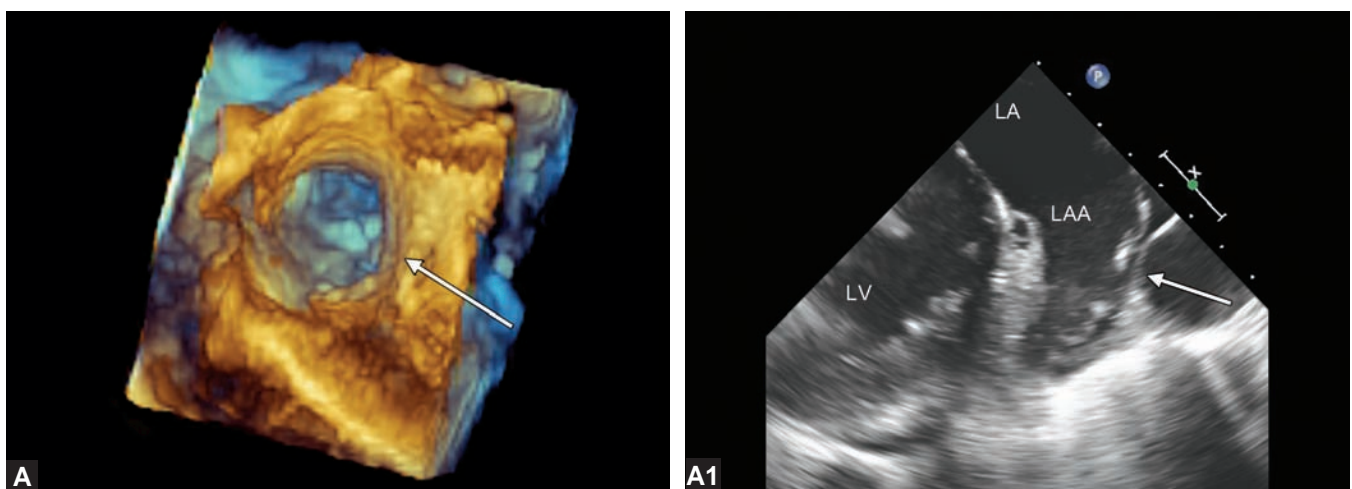
Figs 28.39A and A1
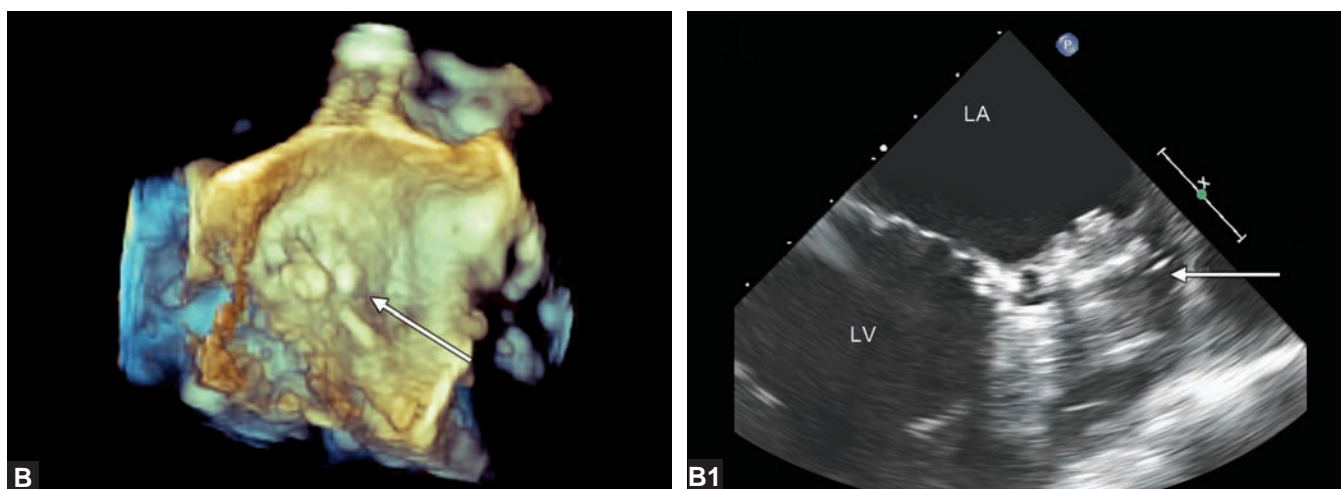
Figs 28.39A and B: LAA appearance before and after Lariat procedure. Appearance of the LAA before (A) and after the Lariat procedure (B). Each figure has a 3D TEE en face zoom image (left) and 2D TEE image (right). (LA: Left atrium; LAA: Left atrial appendage; LV: Left ventricle).

(from 1% in general population to about 10% in the octogenarians).[120] Atrial fibrillation may present with disabling symptoms, thromboembolism and tachycardia-induced cardiomyopathy. Despite its disorderly rhythm, atrial fibrillation is often triggered in an orderly fashion by ectopic beats in the region of pulmonary vein ostia. This insight led to development of techniques for catheter-based pulmonary vein isolation[121] and isolation of other atrial foci.[122] Collectively these procedures are referred to as atrial fibrillation ablation.

Catheter-based atrial fibrillation ablation has been shown in a randomized trial to be more effective than drug therapy in preventing recurrence of paroxysmal atrial fibrillation.[123] At present, catheter ablation is indicated for maintenance of sinus rhythm in selected patients with significantly symptomatic paroxysmal atrial fibrillation who have failed treatment with an antiarrhythmic drug and have normal or mildly dilated left atria, normal or mildly reduced LV function, and no severe pulmonary disease. Additionally, catheter ablation is reasonable to treat symptomatic persistent atrial fibrillation or symptomatic paroxysmal atrial fibrillation in patients with significant left atrial dilatation or with significant LV dysfunction.[124]

In a typical clinical scenario, prior to atrial fibrillation ablation patients undergo either CT or MRI of the chest to define the anatomy of the pulmonary veins and other cardiac structures. Subsequently, patients are brought the electrophysiology suite where 2D TEE imaging is used primarily to exclude intracardiac thrombus and to further delineate cardiac anatomy.[125] Patients then undergo atrial

fibrillation ablation guided by electrical mapping and fluoroscopy. The major shortcomings of such a scenario that CT, MRI, TEE, fluoroscopy, and electrical mapping are not done simultaneously and image integration from various modalities is still a challenge.

Some electrophysiologists opt to use ICE for real time imaging during the ablation procedure.[126,127] In addition to imaging cardiac structures, ICE can also visualize the esophagus and thus monitor for esophageal injury (left atrio-esophageal fistula), a rare but serious complication of the ablation procedure.[128] However, ICE has its own shortcomings: it is invasive, costly, and provides only 2D cross-sectional images.

3D TEE imaging during atrial fibrillation imaging overcomes more of the shortcomings of other imaging modalities. It can provide en face views of pulmonary veins and other cardiac structures in real time.[129] Thus, one can determine the number and location of pulmonary vein ostia. There are typically two pulmonary vein ostia on the right and two ostia on the left (Figs 28.40A to D). However, there are many variations; the most frequent one being the common ostium (antrum) of the two left pulmonary veins or three pulmonary ostia on the right (with the right middle pulmonary vein entering the left atrium directly rather than being a tributary of the right upper pulmonary vein (RUPV; Figs 28.41A and B).[130] During the ablation procedure, 3D TEE can be used to guide the transseptal puncture. In addition, 3D TEE can provide real time 3D anatomic guidance for placement of mapping and ablation catheters that cannot be achieved at present by any other imaging technique (Figs 28.42A to C).[131,132]
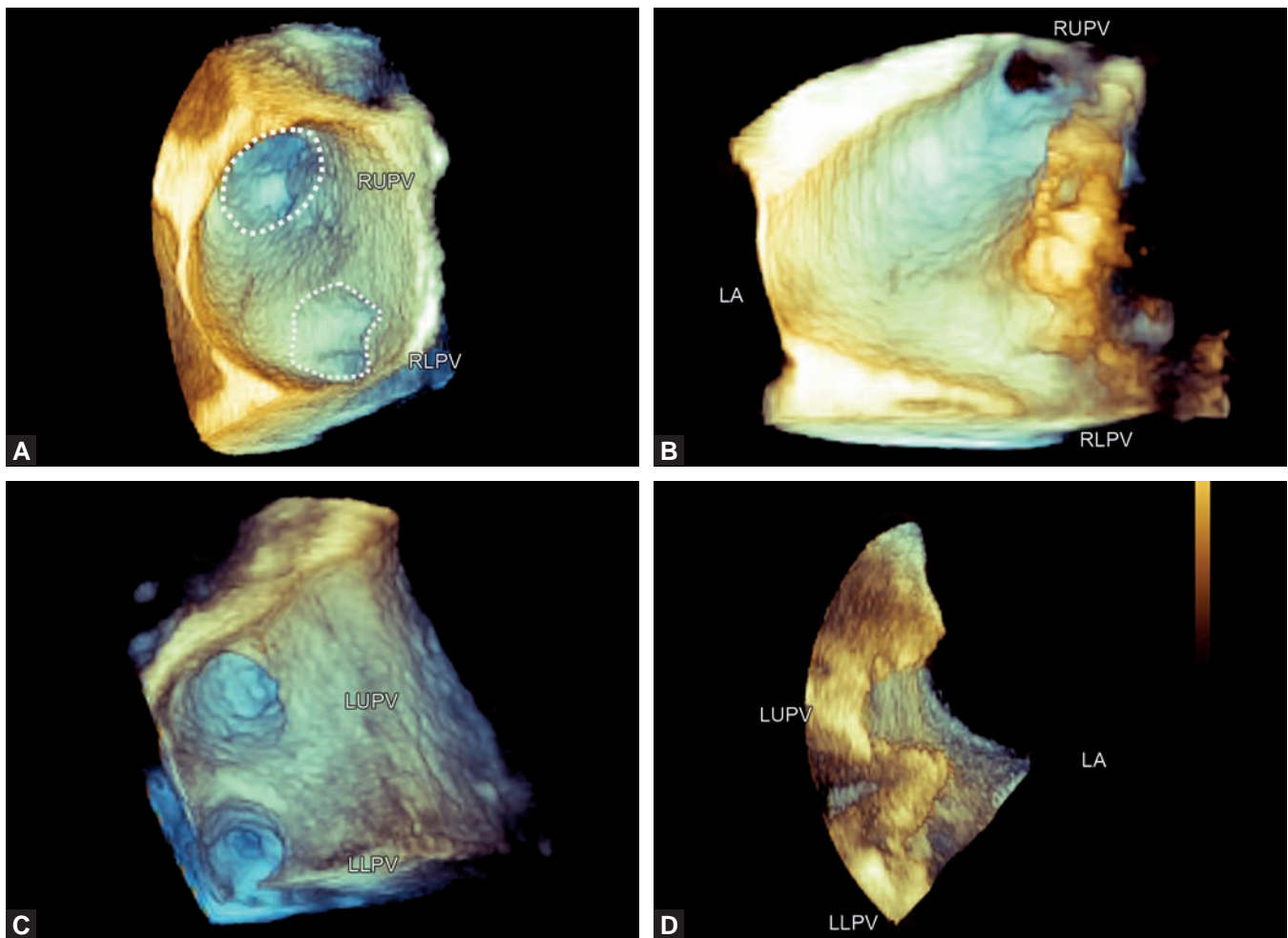
Figs 28.40A to D: 3D TEE appearance of typical pulmonary vein ostia. 3D TEE zoom views of pulmonary vein ostia in the left atrium (LA). With current 3D TEE, all four pulmonary vein ostia cannot be seen at once. Instead one visualizes separately right-sided then left-sided pulmonary vein ostia. (A and B) Ostia of the right-sided pulmonary veins seen en face (A) and in the long axis (B); (C and D) Ostia of the left-sided pulmonary veins seen en face (A) and in the long axis (B). (LUPV: Left upper pulmonary vein; LLPV: Left lower pulmonary vein RUPV: Right upper pulmonary vein; RLPV: Right lower pulmonary vein).

2D and 3D TEE can also be used to monitor for procedural complications such as the pericardial effusion. Doppler imaging is used to assess for pulmonary vein stenosis, a long-term complication of pulmonary vein ablation. Pulmonary vein stenosis is defined as a combination of a diminished diameter of the pulmonary vein ostium (< 0.7 cm; normal ~1.5 cm) and an increase in the peak velocity of the pulmonary vein diastolic (D) wave (> 100 cm/sec; normal 40-60 cm/sec).[125]

MISCELLANEOUS PROCEDURES

The utility of 3DE has also been demonstrated in a variety of other percutaneous procedures such as the closure of the LV pseudoaneurysm, alcohol septal ablation, and right ventricular endomyocardial biopsy.

Left Ventricular Pseudoaneurysm Closure

LV pseudoaneurysm is a rare but potentially serious complication of myocardial Infarction or cardiac surgery. It represents a rupture of the LV free wall that is contained by adherent pericardium or scar tissue. The goal of therapy is to prevent conversion of this contained rupture into complete rupture leading to pericardial tamponade and possibly death. Unrepaired LV pseudoaneurysm has high mortality.
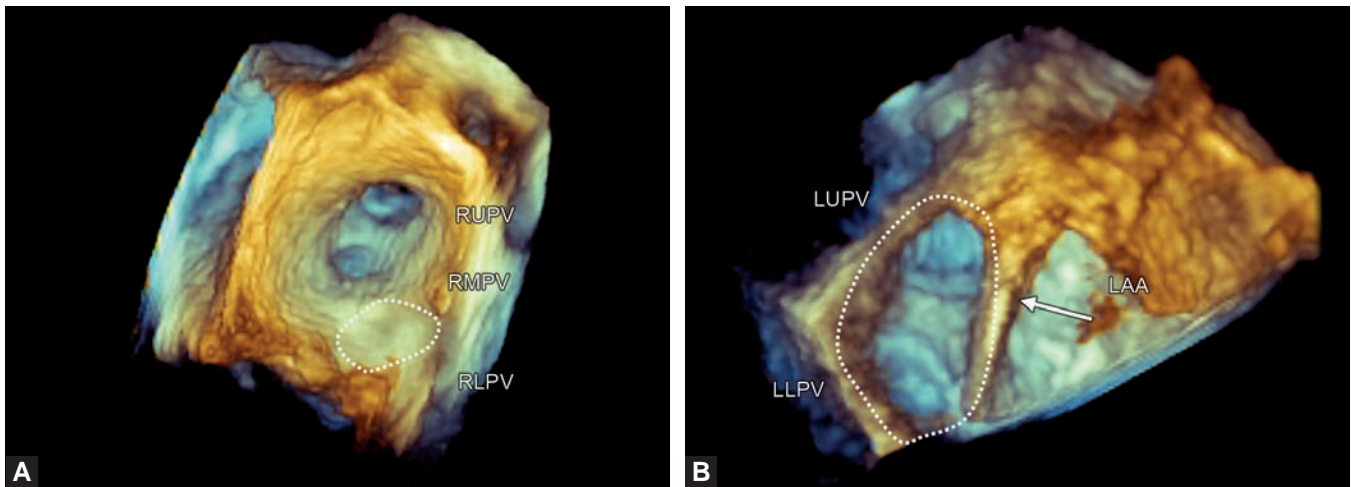
Figs 28.41A and B: 3D TEE appearance of common pulmonary vein variants. (A) 3D TEE zoom en face image demonstrates the most common variant of right sided pulmonary vein ostia, namely the right middle pulmonary vein (RMPV) having a separate left atrial ostium. This is in contrast to most normal individuals in whom the RMPV is a tributary of the RUPV; (B) 3D TEE zoom en face image of the most common variant of left-sided pulmonary ostia, namely the common antrum created by the confluence of the left upper pulmonary vein (LUPV) and the left lower pulmonary vein (LLPV). Irrespective of whether there is one common or two separate left-sided pulmonary ostia, the ligament of Marshall, also known as the left atrial or Coumadin ridge (arrow) separates the pulmonary ostia from the LAA. (RLPV: Right lower pulmonary vein).
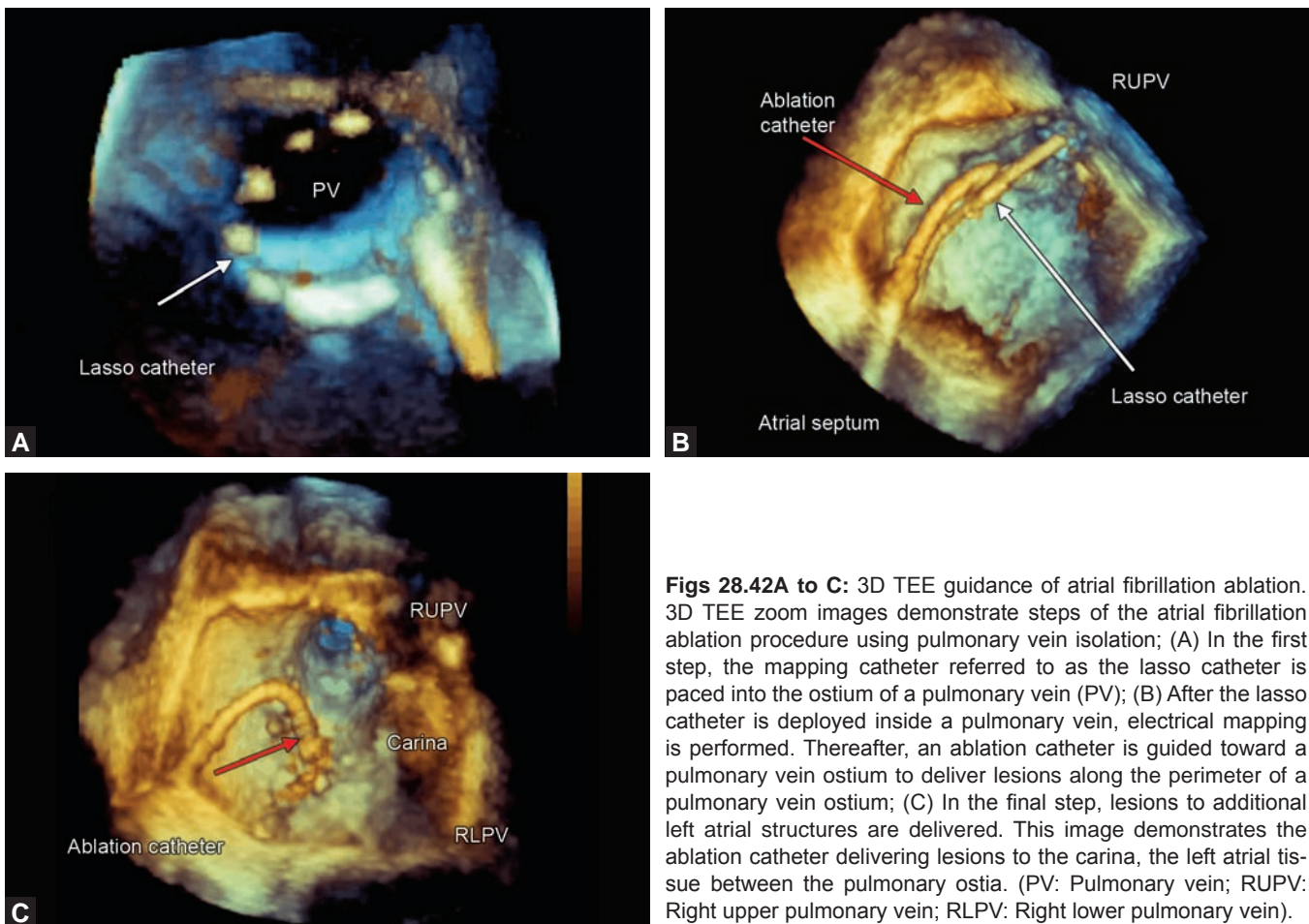
Figs 28.42A to C: 3D TEE guidance of atrial fibrillation ablation. 3D TEE zoom images demonstrate steps of the atrial fibrillation ablation procedure using pulmonary vein isolation; (A) In the first step, the mapping catheter referred to as the lasso catheter is paced into the ostium of a pulmonary vein (PV); (B) After the lasso catheter is deployed inside a pulmonary vein, electrical mapping is performed. Thereafter, an ablation catheter is guided toward a pulmonary vein ostium to deliver lesions along the perimeter of a pulmonary vein ostium; (C) In the final step, lesions to additional left atrial structures are delivered. This image demonstrates the ablation catheter delivering lesions to the carina, the left atrial tissue between the pulmonary ostia. (PV: Pulmonary vein; RUPV: Right upper pulmonary vein; RLPV: Right lower pulmonary vein).
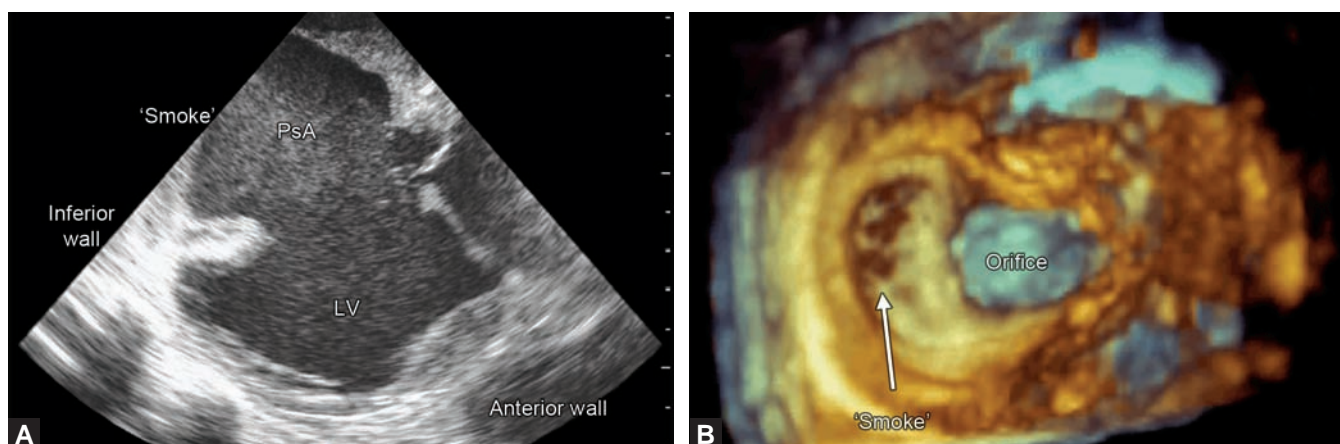
Figs 28.43A and B: 2D/3D appearance of left ventricular pseudoaneurysm. (A) 2D TEE transgastric view demonstrating a large left ventricular (LV) pseudoaneurysm (PsA) in a patient with prior inferior wall myocardial infarction. Note the appearance of spontaneous echo contrast ("smoke") in the pseudoaneurysm space; (B) Full-volume 3D TEE image of the LV pseudoaneurysm. The external wall of the pseudoaneurysm is cropped out to reveal the defect in the inferior wall which creates the orifice of the LV pseudoaneurysm. There is spontaneous echo contrast ("smoke") in the pseudoaneurysm space. (Movie clip 28.43B corresponds to Figure 28.43B).
Courtesy: Images in this figure by Jan R Purgess, Department of Anesthesiology, New York University School of Medicine and New York Veterans Affairs Hospital, New York, NY.

Historically, surgery has been the only means of repairing LV pseudoaneurysm (Figs 28.43A and B and Movie clip 28.43B); however, such surgeries themselves have significant mortality and morbidity as well.[133] Percutaneous closure of an LV pseudoaneurysm was first reported in 2004 from a hospital in the United Kingdom with an off-label use of the Amplatzer™ atrial septal occluder.[134] Experience with percutaneous LV pseudoaneurysm closures is limited to case series, the largest to date consisting of seven patients.[135] Multimodality imaging, including 3DE, is essential for the success of percutaneous LV pseudoaneurysm closure.[136] Utility of 3D TEE of LV pseudoaneurysm closure is similar to that of VSD closure described earlier in this chapter.

Alcohol Septal Ablation for Hypertrophic Obstructive Cardiomyopathy

Alcohol septal ablation, first reported in 1995, is an alternative to surgical myomectomy used for relief of LV obstruction is hypertrophic obstructive cardiomyopathy.[137] It entails intracoronary injection of alcohol into the septal perforator branch supplying the myocardium in the region asymmetric septal hypertrophy. Successful alcohol septal ablation leads to limited iatrogenic septal infarction, septal thinning, and subsequent diminution of mitral septal contact and LV outflow obstruction. The role of 2DE is well established including the off-label use of microbubble echo contrast injected intra-arterially into the septal perforator branch.[138]

3D TEE imaging may improve localization of the mitral-septal contact, which is often displaced eccentrically within the LVOT. However, in contrast to most other percutaneous interventions, 3D TEE imaging cannot provide immediate assessment of procedural success of alcohol septal ablation since LV obstruction relief is expected to occur hours or days after septal infarct completion.

Right Ventricular Endomyocardial Biopsy

Right ventricle (RV) is the primary site of endomyocardial biopsies which are used in the diagnostic workup of myocarditis, infiltrative cardiomyopathies, cardiac transplant rejection, and other myocardial disorders. Although endomyocardial biopsy is often performed using fluoroscopic guidance alone, both TEE and ICE[139] may help define the anatomy better, guide the deployment of the bioptome tip to the desired region of the heart, and potentially increase the safety of the procedure [by avoidance of the tricuspid valve (TV) apparatus, for instance]. The utility of 3DE in RV endomyocardial biopsy has been shown in case reports and case series.[140,141]

ACKNOWLEDGMENTS

▌ REFERENCES

1. Rashkind WJ. Palliative procedures for transposition of the great arteries. Br Heart J. 1971;33(Suppl):69–72.
2. Saric M, Gila P, Ruiz C, et al. Chapter 11: Catheter-based procedures to repair structural heart diseases. In: Lang RM, Shernan SK, Shirali G, editors. Comprehensive Atlas of 3D Echocardiography. 1 Har/Psc ed. Philadelphia, PA: Lippincott Williams & Wilkins; December 20, 2012:219–54.
3. Garcia Fernandez MA, Perk G, Saric M, et al. Chapter 12: Real time three-dimensional transesophageal echocardiography for guidance of catheter based interventions. In Badano LP, Lang RM, Zamorano JL, editors. Textbook of Real time Three-Dimensional Echocardiography. 1st ed. New York, NY: Springer; March 9, 2011: 121–34.
4. Houck RC, Cooke JE, Gill EA. Live 3D echocardiography: a replacement for traditional 2D echocardiography? AJR Am J Roentgenol. 2006;187(4):1092–106.
5. Sugeng L, Shernan SK, Salgo IS, et al. Live 3-dimensional transesophageal echocardiography initial experience using the fully-sampled matrix array probe. J Am Coll Cardiol. 2008;52(6):446–9.
6. Salcedo EE, Quaife RA, Seres T, et al. A framework for systematic characterization of the mitral valve by real time three-dimensional transesophageal echocardiography. J Am Soc Echocardiogr. 2009;22(10):1087–99.
7. Sudhakar S, Khairnar P, Nanda NC. Live/real time three-dimensional transesophageal echocardiography. Echocardiography. 2012;29(1):103–11.
8. Ross J Jr. Transeptal left heart catheterization: a new method of left atrial puncture. Ann Surg. 1959;149(3):395–401.
9. Brockenbrough EC, Braunwald E, Ross J Jr. Transseptal left heart catheterization. A review of 450 studies and description of an improved technic. Circulation. 1962;25:15–21.
10. De Ponti R, Cappato R, Curnis A, et al. Trans-septal catheterization in the electrophysiology laboratory: data from a multicenter survey spanning 12 years. J Am Coll Cardiol. 2006;47(5):1037–42.
11. Silvestry FE, Kerber RE, Brook MM, et al. Echocardiography-guided interventions. J Am Soc Echocardiogr. 2009;22(3):213–31; quiz 316.
12. Ho SY, Chang SD, Liang CC. Simultaneous uterine and urinary bladder rupture in an otherwise successful vaginal birth after cesarean delivery. J Chin Med Assoc. 2010;73(12):655–9.
13. Ho SY. Embryology and anatomy of the atrial septum. In: Thakur R, Natale A, (editors). Transseptal catheterization and interventions. Minneapolis, MN: Cardiotext; 2010:|11-26.
14. Faletra FF, Nucifora G, Ho SY. Imaging the atrial septum using real time three-dimensional transesophageal echocardiography: technical tips, normal anatomy, and its role in transseptal puncture. J Am Soc Echocardiogr. 2011;24(6):593–9.
15. Webster MW, Chancellor AM, Smith HJ, et al. Patent foramen ovale in young stroke patients. Lancet. 1988;2(8601):11–2.
16. Tomlinson DR, Sabharwal N, Bashir Y, et al. Interatrial septum thickness and difficulty with transseptal puncture during redo catheter ablation of atrial fibrillation. Pacing Clin Electrophysiol. 2008;31(12):1606–11.
17. Wieczorek M, Hoeltgen R, Akin E, et al. Use of a novel needle wire in patients undergoing transseptal puncture associated with severe septal tenting. J Interv Card Electrophysiol. 2010;27(1):9–13.
18. Waterston DS. Léčení Fallotovy tetralogie u děí do jednogo roku věki. [Treatment of Fallot's tetralogy in infants under the age of one year.] [Article in Czech] Rozhl Chir. 1962;41:181–3.
19. Søndergaard T, Gotsche H, Ottoson P, et al. Surgical closure of interatrial septal defects by circumclusion. Acta Chir Scand. 1955;109:188–96.
20. Kronzon I, Saric M, Lang RM. Chapter 9: Mitral stenosis. In: Lang R, Goldstein SA, Kronzon I, Khanderia BK, editors. Dynamic Echocardiography: A Case-Based Approach. 1 ed. New York, NY: Springer; July 1, 2010:38–45.
21. Fleming PR. A Short History of Cardiology. Amsterdam, Netherlands—Atlanta, GA: Editions Rodopi Bv; January 1997.
22. Vieussens R. Traité nouveau de la structure et des causes du mouvement naturel du coeur [Treatise on the structure of the heart and the causes of its natural motion]. Toulouse, France;1715.
23. Chandrashekhar Y, Westaby S, Narula J. Mitral stenosis. Lancet. 2009;374(9697):1271–83.
24. Cutler EC, Levine SA. Cardiotomy and valvulotomy for mitral stenosis. Experimental observations and clinical notes concerning an operated case with recovery. Boston Med Surg J. 1923;188:1023–7.
25. Souttar HS. The surgical treatment of mitral stenosis. Br Med J. 1925;2(3379):603–6.
26. Gonzalez-Lavin L. Charles P. Bailey and Dwight E. Harken—the dawn of the modern era of mitral valve surgery. Ann Thorac Surg. 1992;53(5):916–9.
27. Matthews AM. The development of the Starr-Edwards heart valve. Tex Heart Inst J. 1998;25(4):282–93.
28. Edler I, Hertz CH. The use of ultrasonic reflectoscope for the continuous recording of the movements of heart walls. 1954. Clin Physiol Funct Imaging. 2004;24(3):118–36.
29. Starr A, Herr RH, Wood JA. The present status of valve replacement. Special issue on the VII Congress of the International Cardiovascular Society held Sept 14–18, 1965, in Philadelphia. J Cardiovasc Surg. 1965:95–103.
30. Inoue K, Owaki T, Nakamura T, et al. Clinical application of transvenous mitral commissurotomy by a new balloon catheter. J Thorac Cardiovasc Surg. 1984;87(3):394–402.
31. Bonow RO, Carabello BA, Kanu C, et al. ACC/AHA 2006 guidelines for the management of patients with valvular heart disease: a report of the American College of Cardiology/American Heart Association Task Force on Practice Guidelines (writing committee to revise the 1998 Guidelines for the Management of Patients With Valvular Heart Disease): developed in collaboration with the Society of Cardiovascular Anesthesiologists: endorsed by the

Society for Cardiovascular Angiography and Interventions and the Society of Thoracic Surgeons. Circulation. August 1, 2006;114(5):e84–231.

32. Schlosshan D, Aggarwal G, Mathur G, et al. Real-time 3D transesophageal echocardiography for the evaluation of rheumatic mitral stenosis. JACC Cardiovasc Imaging. 2011; 4(6):580–8.

33. Perk, G., Ruiz, C., Saric, M., et al. Real-time three-dimensional transesophageal echocardiography in trans-cutaneous, catheter-based procedures for repair of structural heart diseases. Curr Cardiovasc Imaging Rep. 2009;2(5):363–74.

34. Wilkins GT, Weyman AE, Abascal VM, et al. Percutaneous balloon dilatation of the mitral valve: an analysis of echocardiographic variables related to outcome and the mechanism of dilatation. Br Heart J. 1988;60(4):299–308.

35. Yun KL, Miller DC. Mitral valve repair versus replacement. Cardiol Clin. 1991;9(2):315–27.

36. Oliveira JM, Antunes MJ. Mitral valve repair: better than replacement. Heart. 2006;92(2):275–81.

37. Carpentier A. Cardiac valve surgery–the "French correction." J Thorac Cardiovasc Surg. 1983;86(3):323–37.

38. Binet JP, Carpentier A, Langlois J, et al. [Implantation of heterogenic valves in the treatment of aortic cardio-pathies]. CR Hebd Seances Acad Sci, Ser D, Sci Nat. 1965;261(25):5733–4.

39. Feldman T, Cilingiroglu M. Percutaneous leaflet repair and annuloplasty for mitral regurgitation. J Am Coll Cardiol. 2011;57(5):529–37.

40. Fucci C, Sandrelli L, Pardini A, et al. Improved results with mitral valve repair using new surgical techniques. Eur J Cardiothorac Surg. 1995;9(11):621–6; discuss 626.

41. Alfieri O, Maisano F, De Bonis M, et al. The double-orifice technique in mitral valve repair: a simple solution for complex problems. J Thorac Cardiovasc Surg. 2001; 122(4):674–81.

42. Feldman T, Foster E, Glower DD, et al.; EVEREST II Investigators. Percutaneous repair or surgery for mitral regurgitation. N Engl J Med. 2011;364(15):1395–406.

43. Maisano F, Michev I, La Canna G, et al. Brief description of the percutaneous mitral repair procedure using the MitraClip® device. http://www.ctsnet.org/portals/endovascular/evolvingtechnology/exp_tech1.html, accessed on April 13, 2013.

44. Benenstein R, Saric M. Mitral valve prolapse: role of 3D echocardiography in diagnosis. Curr Opin Cardiol. 2012;27(5):465–76.

45. Feldman T, Wasserman HS, Herrmann HC, et al. Percut-aneous mitral valve repair using the edge-to-edge technique: six-month results of the EVEREST Phase I Clinical Trial. J Am Coll Cardiol. 2005;46(11):2134–40.

46. Faletra FF, Pedrazzini G, Pasotti E, et al. Role of real-time three dimensional transoesophageal echocardiography as guidance imaging modality during catheter based edge-to-edge mitral valve repair. Heart. 2013;99(16):1204–15.

47. Saric M, Kronzon I. Aortic stenosis in the elderly. Am J Geriatr Cardiol. 2000;9:321–9, 345.

48. Ross J Jr, Braunwald E. Aortic stenosis. Circulation. 1968; 38(1 Suppl):61–7.

49. Schwarz F, Baumann P, Manthey J, et al. The effect of aortic valve replacement on survival. Circulation. 1982;66(5): 1105–10.

50. Webb JG, Wood DA. Current status of transcatheter aortic valve replacement. J Am Coll Cardiol. 2012;60(6):483–92.

51. Harken DE, Soroff HS, Taylor WJ, et al. Partial and complete prostheses in aortic insufficiency. J Thorac Cardiovasc Surg. 1960;40:744–62.

52. Brown JM, O'Brien SM, Wu C, et al. Isolated aortic valve replacement in North America comprising 108,687 patients in 10 years: changes in risks, valve types, and outcomes in the Society of Thoracic Surgeons National Database. J Thorac Cardiovasc Surg. 2009;137(1):82–90.

53. Cribier A, Savin T, Saoudi N, et al. Percutaneous translu-minal valvuloplasty of acquired aortic stenosis in elderly patients: an alternative to valve replacement? Lancet. 1986;1(8472):63–7.

54. Ben-Dor I, Pichard AD, Satler LF, et al. Complications and outcome of balloon aortic valvuloplasty in high-risk or inoperable patients. JACC Cardiovasc Interv. 2010;3(11): 1150–6.

55. Cribier A, Eltchaninoff H, Bash A, et al. Percutaneous transcatheter implantation of an aortic valve prosthesis for calcific aortic stenosis: first human case description. Circulation. 2002;106(24):3006–8.

56. Andersen HR, Knudsen LL, Hasenkam JM. Transluminal implantation of artificial heart valves. Description of a new expandable aortic valve and initial results with implantation by catheter technique in closed chest pigs. Eur Heart J. 1992;13(5):704–8.

57. Smith CR, Leon MB, Mack MJ, et al.; PARTNER Trial Investigators. Transcatheter versus surgical aortic-valve replacement in high-risk patients. N Engl J Med. 2011; 364(23):2187–98.

58. Forrest JK. Transcatheter aortic valve replacement: design, clinical application, and future challenges. Yale J Biol Med. 2012;85(2):239–47.

59. Gila P, Kronzon I, Saric M. Chapter 9: Aortic valve. In: Lang RM, Shernan SK, Shirali G, editors. Comprehensive Atlas of 3D Echocardiography. 1 Har/Psc ed. Philadelphia, PA: Lippincott Williams & Wilkins; December 20, 2012: 183–200.

60. Gaspar T, Adawi S, Sachner R, et al. Three-dimensional imaging of the left ventricular outflow tract: impact on aortic valve area estimation by the continuity equation. J Am Soc Echocardiogr. 2012;25(7):749–57.

61. Otani K, Takeuchi M, Kaku K, et al. Assessment of the aortic root using real-time 3D transesophageal echocardiography. Circ J. 2010;74(12):2649–57.

62. Jabbour A, Ismail TF, Moat N, et al. Multimodality imaging in transcatheter aortic valve implantation and post-procedural aortic regurgitation: comparison among cardiovascular magnetic resonance, cardiac computed tomography, and echocardiography. J Am Coll Cardiol. 2011;58(21):2165–73.

63. Jilaihawi H, Doctor N, Kashif M, et al. Aortic annular sizing for transcatheter aortic valve replacement using cross-sectional 3-dimensional transesophageal echocardiography. J Am Coll Cardiol. 2013;61(9):908–16.

64. Smith LA, Dworakowski R, Bhan A, et al. Real-time three-dimensional transesophageal echocardiography adds value to transcatheter aortic valve implantation. J Am Soc Echocardiogr. 2013;26(4):359–69.

65. Jilaihawi H, Chakravarty T, Weiss RE, et al. Meta-analysis of complications in aortic valve replacement: comparison of Medtronic-Corevalve, Edwards-Sapien and surgical aortic valve replacement in 8,536 patients. Catheter Cardiovasc Interv. 2012;80(1):128–38.

66. Latson LA. Transcatheter closure of paraprosthetic valve leaks after surgical mitral and aortic valve replacements. Expert Rev Cardiovasc Ther. 2009;7(5):507–14.

67. Maraj R, Jacobs LE, Ioli A, et al. Evaluation of hemolysis in patients with prosthetic heart valves. Clin Cardiol. 1998;21(6):387–92.

68. Echevarria JR, Bernal JM, Rabasa JM, et al. Reoperation for bioprosthetic valve dysfunction. A decade of clinical experience. Eur J Cardiothorac Surg. 1991;5(10):523–6; discussion 527.

69. Hourihan M, Perry SB, Mandell VS, et al. Transcatheter umbrella closure of valvular and paravalvular leaks. J Am Coll Cardiol. 1992;20(6):1371–7.

70. Sorajja P, Cabalka AK, Hagler DJ, et al. Percutaneous repair of paravalvular prosthetic regurgitation: acute and 30-day outcomes in 115 patients. Circ Cardiovasc Interv. 2011;4(4):314–21.

71. Kronzon I, Sugeng L, Perk G, et al. Real-time 3-dimensional transesophageal echocardiography in the evaluation of post-operative mitral annuloplasty ring and prosthetic valve dehiscence. J Am Coll Cardiol. 2009;53(17):1543–7.

72. Hoffmayer KS, Zellner C, Kwan DM, et al. Closure of a para-valvular aortic leak: with the use of 2 AMPLATZER devices and real-time 2- and 3-dimensional transesophageal echocardiography. Tex Heart Inst J. 2011;38(1):81–4.

73. Rihal CS, Sorajja P, Booker JD, et al. Principles of percutaneous paravalvular leak closure. JACC Cardiovasc Interv. 2012;5(2):121–30.

74. Ruiz CE, Jelnin V, Kronzon I, et al. Clinical outcomes in patients undergoing percutaneous closure of periprosthetic paravalvular leaks. J Am Coll Cardiol. 2011;58(21):2210–7.

75. Saric M, Kronzon I. Chapter 108: Patent ductus arteriosus. In: Lang R, Goldstein SA, Kronzon I, Khanderia BK, editors. Dynamic Echocardiography: A Case-Based Approach. 1 ed. New York, NY: Springer; July 1, 2010: 451–4.

76. Gross RE, Hubbard JP. Surgical ligation of a patent ductus arteriosus. Report of first successful case. JAMA. 1939; 112(8):729–31.

77. Porstmann W, Wierny L, Warnke H. [The closure of the patent ductus arteriosus without thoractomy. (preliminary report)]. Thoraxchir Vask Chir. 1967;15(2):199–203.

78. Warnes CA, Williams RG, Bashore TM, et al. ACC/AHA 2008 Guidelines for the Management of Adults with Congenital Heart Disease: a report of the American College of Cardiology/American Heart Association Task Force on Practice Guidelines (writing committee to develop guidelines on the management of adults with congenital heart disease). Circulation. 2008;118(23):e714–833.

79. Krichenko A, Benson LN, Burrows P, et al. Angiographic classification of the isolated, persistently patent ductus arteriosus and implications for percutaneous catheter occlusion. Am J Cardiol. 1989;63(12):877–80.

80 Roushdya A, El Fikyb A, Ezz el Dine D. Visualization of patent ductus arteriosus using real-time three-dimensional echocardiogram: Comparative study with 2D echocardiogram and angiography. Journal of the Saudi Heart Association. 2012;24(3):177–86.

81. Marek T, Zelizko M, Kautzner J. Images in cardiovascular medicine. Real-time 3-dimensional transesophageal echocardiography imaging: adult patent ductus arteriosus before and after transcatheter closure. Circulation. 2009;120(12):e92–3.

82. Chuang YC, Yin WH, Hsiung MC, et al. Successful transcatheter closure of a residual patent ductus arteriosus with complex anatomy after surgical ligation using an amplatzer ductal occluder guided by live three-dimensional transesophageal echocardiography. Echocardiography. 2011;28(5):E101–3.

83. Lam J, Tanke RB, van Oort A, et al. The use of transesophageal echocardiography monitoring of transcatheter closure of a persistent ductus arteriosus. Echocardiography. 2001; 18(3):197–202.

84 Saric M, Kronzon I. Chapter 105: Congenital heart disease in adults. In: Lang R, Goldstein SA, Kronzon I, Khanderia BK, editors. Dynamic Echocardiography: A Case-Based Approach. 1 ed. New York, NY: Springer; July 1, 2010:438–9.

85. Lewis FJ, Taufic M. Closure of atrial septal defects with the aid of hypothermia; experimental accomplishments and the report of one successful case. Surgery. 1953;33(1):52–9.

86. Gibbon JH Jr. Application of a mechanical heart and lung apparatus to cardiac surgery. Minn Med. 1954;37(3):171–85; passim.

87. King TD, Mills NL. Nonoperative closure of atrial septal defects. Surgery. 1974;75(3):383–8.

88. Vaidyanathan B, Simpson JM, Kumar RK. Transesophageal echocardiography for device closure of atrial septal defects: case selection, planning, and procedural guidance. JACC Cardiovasc Imaging. 2009;2(10):1238–42.

89. Roberson DA, Cui W, Patel D, et al. Three-dimensional transesophageal echocardiography of atrial septal defect: a qualitative and quantitative anatomic study. J Am Soc Echocardiogr. 2011;24(6):600–10.

90. Saric M, Perk G, Purgess JR, et al. Imaging atrial septal defects by real-time three-dimensional transesophageal echocardiography: step-by-step approach. J Am Soc Echocardiogr. 2010;23(11):1128–35.

91. Vettukattil JJ, Ahmed Z, Salmon AP, et al. Defects in the oval fossa: morphologic variations and impact on transcatheter closure. J Am Soc Echocardiogr. 2013;26(2):192–9.

92. Razzouk L, Saric M, Slater JN. Placement of a large Gore-Helex atrial septal occluder device in a patient with

deficient aortic rim and large atrial septal aneurysm. Closing Remarks Newsletter, Spring 2013; Issue XXII.

93. Amin Z. Transcatheter closure of secundum atrial septal defects. Catheter Cardiovasc Interv. 2006;68(5):778–87.

94. Mathewson JW, Bichell D, Rothman A, et al. Absent posteroinferior and anterosuperior atrial septal defect rims: Factors affecting nonsurgical closure of large secundum defects using the Amplatzer occluder. J Am Soc Echocardiogr. 2004;17(1):62–9.

95. Hagen PT, Scholz DG, Edwards WD. Incidence and size of patent foramen ovale during the first 10 decades of life: an autopsy study of 965 normal hearts. Mayo Clin Proc. 1984;59(1):17–20.

96. Lechat P, Mas JL, Lascault G, et al. Prevalence of patent foramen ovale in patients with stroke. N Engl J Med. 1988;318(18):1148–52.

97. Bridges ND, Hellenbrand W, Latson L, et al. Transcatheter closure of patent foramen ovale after presumed paradoxical embolism. Circulation. 1992;86(6):1902–08.

98. Furlan AJ, Reisman M, Massaro J, et al.; CLOSURE I Investigators. Closure or medical therapy for cryptogenic stroke with patent foramen ovale. N Engl J Med. 2012; 366(11):991–99.

99. Meier B, Kalesan B, Mattle HP, et al.; PC Trial Investigators. Percutaneous closure of patent foramen ovale in cryptogenic embolism. N Engl J Med. 2013;368(12):1083–91.

100. Minette MS, Sahn DJ. Ventricular septal defects. Circulation. 2006;114(20):2190–7.

101. Razzouk L, Applebaum RM, Okamura C, et al. The windsock syndrome: subpulmonic obstruction by membranous ventricular septal aneurysm in congenitally corrected transposition of great arteries. echocardiography. 2013 Jul 1. doi: 10.1111/echo.12279 [Epub ahead of print].

102 Saric M, Kronzon I. Chapter 107: Ventricular septal defect and Eisenmenger syndrome. In: Lang R, Goldstein SA, Kronzon I, Khanderia BK, editors. Dynamic Echocardiography: A Case-Based Approach. 1 ed. New York, NY: Springer; July 1, 2010:446–50.

103. Lock JE, Block PC, McKay RG, et al. Transcatheter closure of ventricular septal defects. Circulation. 1988;78(2):361–8.

104. Holzer R, Balzer D, Amin Z, et al. Transcatheter closure of postinfarction ventricular septal defects using the new Amplatzer muscular VSD occluder: Results of a U.S. Registry. Catheter Cardiovasc Interv. 2004;61(2):196–201.

105. Masura J, Gao W, Gavora P, et al. Percutaneous closure of perimembranous ventricular septal defects with the eccentric Amplatzer device: multicenter follow-up study. Pediatr Cardiol. 2005;26(3):216–9.

106 Halpern DG, Perk G, Ruiz C, et al. Percutaneous closure of a post-myocardial infarction ventricular septal defect guided by real-time three-dimensional echocardiography. Eur J Echocardiogr. 2009,10:702–3.

107 Anonymous. Risk factors for stroke and efficacy of antithrombotic therapy in atrial fibrillation. Analysis of pooled data from five randomized controlled trials. Arch Intern Med. July 11, 1994;154(13):1449–57.

108. Blackshear JL, Odell JA. Appendage obliteration to reduce stroke in cardiac surgical patients with atrial fibrillation. Ann Thorac Surg. 1996;61(2):755–9.

109. Cox JL, Sundt TM 3rd. The surgical management of atrial fibrillation. Annu Rev Med. 1997;48:511–23.

110. Salzberg SP, Plass A, Emmert MY, et al. Left atrial appendage clip occlusion: early clinical results. J Thorac Cardiovasc Surg. 2010;139(5):1269–74.

111. Kim R, Baumgartner N, Clements J. Routine left atrial appendage ligation during cardiac surgery may prevent postoperative atrial fibrillation-related cerebrovascular accident. J Thorac Cardiovasc Surg. 2013;145(2):582–9; discussion 589.

112. Katz ES, Tsiamtsiouris T, Applebaum RM, et al. Surgical left atrial appendage ligation is frequently incomplete: a transesophageal echocardiograhic study. J Am Coll Cardiol. 2000;36(2):468–71.

113. Perk G, Biner S, Kronzon I, et al. Catheter-based left atrial appendage occlusion procedure: role of echocardiography. Eur Heart J Cardiovasc Imaging. 2012;13(2):132–8.

114. Cruz-Gonzalez I, Yan BP, Lam YY. Left atrial appendage exclusion: state-of-the-art. Catheter Cardiovasc Interv. 2010;75(5):806–13.

115. Holmes DR, Reddy VY, Turi ZG, et al.; PROTECT AF Investigators. Percutaneous closure of the left atrial appendage versus warfarin therapy for prevention of stroke in patients with atrial fibrillation: a randomised non-inferiority trial. Lancet. 2009;374(9689):534–42.

116. Shah SJ, Bardo DM, Sugeng L, et al. Real-time three-dimensional transesophageal echocardiography of the left atrial appendage: initial experience in the clinical setting. J Am Soc Echocardiogr. 2008;21(12):1362–8.

117. Bartus K, Han FT, Bednarek J, et al. Percutaneous Left Atrial Appendage Suture Ligation Using the LARIAT Device in Patients With Atrial Fibrillation: Initial Clinical Experience. J Am Coll Cardiol. 2013;62(2):108–18.

118. Klein AL, Grimm RA, Murray RD, et al.; Assessment of Cardioversion Using Transesophageal Echocardiography Investigators. Use of transesophageal echocardiography to guide cardioversion in patients with atrial fibrillation. N Engl J Med. 2001;344(19):1411–20.

119. Faletra FF, Ho SY, Auricchio A. Anatomy of right atrial structures by real-time 3D transesophageal echocardiography. JACC Cardiovasc Imaging. 2010;3(9):966–75.

120. Go AS, Hylek EM, Phillips KA, et al. Prevalence of diagnosed atrial fibrillation in adults: national implications for rhythm management and stroke prevention: the AnTicoagulation and Risk Factors in Atrial Fibrillation (ATRIA) Study. JAMA. 2001;285(18):2370–75.

121. Haïssaguerre M, Jaïs P, Shah DC, et al. Spontaneous initiation of atrial fibrillation by ectopic beats originating in the pulmonary veins. N Engl J Med. 1998;339(10):659–66.

122. Pappone C, Rosanio S, Oreto G, et al. Circumferential radiofrequency ablation of pulmonary vein ostia: A new anatomic approach for curing atrial fibrillation. Circulation. 2000;102(21):2619–28.

123. Wilber DJ, Pappone C, Neuzil P, et al.; ThermoCool AF Trial Investigators. Comparison of antiarrhythmic drug therapy and radiofrequency catheter ablation in patients with paroxysmal atrial fibrillation: a randomized controlled trial. JAMA. 2010;303(4):333–40.

124. Fuster V, Rydén LE, Cannom DS, et al.; American College of Cardiology Foundation/American Heart Association Task Force. 2011 ACCF/AHA/HRS focused updates incorporated into the ACC/AHA/ESC 2006 guidelines for the management of patients with atrial fibrillation: a report of the American College of Cardiology Foundation/American Heart Association Task Force on practice guidelines. Circulation. 2011;123(10):e269–367.

125. To AC, Gabriel RS, Park M, et al. Role of Transesophageal Echocardiography Compared to Computed Tomography in Evaluation of Pulmonary Vein Ablation for Atrial Fibrillation (ROTEA study). J Am Soc Echocardiogr. 2011;24(9): 1046–55.

126. Marrouche NF, Martin DO, Wazni O, et al. Phased-array intracardiac echocardiography monitoring during pulmonary vein isolation in patients with atrial fibrillation: impact on outcome and complications. Circulation. 2003; 107(21):2710–6.

127. Jongbloed MR, Bax JJ, de Groot NM, et al. Radiofrequency catheter ablation of paroxysmal atrial fibrillation; guidance by intracardiac echocardiography and integration with other imaging techniques. Eur J Echocardiogr. 2003;4(1):54–8.

128. Schmidt M, Nölker G, Marschang H, et al. Incidence of oesophageal wall injury post-pulmonary vein antrum isolation for treatment of patients with atrial fibrillation. Europace. 2008;10(2):205–9.

129. Faletra FF, Nucifora G, Regoli F, et al. Anatomy of pulmonary veins by real-time 3D TEE: implications for catheter-based pulmonary vein ablation. JACC Cardiovasc Imaging. 2012;5(4):456–62.

130. Pinheiro L, Nanda NC, Jain H, et al. Transesophageal echocardiographic imaging of the pulmonary veins. Echocardiography. 1991;8(6):741–8.

131 Purgess JR, Bernstein S, Saric M. Real-time 3D transesophageal echocardiography: development of a protocol for use in atrial fibrillation ablation procedures. Anesth Analg. 2012;114(Suppl):1–94.

132. Ottaviano L, Chierchia GB, Bregasi A, et al. Cryoballoon ablation for atrial fibrillation guided by real-time three-dimensional transoesophageal echocardiography: a feasibility study. Europace. 2013;15(7):944–50.

133. Frances C, Romero A, Grady D. Left ventricular pseudo-aneurysm. J Am Coll Cardiol. 1998;32(3):557–61.

134. Clift P, Thorne S, de Giovanni J. Percutaneous device closure of a pseudoaneurysm of the left ventricular wall. Heart. 2004;90(10):e62.

135. Dudiy Y, Jelnin V, Einhorn BN, et al. Percutaneous closure of left ventricular pseudoaneurysm. Circ Cardiovasc Interv. 2011;4(4):322–26.

136. Kapadia SR, Tuzcu EM. Plugging holes: expanding horizon for structural interventions. Circ Cardiovasc Interv. 2011;4(4):308–10.

137. Sigwart U. Non-surgical myocardial reduction for hypertrophic obstructive cardiomyopathy. Lancet. 1995;346(8969):211–4.

138. Faber L, Seggewiss H, Gleichmann U. Percutaneous transluminal septal myocardial ablation in hypertrophic obstructive cardiomyopathy: results with respect to intraprocedural myocardial contrast echocardiography. Circulation. 1998;98(22):2415–21.

139. Silvestry FE, Kerber RE, Brook MM, et al. Echocardiography-guided interventions. J Am Soc Echocardiogr. 2009; 22(3):213–31; quiz 316.

140. McCreery CJ, McCulloch M, Ahmad M, deFilippi CR. Real-time 3-dimensional echocardiography imaging for right ventricular endomyocardial biopsy: a comparison with fluoroscopy. J Am Soc Echocardiogr. 2001;14(9):927–33.

141. Scheurer M, Bandisode V, Ruff P, et al. Early experience with real-time three-dimensional echocardiographic guidance of right ventricular biopsy in children. Echocardiography. 2006;23(1):45–9